The
PHILOSOPHICAL MAGAZINE

FIRST PUBLISHED IN 1798

L. 44 SEVENTH SERIES No. 357 October 1953

A Journal of Theoretical Experimental and Applied Physics

PRICE 15s. 0d.
Annual Subscription £8 0s. 0d. payable in advance

AND PUBLISHED BY TAYLOR & FRANCIS LTD., RED LION COURT, FLEET ST., LONDON, E.C.4.

CX. *A Study of Charge Exchange by Helium Ions in Metals*

By G. A. Dissanaike
Cavendish Laboratory, Cambridge *

[Received July 4, 1953]

Abstract

A study has been made of the equilibrium fractions of He^0, He^+ and He^{++} in a helium beam traversing metallic foils of beryllium, aluminium and silver at energies from 0·13 to 1·1 Mev. The equilibrium fractions have been found to be independent of the metals used. The ratio σ_l/σ_c of the cross sections for electron loss and capture respectively by the helium ions is proportional to v^m, where v is the ion velocity. In the exchange $He^0 \rightleftharpoons He^+$ the exponent m is equal to $3{\cdot}08 \pm 0{\cdot}10$ in the energy range 0·13 to 0·6 Mev studied. In the exchange $He^+ \rightleftharpoons He^{++}$ m appears to be constant at $5{\cdot}10 \pm 0{\cdot}12$ for energies between 0·43 and 1·1 Mev, but decreases steadily with decreasing energy below this region.

For the He^{++} ion, the speed for which $\sigma_l = \sigma_c$ is found to be 2·55 times that of the orbital electron in the hydrogen atom, and is almost exactly twice as great as the corresponding speed for the He^+ ion.

§ 1. Introduction

A study of charge exchange of light ions in passing through matter is of interest in the understanding of the processes of electron capture and electron loss and of the energy loss of the ions, especially near the end of their range where charge exchange is most frequent.

The subject of charge exchange has been widely studied for light ions and the early work has been reviewed by Rüchardt (1933). The first evidence for electron capture by high energy alpha-particles was obtained by Henderson (1922), and the phenomenon was studied more closely for energies above 0·65 Mev by Rutherford (1924), Kapitza (1924), Henderson (1925), and Briggs (1927) using natural sources. Considerable work has also been carried out below 0·1 Mev and is summarized by Massey and Burhop (1952). Recently Snitzer (1953) has investigated the charge exchange for alpha-particles in different gases from 0·1 Mev to 0·48 Mev. Similar work has been reported for hydrogen beams in gases by Keene (1949), Montague (1951), Ribe (1951), and Kanner (1951), and in metals by Hall (1949). Theoretical interpretations of these exchange processes have been attempted using classical mechanics by Fowler (1924) and Thomas (1927), and on quantum-mechanical ideas by Oppenheimer (1928) and Brinkman and Kramers (1930).

* Communicated by A. P. French.

The present work describes experiments on alpha-particles in different metals for energies from 0·13 MeV to 1·1 MeV. For this energy range it has been of interest to consider the results in the light of the simple considerations made by Bohr (1948) in a general survey of the exchange phenomena.

§ 2. Description of Apparatus

2.1. *General*

The general arrangement of the target and detector systems is shown schematically in figs. 1 (*a*) and 1 (*b*). A beam of He^+ ions, stabilized to

Fig. 1

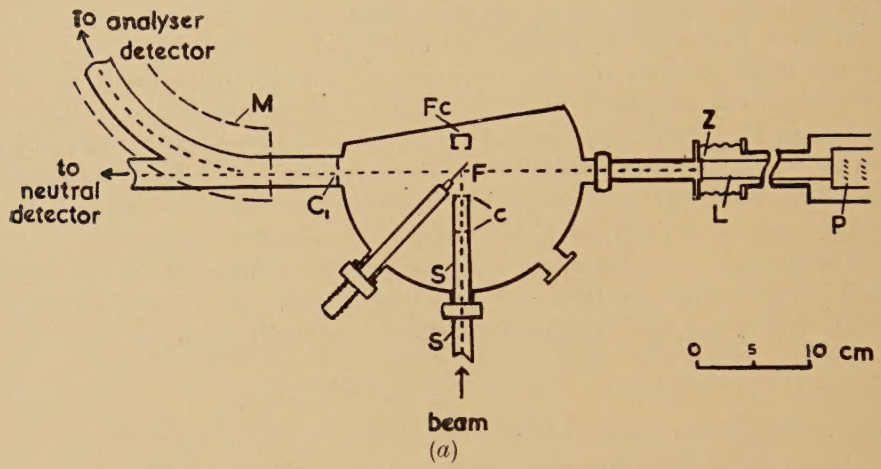

(*a*)

The target and detector arrangement. (Horizontal section.)

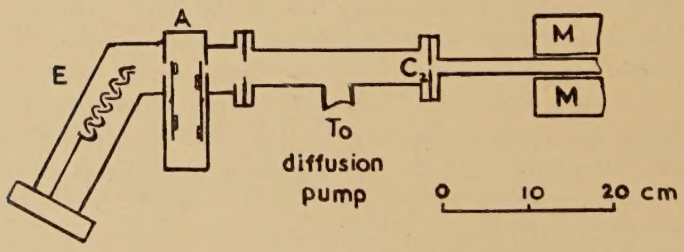

(*b*)

The neutral detector system with the secondary electron multiplier E. (Vertical section.)

within ± 1 kev, from the Cavendish Laboratory Electrostatic Generator entered the target box through steel tubes SS which shielded the beam from the stray field of the magnetic analyser. Collimating apertures CC (No. 32 drill size) positioned the beam centrally on the target foil F. The beam current was collected and measured in a Faraday cage Fc. Particles scattered at 90° to the incident direction (having undergone a single nuclear collision in the foil) passed through aperture C_1 into the

analyser between pole pieces MM, and with the magnetic field zero entered the secondary electron multiplier assembly (fig. 1 (*b*)) which will be referred to as the neutral detector. The detector solid angle was limited by the aperture C_2 of diameter 3·5 mm, C_1 merely preventing any scattering from the inner walls of the waveguide. The whole detector system was carefully aligned with a light source at the target position. Ten collodion foils of varying thickness arranged in two sets in the foil changer A enabled stopping thicknesses in the range 0·1 to 7·4 mm air at N.T.P. to be introduced in the path of the scattered particles. An auxiliary mercury diffusion pump system was used to help maintain a good vacuum. A Philips gauge, not shown, registered the pressure near the secondary electron multiplier. The pressure throughout the experiment did not exceed $1{\cdot}5\times10^{-5}$ mm of mercury.

The charged particles analysed by the magnetic field were detected by an arrangement similar to the one used for the monitoring, which consisted of a zinc sulphide screen Z and photomultiplier tube P. A lucite rod L (53 cm long) was used as a light guide so that the multiplier could be removed from the influence of the analyser field. Measurements were made with two different magnetic analysers. The first, a 90° focussing analyser (Burcham and Freeman 1949), was used in the study of the He^0 content and of the He^+ and He^{++} groups for energies up to 0·6 MeV, and is the one generally referred to in this description. A 60° focussing analyser was used for the comparison of the intensities of the He^+ and He^{++} groups between 0·6 MeV and 1·1 MeV. The analysers were calibrated in terms of magnet current for energies up to about 3·0 MeV in the way described by Burcham and Freeman (1949). The calibration of the 60° analyser was extended to 4·4 MeV using the particle groups from the reactions $^2D(dp)^3T$, $^{12}C(dp)^{13}C$, $^9Be(d\alpha')^7Li^*$ and $^9Be(d\alpha)^7Li$. These calibrations were checked during the experiment using the alpha-particles from $^{19}F(p\alpha')^{16}O^*$ and the elastically scattered protons from thin films of beryllium, silver and aluminium. By deducing the alpha-particle energies in the experiment from the positions of the He^+ group (which should give exactly four times the required energy value) it was possible to reduce the error in the energy measurement to within ±5 kev for the energies studied.

2.2. *Target Foils*

For the comparison of the He^+ and He^{++} contents, thin self-supporting foils of beryllium, aluminium and silver of thickness between 0·3 and 0·7 mm air equivalent at N.T.P. were used. The spread in energy of the scattered particles as they emerged from the foils ranged from 50 to 90 kev. For the study of the He^0 content, however, where the energy distribution of the particles could not be analysed as for the charged components, it was necessary to reduce this energy spread considerably in order to define the energy within a narrow interval. The metal was therefore evaporated on thin collodion film ; when the beam was directed

into the backing, the collodion burnt off leaving a film of the metal. Silver and aluminium foils of between 0·15 mm and 0·3 mm air equivalent at N.T.P. were obtained in this way, producing an energy spread of less than 30 kev in the scattered particles. In using such thin foils it was important to consider the effect due to the scattering from the carbon left by the burnt collodion and also gradually built up during the bombardment; the particles scattered from carbon have energies smaller than those from the metal itself and would therefore give rise to a higher He^0 content. This effect was found to be serious in the case of aluminium and the final measurements were made using a self-supporting foil of 0·2 mm air equivalent at N.T.P. prepared with special care. The foils withstood quite satisfactorily the beam currents (up to 50 mμA concentrated on an area 0·06 cm^2) used in the experiment.

2.3. *Detectors*

(*a*) *Charged Particles*

A zinc sulphide screen and an E.M.I. photomultiplier (type 5032) were used for the analyser detector and for the monitoring system. In the latter a thin aluminium foil ($\sim$0·2 mm air at N.T.P.) was placed in front of the ZnS screen to prevent any light from the target box from entering the detector. The efficiency of detection of particles below about 0·6 MeV was well below 100% and depended on the energy of the particles. In studying the charged components with the magnetic analyser, however, the efficiency of detection would be the same for a particular energy in both He^+ and He^{++} groups provided the detecting system were not influenced by the stray field of the analyser. The use of the light guide ensured this condition and did not appreciably reduce the size of the pulses in the detector. To ensure stability a high-tension battery unit was used to supply the voltage direct to each dynode of the photomultiplier.

(*b*) *Neutral Particles*

A secondary-electron-multiplier was used for the study of the He^0 content. Successful use of these counters for the detection of particles has been reported by many workers and recently reviewed by Allen (1950). The efficiency of detection of alpha-particles and protons above about 5 kev has been found to be near 100% and independent of the energy of the particles. The multiplier used in the present work was of the design developed in the Cavendish Laboratory by Baxter (1949). The dynodes were of beryllium-copper alloy activated by a thin layer of beryllium oxide. The multiplier was encased in steel to ensure adequate magnetic shielding. In the experiment about 300–350 volts per stage were used on the dynodes.

The use of the secondary-electron-multiplier to measure the He^0 content required a detailed knowledge of its response to both charged and neutral particles and to photons. The full discussion of this problem is rather lengthy and is therefore given in the separate section that follows.

§ 3. The Performance of the Secondary Electron Multiplier

In the experimental arrangement (fig. 1 (*b*)) the first dynode surface 'looked' directly at the target and was found to be sensitive to the x-rays given off during the bombardment. The pulse-height distributions for alpha-particles and for the background radiation are however essentially different and it was found possible to bias out the background satisfactorily. As an example, fig. 2 (obtained using the Hutchinson–Scarrott kicksorter, 1951) shows differential bias curves due to scattered alpha-particles of energy 0·6 MeV and the associated background radiation; curve A is obtained without the magnetic field on which deflects the charged particles away from the detector, and therefore represents the total contribution of particles and background; curve B is obtained with

Fig. 2

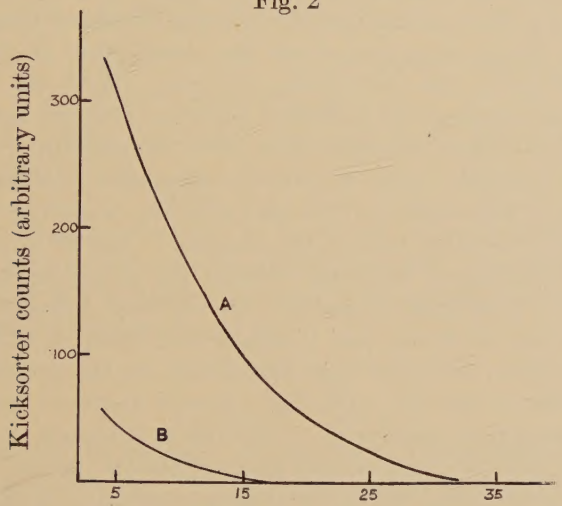

Differential bias curves for 0·6 MeV alpha-particles and associated background radiation. Curve A shows the total contribution due to the particles plus background, curve B due to the background alone.

the magnetic field on and with a stopping foil to cut off the undeflected neutral particles, and therefore gives the background contribution alone. The relative intensity of this background contribution was found to increase with increasing energy of bombardment and was thus more difficult to bias out at high energies. In the experiment a bias of 28 volts ensured that the pulses counted were entirely due to the alpha-particles for the energies below 0·6 MeV that were studied.

The use of the detector to compare the intensities of the neutral and charged components of the helium beam presupposes the same efficiency of detection for all charge states at the same energy. This is a reasonable assumption to make since the mean free path for electron capture by the alpha-particle is much less than 10^{-3} mm air equivalent for all energies used (Rutherford 1924). An experimental proof of the constant efficiency

was possible. From the curves of fig. 2 the pulse-height distribution due to charged and uncharged alpha-particles together may be obtained. At the same energy, the differential bias curve obtained with the magnetic field on, but with no stopping foil to cut off the neutrals, gives the pulse-height distribution due to the neutral particles alone once the x-ray background is subtracted. It was found that the two distributions so obtained could be made to coincide quite satisfactorily by multiplying the ordinates of one of them by a suitable constant factor, which clearly implies a similar response to charged and uncharged particles by the detector.

§ 4. Experimental Procedure

The experiment was carried out in two stages. Firstly, the fraction of the He^0 content in the total scattered beam was obtained using the neutral detector. The beam was monitored by observation of the scattered particles at 90° using the scintillation counter. With the magnet field zero, the detector counted all scattered particles, charged and uncharged. With the magnet current increased from zero, the counting rate decreased suddenly to a constant value which was thereafter independent of the magnet current ; this confirmed the fact that the detecting systems were not influenced by the stray field of the analyser. The counting rates were then observed alternately with and without the magnetic field in several repeated runs at a particular energy. In the measurements a stopping foil of appropriate thickness was interposed in front of the detector to cut off any particles scattered from the carbon on the targets.

The intensities of the He^+ and He^{++} groups analysed by the magnet spectrometer were then compared. A plot of the counting rate against the magnet current gave the position and shape of the two peaks. A resolution of 2 to 4% in energy was used in the analyser system, and since the energy spread of the detected particles was much greater than the energy interval accepted by the analyser, the ratio of the heights of the peaks gave directly the proportion of He^+ to He^{++} ions in the beam. Several runs were made over the top of each peak at a particular energy. The beam was monitored in one of two ways. With the 60° focussing analyser, the beam current was measured using a current amplifier and integrator arrangement; with the 90° focussing analyser, it was found more convenient to monitor on the scattered neutral particles detected by the secondary electron multiplier.

In the case of beryllium, two groups of scattered particles, from the metal and from oxygen impurity, were observed. The oxygen-peak was nearly twice as high as the beryllium-peak. The equilibrium ratio obtained here corresponded to a stopping material of beryllium oxide rather than to the metal itself. For energies below about 0·5 Mev the contribution due to the ' tail ' of the He^+ group scattered from beryllium was appreciable at the position of the He^{++} group from oxygen, and a subtraction procedure was necessary to separate them.

§ 5. Analysis of Experimental Results

5.1. *Conditions for Charge Equilibrium*

The fractions of He^0, He^+ and He^{++} present in the beam can be related to the cross sections for capture and loss of electrons.

Let $f_0(x)$, $f_1(x)$ and $f_2(x)$ represent the fractions of He^0, He^+ and He^{++} ions respectively in the beam at a variable depth in the foil, and x the number of atoms per unit area in that depth. Let σ_{01} and σ_{10} denote the cross sections for loss and for capture of electrons respectively in the exchange $He^0 \rightleftarrows He^+$, and σ_{12} and σ_{21} the corresponding cross sections for the exchange $He^+ \rightleftarrows He^{++}$. Then, if we neglect the cross sections for capture and loss of two electrons in a single encounter, we may write for the change in composition of the beam in traversing a layer dx,

$$\left.\begin{aligned} df_0/dx &= \sigma_{10}f_1 - \sigma_{01}f_0, \\ df_1/dx &= \sigma_{01}f_0 - \sigma_{10}f_1 + \sigma_{21}f_2 - \sigma_{12}f_1, \\ df_2/dx &= \sigma_{12}f_1 - \sigma_{21}f_2. \end{aligned}\right\} \quad . \quad . \quad . \quad (1)$$

The mean free path for charge exchange in the $He^0 \rightleftarrows He^+$ transition may be expressed by $\Delta x_{01}=(\sigma_{01}+\sigma_{10})^{-1}$ and for the $He^+ \rightleftarrows He^{++}$ transition by $\Delta x_{12}=(\sigma_{12}+\sigma_{21})^{-1}$. Since the cross sections remain very nearly constant for a change of energy in the beam corresponding to one mean free path, we may expect charge equilibrium to be established for $x \gg \Delta x_{01}$ or Δx_{12}. With this condition satisfied the equilibrium composition of the beam is given from eqns. (1) by

$$\left.\begin{aligned} f_1(x)/f_0(x) &= \sigma_{01}/\sigma_{10}, \\ f_2(x)/f_1(x) &= \sigma_{12}/\sigma_{21}. \end{aligned}\right\} \quad . \quad . \quad . \quad . \quad . \quad . \quad (2)$$

The thickness of the metallic foils used was several times the mean free path for charge exchange ; hence the measured intensities n_0, n_1 and n_2 respectively of He^0, He^+ and He^{++} ions in the beam emerging from the foil were proportional to the quantities f_0, f_1 and f_2 of eqns. (2).

5.2. *Experimental Results*

Figures 3 and 4 show the values of the ratios n_1/n_0 and n_2/n_1 respectively plotted (logarithmically) as functions of the energy E of the alpha-particles. The results show no difference in the charge state of the helium beam, within the accuracy of the experiment, for the different metals used. Figure 3 shows that the experimental points are closely fitted by a straight line, implying that σ_{01}/σ_{10} is proportional to $E^{m'}$, where m' is constant over the whole energy range studied. The value of m' is $1{\cdot}54 \pm 0{\cdot}05$.

The plot of $\log(n_2/n_1)$ versus $\log E$, fig. 4, appears to be linear for energies 0·43 to 1·1 MeV with a slope of $2{\cdot}55 \pm 0{\cdot}06$ over this limited range. For energies below 0·4 MeV the results fit closely a relation of the form

$$\sigma_{12}/\sigma_{21} = 0{\cdot}019 - 0{\cdot}064E + 1{\cdot}93E^2 \quad (E \text{ in MeV}).$$

The equilibrium charge distribution of the helium beam as a function of the energy is shown in fig. 5. The values are taken from the smooth

curves through the experimental points for all the metals used. The fraction f_0 of the He^0 content in the beam obeys closely the relation

$$f_0 = -0{\cdot}122 + 0{\cdot}119/E - 0{\cdot}0033/E^2,$$

for energies between 0·2 and 0·6 MeV, and the curve above 0·6 MeV has been extrapolated using this relation.

5.3. *Errors*

The main error in the experiments arises from the uncertainty in the energy measurements, estimated to be within ± 5 kev. For energies above 0·5 MeV the error in each of the ratios n_1/n_0 and n_2/n_1 is less than

Fig. 3

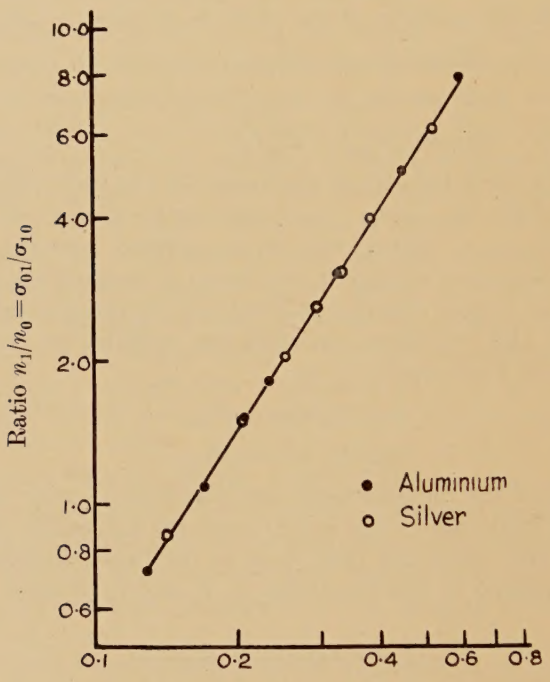

The ratio σ_{01}/σ_{10} of the loss to capture cross sections for the exchange $He^0 \rightleftharpoons He^+$ in metals as a function of the alpha-particle energy.

2%, but increases to about 5% at energies below 0·2 MeV. In the results for beryllium a further error may arise for energies below about 0·4 MeV as a result of the subtraction procedure used to analyse the composition of the beam (see § 4).

A few systematic errors are also possible (some of them have already been considered in §§ 2 and 3). Effects due to light and background radiation have been successfully eliminated, and by the use of a suitable collimating arrangement errors due to particles multiply scattered in the analyser wave guide have been avoided. Deposits of carbon or thin oil films on the target could have had serious effects. The former appeared

Fig. 4

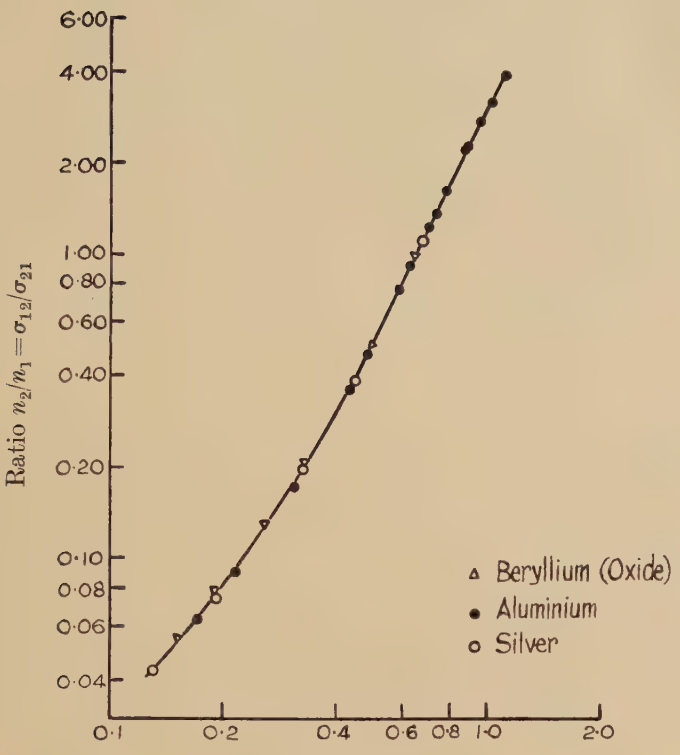

Energy in MeV.

The ratio σ_{12}/σ_{21} of the loss to capture cross sections for the exchange $He^{+} \rightleftharpoons He^{++}$ in metals as a function of the alpha-particle energy.

Fig. 5

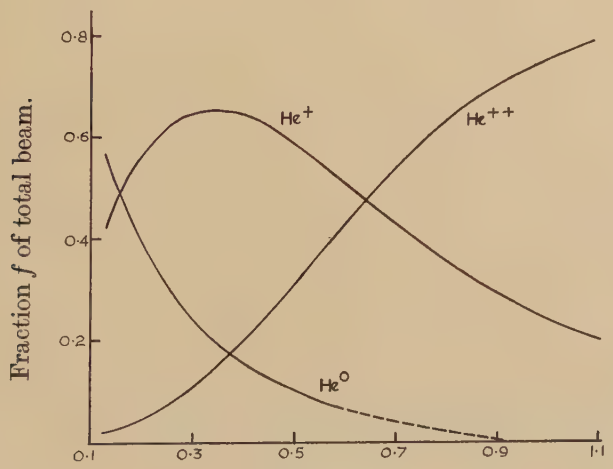

Energy in MeV.

The equilibrium charge distribution of a helium beam in metals as a function of the energy.

to be serious only in the collodion-backed foils of aluminium, which were therefore not used. No oil diffusion pumps were used near the apparatus nor were there any visible traces of oil film on the targets bombarded. Checks were however made from time to time at a particular energy to test for consistency in the results. No foils were bombarded for more than two hours. The equality of response of the neutral detector to both charged and uncharged particles has been established, as discussed in § 3.

In the study of the He^0 content, the energy spread of the scattered particles was between 25 and 30 kev. The spread, however, does not give rise to appreciable errors as the variations of the capture and loss cross-sections in this energy interval are small and approximately linear.

§ 6. Theory

6.1. *Electron Loss*

Bohr (1948), considering electron loss as a simple ionization process, showed that for velocities v of the particle much greater than $v_0=e^2/h$ (the electron velocity in the first Bohr orbit of hydrogen), the cross section σ_l for electron loss should be proportional to $(v_0/v)^n$ where n ranges from 0 to 2 depending on the charge number Z of the material. n is equal to 2 for the lightest nuclei, but should decrease as Z increases, and be zero for the heaviest nuclei where the atomic field is so strong that any collision in which the particle penetrates the atomic region would lead to the ionization of the particle. For velocities v approaching v_0 there is no adequate theory of the interaction as neither classical (orbital) pictures nor simplified quantum ideas (Born approximation) can be applied. It is however expected that for $v\sim v_0$, $\sigma_l\sim\pi a_0^2$ where a_0 is the Bohr radius $(=\hbar^2/me^2)$.

6.2. *Electron Capture*

For the capture of electrons in lighter substances Brinkman and Kramers (1930), using the Born approximation, showed that for $v\gg v_0$, σ_c (the cross section for electron capture) is proportional to v^{-12}. For heavier substances Bohr (1948) estimated that for $v>v_0$, σ_c should be proportional to v^{-6}. He used simple statistical considerations together with the assumption that capture was most probable for those electrons in the atom with orbital velocities comparable with the velocity v of the particle. As the velocity v approaches v_0, σ_c becomes large, but it cannot much exceed the geometrical cross section of the atom and therefore becomes less dependent on the velocity v.

§ 7. Discussion

It follows from the considerations of § 6 that σ_l/σ_c should increase with increasing Z and, for $v\gg v_0$, should be proportional to v^m where $m\approx 5$ for intermediate Z corresponding to the metals studied. As the velocity decreases m would be expected to decrease, and for $v\sim v_0$, σ_l/σ_c should be of order unity. In the experiments σ_l/σ_c is given for He^+ ions by n_1/n_0 and for He^{++} ions by n_2/n_1.

In fig. 6 the experimental values of m are plotted as functions of the quantity (v/v_0). For comparison some of the values obtained by Hall (1949) for protons in metals (except gold) and by Henderson (1925) for high energy alpha-particles in metals are included. The experimental results for the exchange $He^+ \rightleftharpoons He^{++}$ agree in the main with the theoretical expectations, though Henderson's values of m for alpha-particles of higher energy $(v > 3{\cdot}5v_0)$ show a steady decrease with increasing velocity. On the other hand, the exchanges $He^0 \rightleftharpoons He^+$ (this work) and $H^0 \rightleftharpoons H^+$ (Hall

Fig. 6

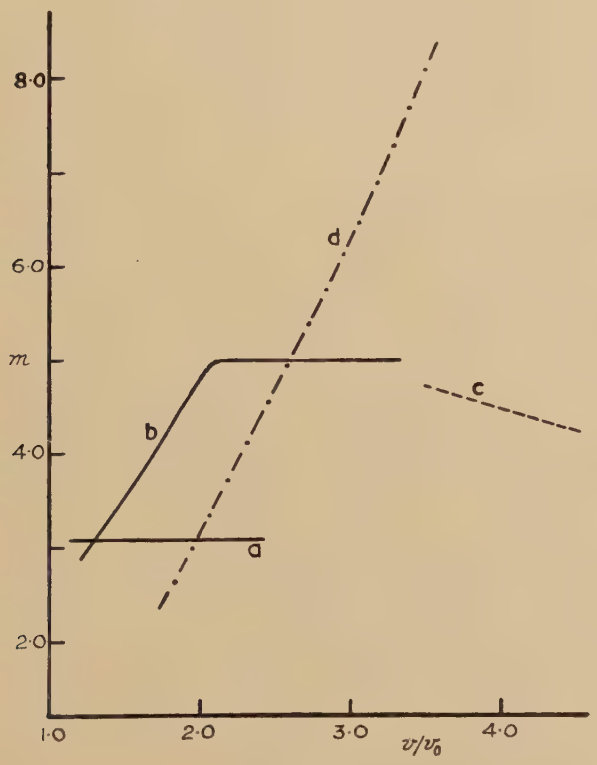

The exponent m (in $\sigma_l/\sigma_c \propto v^m$) plotted as a function of v/v_0. The curves represent the following exchanges in metals: (*a*) $He^0 \rightleftharpoons He^+$ (present work), (*b*) $He^+ \rightleftharpoons He^{++}$ (present work), (*c*) $He^+ \rightleftharpoons He^{++}$ (Henderson), (*d*) $H^0 \rightleftharpoons H^+$ (Hall).

1949) exhibit no such agreement. It is significant that for both protons and alpha-particles the charge exchange behaviour is independent of the atomic number Z of the metal used. It may be that, in a metal foil, the charge transfer properties are determined by the lattice and electron band structure rather than by the electronic configurations of individual atoms. If this were so the usual theoretical treatments which deal only with single collision effects would be inapplicable.

The results obtained in the present experiments may also be compared with the results of Snitzer (1953) for the charge exchange of alpha-particles of energies between 0·1 and 0·48 MeV in the gases hydrogen, helium, air and argon. These do, by contrast, exhibit a definite dependence on Z. Snitzer's results also show that in gases m increases with increasing velocity v for the exchange $He^0 \rightleftharpoons He^+$, but is constant at a value between 5·1 and 6·3 in the exchange $He^+ \rightleftharpoons He^{++}$. The equilibrium charge distribution of a helium beam in hydrogen has an energy dependence remarkably close to that in metals, although the absolute values of f_0, f_1, and f_2 are not quite the same.

The salient features of the charge distributions for both metals and gases are summarized in table 1. The velocity of the particle for which

Table 1

Stopping material	E_{01} (MeV)	E_{02} (MeV)	E_{12} (MeV)	f_1 (max)	E_1 (MeV)	v_{01}/v_0	v_{12}/v_0
Metals	0·157	0·370	0·645	0·66	0·350	1·25	2·54
Hydrogen	0·148	0·370	0·660	0·76	0·340	1·22	2·58
Helium	0·145	0·430	0·800	0·72	0·410	1·21	2·84
Air	0·098	0·340	0·650	0·76	0·300	0·99	2·56
Argon	0·155	0·330	0·580	0·77	0·290	1·08	2·42

E_{01}, E_{02}, and E_{12} are the energies corresponding to $n_0=n_1$, $n_0=n_2$ and $n_1=n_2$ respectively. v_{01}, v_{12} are the velocities corresponding to E_{01}, E_{12}. $v_0=e^2/\hbar=2{\cdot}19\times10^8$ cm sec^{-1}. f_1(max)=maximum value of He^+ fraction in beam, E_1 the energy at this value.

$\sigma_l=\sigma_c$ is significant since, according to any simple theory of electron transfer, the processes of capture and loss become equally probable when the linear velocity of the ion becomes about equal to the orbital velocity of the transferred electron. It is interesting to note that the results on the passage of ions through metals seem to bear out this hypothesis. Table 2 shows the extent of the agreement, the experimental values being

Table 2

Exchange	$v_{\sigma_c=\sigma_l}$ (in $e^2/\hbar$ units)	Orbital velocity of transferred electron (in $e^2/\hbar$ units)
$H^0 \rightleftharpoons H^+$	0·95	1·00
$He^0 \rightleftharpoons He^+$	1·25	1·34
$He^+ \rightleftharpoons He^{++}$	2·55	2·35

taken from the present work and from that of Hall (1949), and the electron orbital velocities being defined by the known values of the corresponding ionization potentials. From the work of Snitzer (1953) it appears that a

similar correspondence can be made when the stopping material is a gas although the agreement is certainly not as good.

Acknowledgments

The author is much indebted to Professor W. E. Burcham for suggesting the experiment, and to Dr. A. P. French for helpful discussions. He is grateful to the Ceylon Government for the award of a scholarship.

References

Allen, J. S., 1950, *Proc. Inst. Radio Engrs., N.Y.*, **38,** 346.
Baxter, A. S., 1949, *Thesis*, University of Cambridge.
Bohr, N., 1948, *Kgl. Danske Videnskab. Selskab, Mat.-fys. Medd.*, **18,** No. 8.
Briggs, G. H., 1927, *Proc. Roy. Soc.* A, **114,** 341.
Brinkman, H. C., and Kramers, H. A., 1930, *Proc. Akad. Amsterdam*, **33,** 973.
Burcham, W. E., and Freeman, J. M., 1949, *Phil. Mag.*, **40,** 807.
Fowler, R. H., 1924, *Phil. Mag.*, **47,** 416.
Hall, T., 1949, *Phys. Rev.*, **79,** 504.
Henderson, G. H., 1922, *Proc. Roy. Soc.* A, **102,** 496 ; 1925, *Ibid.*, **109,** 157.
Hutchinson, G. W., and Scarrott, G. G., 1951, *Phil. Mag.*, **42,** 792.
Kanner, H., 1951, *Phys. Rev.*, **84,** 1211.
Kapitza, P., 1924, *Proc. Roy. Soc.* A, **106,** 602.
Keene, J. P., 1949, *Phil. Mag.*, **40,** 369.
Massey, H. S. W., and Burhop, E. H. S., 1952, *Electronic and Ionic Impact Phenomena* (Oxford : University Press), Ch. VIII.
Montague, J. H., 1951, *Phys. Rev.*, **81,** 1026.
Oppenheimer, J. R., 1928, *Phys. Rev.*, **31,** 66, 349.
Ribe, F. L., 1951, *Phys. Rev.*, **83,** 1217.
Rüchardt, E., 1933, *Handbuch der Physik*, **22,** 103.
Rutherford, E., 1924, *Phil. Mag.*, **47,** 277.
Snitzer, E., 1953, *Phys. Rev.*, **89,** 1237.
Thomas, L. H., 1927, *Proc. Roy. Soc.* A, **114,** 561.

CXI. *Electrical Interaction of a Dislocation and a Solute Atom*

By A. H. Cottrell, S. C. Hunter and F. R. N. Nabarro
Department of Metallurgy, University of Birmingham*

[Received July 16, 1953]

Summary

In the dilatation field of an edge dislocation in a metal the Fermi energy and ground state of the conduction electrons are both altered. To preserve a constant level of the Fermi surface everywhere, a charge shift occurs by a redistribution of the electrons and an electrical dipole is formed on the dislocation. Mott's estimate of the effective charge on a solute atom in copper is used in a calculation of the electrical interaction of such an atom with an edge dislocation. For the copper-based alloys considered, the calculations suggest that this electrical interaction is between 1/3 and 1/6 of the corresponding elastic interaction.

§ 1. Introduction

From time to time evidence has been presented to show that the strengthening of metals by alloying elements in solid solution depends on the difference in valency of the solute and solvent atoms as well as on the difference in size. For example, Dorn, Pietrokowsky and Tietz (1950) showed that silver hardens aluminium twice as intensely as does zinc, even though it produces no lattice parameter charge whereas zinc produces an expansion. Other alloying elements showed similar effects, although to express the effects of atomic size and valency in a single empirical formula it proved necessary to assume that the valency of aluminium was 2. In a similar investigation of copper alloys containing zinc, gallium, germanium, and arsenic, it was shown by Allen, Schofield and Tate (1951), that all the alloys studied gave the same stress–strain curve at the same electron concentration, irrespective of atomic concentration. In interpreting their results the authors suggested that high positive charges on the solute atoms in solution might be the cause of hardening. This interpretation is not quite certain since Meyer (1951) has observed that the product ϵc is fairly constant for the alloys which gave the same stress-strain curve; here c is atomic concentration and $\epsilon=(1/a)(da/dc)_{c=0}$, where a is the lattice constant. He suggests that lattice distortion could be the cause of hardening in these alloys. This does not of course rule out a valency effect since the extra electrons which remain localized to the higher valency atoms in solution may produce a local expansion of the lattice round these atoms.

* Communicated by the Authors.

The purpose of the work described below was to examine the position from a theoretical standpoint ; to see what electrical interaction might be expected between a dislocation and a charged solute atom, and how this would compare with the corresponding elastic interaction. That an edge dislocation in a metal should possess an electric field is to be expected on general grounds, and the view has already been expressed by Mott (private communication) that there should be an electrical interaction with a solute atom. Landauer (1951) has already used the idea of an electrical dipole round an edge dislocation in another connection.

§ 2. Charge Potential Round an Edge Dislocation

Following the usual Wigner–Seitz approximation we write the energy of an electron in a state with a wave number k in an unstrained lattice as

$$E(k)=E_0+\frac{\hbar^2k^2}{2m}, \quad . \quad . \quad . \quad . \quad . \quad . \quad . \quad . \quad (1)$$

where E_0 is the energy of the ground state of the electron. In a homogeneously strained lattice the corresponding expression is

$$E(k)=E_0+E_1\Delta+\frac{\hbar^2k^2}{2m}, \quad . \quad . \quad . \quad . \quad . \quad . \quad . \quad (2)$$

where $(E_0+E_1\Delta)$ is now the energy of the ground state, Δ is the dilatation, and

$$E_1=(\partial E_0/\partial\Delta)_{\Delta=0}. \quad . \quad . \quad . \quad . \quad . \quad . \quad . \quad (3)$$

This distortion changes the wave number at the surface of the Fermi distribution from k_0 to $k_0(1+\Delta)^{-1/3}$. The total energy of the n conduction electrons in the lattice is thus

$$n\left[E_0+E_1\Delta+\frac{3}{5}\frac{\hbar^2k_0^2(1+\Delta)^{-2/3}}{2m}\right]. \quad . \quad . \quad . \quad . \quad . \quad (4)$$

A formula for E_1 is

$$E_1=V(r_0)-E_0, \quad . \quad . \quad . \quad . \quad . \quad . \quad . \quad . \quad (5)$$

where $V(r_0)$ is the value at the boundary of the Wigner–Seitz cell of the periodic lattice potential (Bardeen 1938, Hunter and Nabarro 1953). Numerical values given by Mott and Jones (1936) for $[V(r_0)-E_0]$ are 2·3 ev for silver and 1·3 ev for sodium. For metals where the ion–ion interaction can be neglected, E_1 can be found quite easily from the Fermi energy ; in such cases the equilibrium lattice parameter is determined by the condition that the derivative of the total energy of the conduction electrons with respect to Δ should vanish at $\Delta=0$. Applied to (4) this gives

$$E_1=\frac{2}{5}\frac{\hbar^2k_0^2}{2m}. \quad . \quad . \quad . \quad . \quad . \quad . \quad . \quad . \quad (6)$$

Since the effect of the ion–ion interaction is only to increase the equilibrium spacing a certain amount (about 10% for copper), from the value

at which the energy in (4) is a minimum to a value where the slope of the $E_0(r)$ curve is not greatly altered, the formula in (6) remains a fair approximation to E_1 in cases where the ion–ion interaction is not negligible ; we shall therefore use it in the following estimates.

To deal with the inhomogeneously strained lattice in the field of a dislocation we first regard the crystal as divided up into a number of small pieces, each homogeneously strained to the average value in that part of the field. So far, each piece is electrically neutral. However, the level at the top of the Fermi distribution now differs from one piece to another. To correct this, and make the Fermi surface level everywhere, the electrons redistribute themselves so that there is a shift of charge from piece to piece (Hunter and Nabarro 1953).

Before this charge shift, the energy at the Fermi surface. in a piece where the dilatation is Δ, is

$$E_0+E_1\Delta+\frac{\hbar^2k_0^2}{2m}(1+\Delta)^{-2/3},$$

which to the first order in Δ is

$$E_0+\frac{\hbar^2k_0^2}{2m}+\left(E_1-\frac{2}{3}\frac{\hbar^2k_0^2}{2m}\right)\Delta. \quad . \quad . \quad . \quad . \quad . \quad . \quad (7)$$

The third term here measures the difference between the local level of the Fermi surface and its average value. This difference is removed by the charge shift. Hence the charge potential at this place, due to the rearrangement of the electrons is, substituting for E_1 from (6),

$$\frac{4}{15}\frac{\hbar^2k_0^2}{2m}\Delta, \quad . \quad . \quad . \quad . \quad . \quad . \quad . \quad . \quad . \quad . \quad (8)$$

apart from a constant which measures the average dilatation through the lattice and vanishes for a dislocation in linear elasticity theory. This charge potential is the same as the electrical interaction energy of a unit charged ion placed in this part of the field.

§ 3. Interaction with a Solute Atom

For an edge dislocation the shift of electrons is towards the expanded side of the dislocation field, and away from the half-plane. The dilatation is greatest in the region within one atomic spacing of the edge of the half-plane, and its value here is about $1/8$. Hence the electrical contribution to the binding energy of a solute atom and a dislocation is of order

$$\frac{1}{30}\frac{\hbar^2k_0^2}{2m}, \quad . \quad . \quad . \quad . \quad . \quad . \quad . \quad . \quad . \quad . \quad (9)$$

per electronic unit of charge on the atom. For a unit charged ion in copper this is about $\frac{1}{4}$ ev.

According to the calculations of Mott (1936, 1937), the effective charge on a z-valent ion in copper is about $0{\cdot}075\ (z-1)$ unit electronic charges.

We shall use this result, although it may be seriously in error when the ion is in a heavily strained region of the lattice, such as exists at the centre of a dislocation. The electrical binding energy of the ion with an edge dislocation should thus be about $0{\cdot}02\ (z-1)$ ev ; that is, about 0·02, 0·04, 0·06, and 0·08 ev respectively, for zinc, gallium, germanium, and arsenic, in copper. The corresponding elastic binding energy, from the formula of Cottrell (1948), is as follows :

	Zn	Ga	Ge	As
ϵ	0·062	0·078	0·090	0·130
Elastic binding energy, in ev	0·125	0·163	0·188	0·272

Here ϵ has been calculated from the lattice parameter measurements of Hume-Rothery, Lewin and Reynolds (1936), and Owen (1947).

The elastic binding energy is thus some 3 to 6 times greater than the electrical one in these copper-based alloys. It appears that in these alloys the role of the electrical interaction is secondary to that of the elastic interaction. Its importance in other alloys cannot be ascertained until more is known of the effective charges on solute atoms in them.

Acknowledgements

This study was made in the Department of Theoretical Metallurgy, University of Birmingham, under the general direction of the late Professor D. Hanson, during the period in which one of us (S.C.H.) held a maintenance grant from the Department of Scientific and Industrial Research.

References

Allen, N. P., Schofield, T. H., and Tate, A. E. L., 1951, *Nature, Lond.*, **168,** 378.

Bardeen, J., 1938, *J. Chem. Phys.*, **6,** 372.

Cottrell, A. H., 1948, *Report on Strength of Solids* (London : Physical Society), p. 30.

Dorn, J. E., Pietrokowsky, P., and Tietz, T. E., 1950, *Trans. Amer. Inst. Min. Met. Eng.*, **188,** 933.

Hume-Rothery, W., Lewin, G. F., and Reynolds, P. W., 1936, *Proc. Roy. Soc.* A, **157,** 167.

Hunter, S. C., and Nabarro, F. R. N., 1953. To be published.

Landauer, R., 1951, *Phys. Rev.*, **82,** 520.

Meyer, M. A., 1951, *Some Aspects of the Hardness of Metals* (Delft : Laboratorium voor Technische Physica).

Mott, N. F., 1936, *Proc. Camb. Phil. Soc.*, **32,** 281 ; 1937, *Proc. Phys. Soc.*, **49,** 258.

Mott, N. F., and Jones, H., 1936, *Theory of the Properties of Metals and Alloys* (Oxford : Clarendon Press), p. 264.

Owen, E. A., 1947, *J. Inst. Metals*, **73,** 471.

CXII. *On the Analysis of τ-Meson Data and the Nature of the τ-Meson*

By R. H. Dalitz
Department of Mathematical Physics, University of Birmingham*

[Received July 1, 1953]

Abstract

A convenient method of representation is proposed (§ 2) for data on τ-meson decay configurations, applicable when the unlike outgoing π-meson is not distinguished. The relation between the spin and parity of the τ-meson and the distribution of decay configurations is obtained for some simple cases. The hypothesis that the τ- and χ-mesons are identical requires a non-zero spin for this particle and the available data on τ-meson decay does not exclude this possibility. However, observations in which the unlike outgoing π-meson is not distinguished are relatively ineffective in discriminating between the various possibilities. The distortions which strong meson–meson attraction may produce in τ-decay configurations are discussed ; the present data offers no evidence on this effect.

§ 1. Introduction

The existence of a τ-meson whose mass is $978 \pm 6\, m_e$ and which decays into three π-mesons is now well established (Brown *et al.* 1949). Although mass measurements on the outgoing particles in high energy cosmic ray stars suggest (Daniel and Perkins 1953) that only a small proportion ($<20\%$) of the heavy mesons produced could possibly be τ-mesons, the number of τ-decay events observed in photographic emulsions has become quite considerable, presumably because of the very characteristic τ-decay pattern. About fourteen clear examples of the process $\tau^{\pm} \rightarrow \pi^{\pm} + \pi^{+} + \pi^{-}$ are now available. In each event the angles between the outgoing meson tracks, and also the individual meson energies, have been measured, but it is not known which track is produced by the meson whose charge is opposite to that of the τ-meson (we shall generally refer to this π-meson as the ' unlike ' meson). In § 4, it will be seen that the frequency distribution predicted for the decay configuration depends rather less sensitively on the nature of the τ-meson when this additional information is lacking ; however, since such a complete identification of the decay process may well not be generally possible until τ-mesons may be artificially produced, it seems worthwhile to present an analysis appropriate to the data available at the present stage and to discuss what one may hope to learn concerning the τ- and π-mesons when more

* Communicated by Professor R. E. Peierls.

events have been observed. The τ-meson properties of first interest are those related to the conservation laws of physics, the mass, charge, intrinsic spin, parity and (possibly) isotopic spin. The charge of the τ-meson is known to have magnitude $|e|$ and the experimental data on its mass has recently been discussed by Rochester and Butler (1953). Concerning the isotopic spin properties, one type of observation which could lead to some information has been discussed recently (Dalitz 1953). A phenomenological description of the decay for assumed spin and parity may also allow the determination of other parameters relevant to the τ-meson, which may provide guidance in a more detailed theory of the τ-meson. The existence of any strong interactions between the outgoing π-mesons would be expected to influence the decay configuration considerably (Brueckner and Watson 1952), so that a study of the decay events may also provide some evidence concerning the meson–meson interaction.

§2. The Specification and Analysis of τ-Meson Decay Events

In the decay of a τ-meson at rest, the three outgoing π-mesons have zero total momentum and a total kinetic energy of $E=(m_\tau-3m_\pi)c^2$, so that, apart from the spatial orientation, the specification of the decay configuration requires two parameters. A convenient choice would be the energy of the unlike meson and the magnitude of the difference between the energies of the like mesons. However, it is not possible to distinguish between the outgoing mesons in the present data, so that a choice of parameters which is symmetrical between the three π-mesons is more appropriate. Denoting the total kinetic energy of the π-mesons by E and the individual kinetic energies by ϵ_1, ϵ_2, ϵ_3, define

$$\alpha_i=\epsilon_i-E/3 \quad (i=1, 2, 3). \qquad (2.1)$$

These α_i then have zero sum, thus $\Sigma_i\alpha_i=0$. If E and the α_i are known, the decay configuration is specified. If the unlike meson is unidentified, two symmetrical functions,

$$Y=-(\alpha_1\alpha_2+\alpha_2\alpha_3+\alpha_3\alpha_1)=-\Sigma\alpha_1\alpha_2, \quad Z=\alpha_1\alpha_2\alpha_3, \qquad (2.2)$$

may conveniently be used to specify the configuration uniquely, since, for given (Y, Z) the α_1, α_2, α_3 are the three roots of the cubic equation

$$\alpha^3-Y\alpha-Z=0. \qquad (2.3)$$

Y and Z are limited firstly by the condition that (2.3) has three real solutions, which requires that $Z^2\leqslant 4Y^3/27$, and secondly by the requirement that the outgoing mesons have total momentum zero. A necessary and sufficient condition that the momenta p_1, p_2, p_3 satisfy the triangular inequalities $p_1+p_2\geqslant p_3$, $p_2+p_3\geqslant p_1$, $p_3+p_1\geqslant p_2$, which are necessary and sufficient to allow a choice of $\mathbf{p}_1$, $\mathbf{p}_2$, $\mathbf{p}_3$ satisfying $\mathbf{p}_1+\mathbf{p}_2+\mathbf{p}_3=0$, is that

$$(p_1+p_2+p_3)(p_1+p_2-p_3)(p_1-p_2+p_3)(p_1+p_2-p_3)=16m_\pi{}^2\left(\frac{E^2}{12}-Y\right)\geqslant 0.$$

so that Y, Z are limited by the inequalities

$$Y \leqslant E^2/12 \text{ and } Z \leqslant \sqrt{(4Y^3/27)} \leqslant E^3/108. \quad . \quad . \quad . \quad . \quad (2.4)$$

As the uncertainty in the measurement of individual meson energies is often quite large, it will be more appropriate to use the ratios of the meson energies, which may be deduced from the more accurately known angles between the meson tracks. Accordingly, co-ordinates (λ, θ) which are functions of these ratios, may be defined by

$$Y = \lambda E^2/12,\ Z = \lambda^{3/2} \sin\theta\ E^3/108 = \eta E^3/108, \quad . \quad . \quad . \quad (2.5)$$

where it is convenient to define the quantity $\eta = \lambda^{3/2} \sin\theta$. The inequalities (2.4) then correspond to $0 \leqslant \lambda \leqslant 1$ and $-\pi/2 \leqslant \theta \leqslant \pi/2$.

The kinetic energy of an outgoing π-meson cannot exceed $2E/3$, which is close to 50 Mev since the experimental data gives $E = 76{\cdot}5 \pm 3$ Mev. Consequently it is reasonable to adopt a non-relativistic description, since the resulting errors are at most a few per cent, small compared with other uncertainties in the data. The expression for the energy distribution of the three π-mesons may be written in the general form

$$F(\epsilon_1, \epsilon_2, \epsilon_3)\delta(\epsilon_1+\epsilon_2+\epsilon_3-E)\delta(\mathbf{p}_1+\mathbf{p}_2+\mathbf{p}_3)d^3p_1\, d^3p_2\, d^3p_3,$$

where $F(\epsilon_1, \epsilon_2, \epsilon_3) = F(\epsilon_2, \epsilon_1, \epsilon_3)$ since the like mesons (1, 2) are indistinguishable. Non-relativistically this may be reduced to

$$8\pi^2 m_\pi{}^2 F(\epsilon_1, \epsilon_2, \epsilon_3)\delta(\epsilon_1+\epsilon_2+\epsilon_3-E)\, d\epsilon_1\, d\epsilon_2\, d\epsilon_3.$$

If the unlike particle cannot be identified the same configuration may occur in three ways and the total frequency is then the sum of the three separate frequencies, thus

$$[8\pi^2 m_\pi{}^2(F(\epsilon_1, \epsilon_2, \epsilon_3)+F(\epsilon_2, \epsilon_3, \epsilon_1) + F(\epsilon_3, \epsilon_1, \epsilon_2))]\, \delta(\epsilon_1+\epsilon_2+\epsilon_3-E)\, d\epsilon_1\, d\epsilon_2\, d\epsilon_3. \quad . \quad . \quad . \quad (2.6)$$

The function within the square brackets is a symmetrical function of $\epsilon_1, \epsilon_2, \epsilon_3$ and thus of $\alpha_1, \alpha_2, \alpha_3$, so that it may be expressed as a function of E and of Y, Z and hence of λ, θ, say $\phi(\lambda, \theta) \equiv \Phi(\lambda, \eta)$. If we write $\zeta = \alpha_1+\alpha_2+\alpha_3$, then (2.6) may be written as

$$\phi(\lambda, \theta)\delta(\zeta)\, d\alpha_1\, d\alpha_2\, d\alpha_3 = \phi(\lambda, \theta)\, \delta(\zeta)\, \frac{\partial(\alpha_1, \alpha_2, \alpha_3)}{\partial(\zeta, \lambda, \eta)}\, d\zeta\, d\lambda\, d\eta. \quad . \quad . \quad . \quad (2.7)$$

The ratio of the volume elements $d\alpha_1\, d\alpha_2\, d\alpha_3$ and $d\zeta\, d\lambda\, d\eta$, namely $\partial(\alpha_1, \alpha_2, \alpha_3)/\partial(\zeta, \lambda, \eta)$, is equal to the magnitude of

$$(\alpha_1-\alpha_2)(\alpha_2-\alpha_3)(\alpha_3-\alpha_1)1296/E^5,$$

which equals $\sqrt{(4Y^3-27Z^2)}\ 1296/E^5 = 36\sqrt{3}\lambda^{3/2} \cos\theta/E^2$. Integrating over ζ, (2.7) becomes, apart from some numerical factors,

$$\phi(\lambda, \theta)\, d\lambda\, d\theta. \quad . \quad . \quad . \quad . \quad . \quad . \quad . \quad . \quad (2.8)$$

The following considerations lead to a very convenient realization of the co-ordinates defined above. For an equilateral triangle YUV (see fig. 1), the sum PL+PM+PN of the perpendiculars to the sides from any point P within the triangle equals the altitude of the triangle. Hence

a decay event may be uniquely specified by a point P such that the perpendiculars (PL, PM, PN) are proportional to the meson energies (ϵ_1, ϵ_2, ϵ_3). Interchange of two of these energies corresponds to the reflection of P in a corresponding altitude of the triangle so that, corresponding to the incomplete identification of the mesons, the event is represented a point in each of the six sub-triangles of YUV. The distribution in any sub-triangle is obtainable from that in AOV by successive reflections in the altitudes, so that one need consider only that ordering of the meson energies for which P lies within AOV. The Cartesian co-ordinates (x, y) with respect to the axes OX, OY are given by

$$x=\sqrt{3}(\epsilon_1-\epsilon_2)/E,\quad y=(2\epsilon_3-\epsilon_1-\epsilon_2)/E,$$

where the altitude of the triangle has been taken as 3 units. It may now be readily verified that the polar co-ordinates (r, ϕ) of P are ($\lambda^{1/2}$, $-\theta/3$). The points representing decay events are therefore confined

Fig. 1

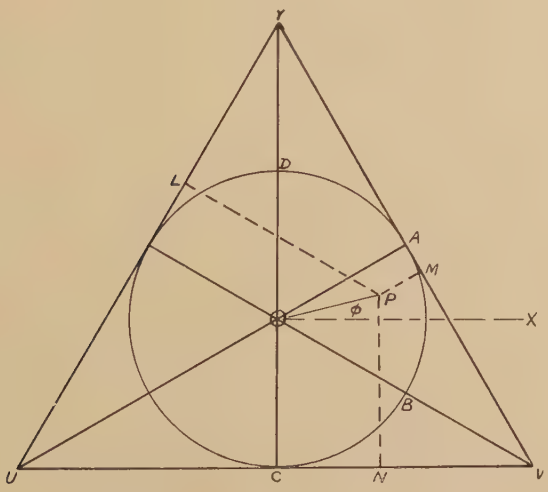

to the interior of the circle inscribed to the triangle YUV, since momentum conservation requires $\lambda \leqslant 1$. In plotting decay events on this diagram, the momenta have been calculated from the observed angles between the meson tracks, and the energy ratios from the squares of these momenta, so that the representation expresses angular relations in the decay and is not modified by relativistic effects. When the co-ordinates are given, the corresponding configuration of the decay process may be quickly obtained by reference to this diagram.

If the function $\phi(\lambda, \theta)$ is independent of λ, θ which is the case, for example, when F is independent of ϵ_1, ϵ_2, ϵ_3, the experimental points should be distributed randomly over the area AOB, since the element of area is $r\,dr\,d\phi = d\lambda\,d\theta/6$. The limited data available is displayed in fig. 2 and although there appears to be some tendency to favour the

upper and outer part of AOB the distribution obtained is not yet significantly different from a random distribution. The corner A corresponds to decay events in which one π-meson is rather slow and a tendency to favour this corner may perhaps result from some initial experimental bias favouring detection of this particular decay configuration. The distribution to be expected according to various hypotheses will be obtained in § 4, where it will be shown that the present statistics are insufficient to allow discrimination between the alternatives considered.

Fig. 2

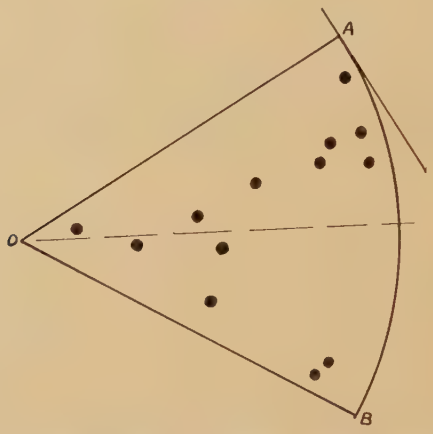

The data from 13 τ-meson decay events.

§ 3. Considerations on the Nature of the τ-Meson

The questions of most direct interest concerning the τ-meson relate to its intrinsic spin, its parity and to the applicability of the notion of isotopic spin. If the τ-meson is some kind of meson–nucleon complex occurring in consequence of the interaction between the meson and nucleon fields, it would follow that the τ-meson would have a definite isotopic spin, if charge independence be established for the meson–nucleon interaction. If the τ-meson needs specification by some new field coupled directly to the meson and nucleon fields, these interactions may still satisfy charge independence and the τ-meson may still have a definite isotopic spin. Some evidence concerning the applicability of isotopic spin to the τ-meson may be obtainable from the study of the branching ratio for the decay processes $\tau^{\pm} \rightarrow \pi^{\pm} + \pi^{+} + \pi^{-}$ and $\tau^{\pm} \rightarrow \pi^{\pm} + \pi^{0} + \pi^{0}$, as discussed earlier (Dalitz 1953). At the present, there is certainly no evidence requiring that the τ-meson should satisfy charge independence: nevertheless, in this and the following section, we shall indicate what additional consequences would follow if this notion were applicable.

The configuration of the three mesons resulting from τ-meson decay will depend on the spin j and parity w of the τ-meson. The configuration is completely specified by the momenta $\mathbf{p}_1$, $\mathbf{p}_2$ of the like particles and

the matrix element for decay to this configuration must be an irreducible tensor of rank j and parity $(-1)^3 w$, formed from $\mathbf{p}_1$, $\mathbf{p}_2$ and symmetrical for interchange of the suffices 1, 2, since the π-meson satisfies Bose statistics. If $w=-(-1)^j$ such a tensor is easily found (e.g. $Y_m{}^j(\mathbf{p}_1)+Y_m{}^j(\mathbf{p}_2)$) so that the decay is then not forbidden by angular momentum and parity conservation. If $w=+(-1)^j$, then for every j except $j=0$, such a tensor may be formed, for example, by multiplying the tensor just formed for $(j-1,\ w'=-(-1)^{j-1})$ by the pseudovector $\mathbf{p}_1\ \mathbf{p}_2(p_1{}^2-p_2{}^2)$ and extracting the irreducible tensor of rank j from the product. For $j=0$, however, we are required to form a pseudoscalar from the vectors $\mathbf{p}_1$, $\mathbf{p}_2$, which is not possible. The 3 π-decay, therefore, is forbidden by angular momentum and parity conservation only for a scalar heavy meson.

The selection rules for decay of a heavy meson into (*a*) two π-mesons or (*b*) one π-meson and a photon, which are allowed as far as energy and momentum conservation are concerned, are well known. For case (*a*), they may be simply obtained by noting that, since the final state is specified by the relative momentum $\mathbf{p}$ of the mesons, the matrix element for decay of a particle of spin j must be given by $Y_m{}^j(\mathbf{p})$. Since this tensor has parity $(-1)^j$, the 2π-decay is therefore forbidden by angular momentum and parity conservation for $w=-(-1)^j$. If isotopic spin is a good quantum number, then since interchange of the mesons corresponds to $\mathbf{p}\rightarrow-\mathbf{p}$ and the mesons satisfy Bose statistics, the 2π-decay is allowed only for even or odd j according as the isotopic spin is even or odd. For states with even j and odd isotopic spin, the 2 π-decay may still proceed unfavourably through electromagnetic interactions which violate charge independence, though one might then expect that the decay $\tau^{\pm}\rightarrow\pi^{\pm}+\pi^0+\gamma$ would be more probable. For case (*b*), the final state is specified by the relative momentum $\mathbf{p}$ and the photon polarization vector $\mathbf{e}$ which satisfy $\mathbf{e}\cdot\mathbf{p}=0$ since the photon is a transverse wave, and the matrix element for the decay to this state must be a linear function of $\mathbf{e}$. For every j (except $j=0$) such a matrix element may be formed for parity $w=(-1)^j$ or $-(-1)^j$ by multiplying $Y_m{}^{j-1}(\mathbf{p})$ by $\mathbf{e}\times\mathbf{p}$ or $\mathbf{e}$ respectively and extracting the irreducible tensor of rank j. However, no non-zero scalar or pseudoscalar can be formed, so that angular momentum conservation forbids (π, γ) decay for a heavy meson of spin $j=0$. In view of the number of 3 π-decay events observed, it has been natural to suppose that the τ-meson is pseudoscalar, since the 3 π-decay would then be the only allowed decay process involving π-mesons alone and other decay processes involving photons (e.g. $\tau^{\pm}\rightarrow\pi^{\pm}+\pi^0+\gamma$) might well be less probable.

Recently, however, a number of events described as χ-meson decay have been found from which a charged π-meson of unique energy 110 Mev results (Menon and O'Ceallaigh 1953). If it is supposed that the neutral particle produced in this decay is a π^0-meson, these events may be interpreted as the decay of a particle of mass about 980 m_e. Also the analysis of V^0-particle decay (Armenteros *et al.* 1951, Barker 1953,

Thompson *et al.* 1953) strongly suggests that there exists a V_2^0-meson which decays into two π-mesons with a Q-value corresponding to a V_2^0 mass of 962 m_e. It is very plausible that this V_2^0 meson is the neutral counterpart of the χ-meson and an attractively simple representation of the data is offered by the further hypothesis (Menon and O'Ceallaigh 1953) that the τ- and χ-mesons are identical, the events observed representing two alternative decay schemes of the (τ, χ) particle. In this case the (τ, χ) particle could not have spin $j=0$ but must be a particle of parity $(-1)^j$ if its spin is $j(\geqslant 1)$—if isotopic spin is rigorously applicable, j is restricted to odd values. On the other hand, the hypothesis that the neutral particle in χ-decay is a photon is still compatible with the hypothesis of a (τ, χ) particle and also requires that this particle have $j \neq 0$. If the parity of this particle is $(-1)^j$, then both 2π- and (π, χ)-decay may compete with 3π-decay, although, for j even, the 2π-decay will be relatively unfavoured if charge independence is a good approximation. If the parity is $-(-1)^j$, the χ-decay would have to be (π, γ)-decay. The hypothesis that the τ-meson is a particle of spin 1 is therefore of particular interest, and if the hypothesis $\chi \equiv \tau$ is to be maintained, we must examine whether the consequences for the 3π-decay pattern are then in agreement with the data.

§ 4. Discussion of Some Particular Hypotheses

The decay of the τ-meson into the π-meson states of momenta $\mathbf{p}_1, \mathbf{p}_2, \mathbf{p}_3$ (in this and the next section, the suffix 3 will refer to the unlike meson) will be described by a matrix element $M(\mathbf{p}_1, \mathbf{p}_2, \mathbf{p}_3)$. Corresponding to the analysis of the final state into partial waves of definite angular momentum, this matrix element may be written as the sum of a number of terms of definite form with coefficients depending on the energies of the mesons. It will be assumed that only low angular momenta are important and that these coefficients may be expanded in powers of the meson energies. This supposes the region of production to be small compared with the meson wavelengths and neglects the effects of any strong interactions between the mesons after the decay. These effects will be discussed briefly in § 5, following the viewpoint of Brueckner and Watson (1951) that the main features of these interaction effects will not depend on the details of the production process.

(1) *The Hypothesis of a Pseudoscalar τ-Meson*

Since there is no change in intrinsic parity, $M(\mathbf{p}_1, \mathbf{p}_2, \mathbf{p}_3)$ is a scalar whose general form is

$$M(\mathbf{p}_1, \mathbf{p}_2, \mathbf{p}_3) = M_0(p_1, p_2, p_3) + \Sigma \mathbf{p}_1 \cdot \mathbf{p}_2 M_3'(p_1, p_2, p_3) + \Sigma(\mathbf{p}_1 \cdot \mathbf{p}_3 \mathbf{p}_2 \cdot \mathbf{p}_3 - \tfrac{1}{3}\mathbf{p}_1 \cdot \mathbf{p}_2 \mathbf{p}_3^2) M_3''(p_1, p_2, p_3) + \ldots . \quad (4.1)$$

of which the successive terms describe the emission of s-wave mesons, of one s-wave and two p-wave mesons, and of one d-wave and two p-wave mesons respectively. The summations are over all permutations of (123)

and $M(\mathbf{p}_1, \mathbf{p}_2 : \mathbf{p}_3)$ is required to be symmetric for interchange of (12), because of the Bose statistics. By expanding the scalar coefficients in powers of p_1^2, p_2^2, p_3^2, making use of the energy conservation relation $(p_1^2+p_2^2+p_3^2)=2m_\pi E$, momentum balance $\mathbf{p}_1+\mathbf{p}_2+\mathbf{p}_3=0$ and the symmetry of M, (4.1) may be reduced to the form

$$M=A+a\alpha_3+b\alpha_1\alpha_2+c\alpha_3^2+ \quad . \quad . \quad . \quad . \quad . \quad (4.2)$$

A, a, b, c being constants and α_1, α_2, α_3 being defined by (2.1). In (4.2), A contains contributions from all partial waves, a arises from the energy dependence of the s-waves and from $s-p$ interference, b and c from the p-waves alone or from higher effects, and so on. The function of interest is $\phi(\lambda, \theta)$ which is proportional to

$$\Sigma(AA^*+\alpha_3 2\mathscr{R}(aA^*)+\alpha_3^2(aa^*+2\mathscr{R}(cA^*))+2\alpha_1\alpha_2\mathscr{R}(bA^*))$$
$$=3AA^*+\lambda(2aa^*+2\mathscr{R}(2cA^*-bA^*))E^2/12+. \quad . \quad . \quad . \quad . \quad (4.3)$$

Although the term a in (4.2) allows a considerable range of variation in the energy distribution of the unlike meson, the cross terms between a and A vanish in the symmetrized function $\phi(\lambda, \theta)$ whose (λ, θ) dependence arises from higher order terms. The fact that the unlike meson cannot be identified leads here to an insensitive dependence of the observable phenomena on the details of the theory. Consequently, apart from meson–meson interaction effects, the decay may be expected to be isotropic. Also, if a is negligible, the orbital state of the outgoing mesons is totally symmetric (of the representation [3]) which implies a branching ratio of $\frac{1}{4}$ for the τ-decay involving neutral mesons if isotopic spin is a good quantum number (Dalitz 1953). The term a, and possibly the effects of meson–meson interactions, will lead to an admixture of [21] orbital symmetry which would increase this branching ratio.

(2) *The Hypothesis of a Vector τ-Meson*

The matrix element must be a pseudovector and, including the possibilities up to a final (p^2d) or (sd^2) configuration, its form is uniquely

$$M(\mathbf{p}_1, \mathbf{p}_2, \mathbf{p}_3)=B\mathbf{p}_1\times\mathbf{p}_2(p_1^2-p_2^2). \quad . \quad . \quad . \quad . \quad (4.4)$$

Averaging over the orientations of the initial τ-meson then leads to

$$F(\epsilon_1, \epsilon_2 ; \epsilon_3)=4m_\pi^4B^2(\epsilon_1-\epsilon_2)^2[\epsilon_3(2E-3\epsilon_3)-(\epsilon_1-\epsilon_2)^2]/3, \quad . \quad (4.5)$$

which corresponds to a distribution function

$$\phi(\lambda, \theta)\sim\lambda(1-\lambda). \quad . \quad . \quad . \quad . \quad . \quad . \quad . \quad . \quad (4.6)$$

Since the matrix element (4.4) is zero if two of the π-mesons have parallel paths or if the like mesons have equal energies, it may be easily understood why the centre and edge of the circle in fig. 1 are unfavoured. The matrix element (4.4) leads to a final state of orbital symmetry [21] which corresponds to equal probability for the two modes of 3π-decay for the τ-meson if the notion of isotopic spin is applicable. In this case, since the only decay observed with certainty to yield a single charged

π-meson is the χ-decay, the hypothesis of (τ, χ) identity would be compatible only if this decay is the predominant mode of decay for the particle.

(3) *The Hypothesis of a Pseudovector τ-Meson*

The matrix element must be a vector. The simplest decay is emission of two s-wave and one p-wave particle for which $M(\mathbf{p}_1, \mathbf{p}_2 ; \mathbf{p}_3)$ is proportional to $\mathbf{p}_3$, giving

$$F(\epsilon_1, \epsilon_2 ; \epsilon_3)=C\epsilon_3, \quad . \quad . \quad . \quad . \quad . \quad . \quad . \quad . \quad (4.7)$$

so that the distribution function is the constant

$$\phi(\lambda, \theta)=8\pi^2 m_\pi{}^2 CE. \quad . \quad . \quad . \quad . \quad . \quad . \quad . \quad . \quad (4.8)$$

This matrix element leads to a final state of orbital symmetry [21], its symmetric part $\frac{1}{3}(\mathbf{p}_1+\mathbf{p}_2+\mathbf{p}_3)$ being zero owing to momentum conservation. Remarks similar to those at the end of the last paragraph apply also to this case except that here the χ-decay must be of the (π, γ) type.

(4) *Higher Spin Values*

For spin j, even the simplest forms for M rapidly increase in number with j, so that the predicted distributions offer a considerable range of possibilities. For the cases $2+$, $3-$, however, the simplest M is unique and leads to the expressions $(1-\lambda)$ and $(1-\lambda)(1-\frac{1}{5}\lambda)$ for the function ϕ, respectively.

For cases (1), (2) and (3) the energy distribution of the unlike meson is plotted in fig. 3. To emphasize the loss of sensitivity resulting from the incomplete identification of the decay, the energy distributions predicted* for the slowest and fastest meson and for all mesons, irrespective of charge, are plotted in fig. 4 and compared with the available data. This effect is particularly marked in the pseudovector case, where the distributions of fig. 4 agree with those for the pseudoscalar case, despite the marked difference in the distribution for the unlike meson. The data available at present are clearly inadequate to discriminate between the various possibilities discussed here.

---

* Given the function $\Phi(\lambda, \eta)$, the energy distribution of all particles is given by

$$P(\epsilon)=\int_0^{\sqrt{(1-y^2)}} \Phi(x^2+y^2, y(y^2-3x^2))\, dx,$$

where $y=(3\epsilon-E)/E$. The distribution $Q_s(\epsilon)$ of the slowest particle is given by $Q_s(\epsilon)=P(\epsilon)$ for $\epsilon<E/6$, since ϵ is then necessarily the slowest particle, whereas for $E/6<\epsilon<E/3$,

$$Q_s(\epsilon)=\int_0^{-y\sqrt{3}} \Phi(x^2+y^2, y(y^2-3x^2))\, dx,$$

corresponding to integration over the sector OCB of fig. 1. The distribution $Q_f(\epsilon)$ of the fastest particle is given by $Q_f(\epsilon)=P(\epsilon)$ for $\epsilon>E/2$, whereas for $E/3<\epsilon<E/2$, $Q_f(\epsilon)$ is found by integrating Φ from 0 to $+y\sqrt{3}$. Q_f and Q_s differ in form only in virtue of any η-dependence of Φ.

§ 5. Some Possible Meson–Meson Interaction Effects

In the emission of π-mesons in cosmic ray stars, a marked correlation in the directions and energies of pairs of π-mesons has been found by Danysz, Lock and Yekutieli (1952), who tentatively suggested that these meson pairs may result from the decay of a short lived ζ^0-meson (see

Fig. 3

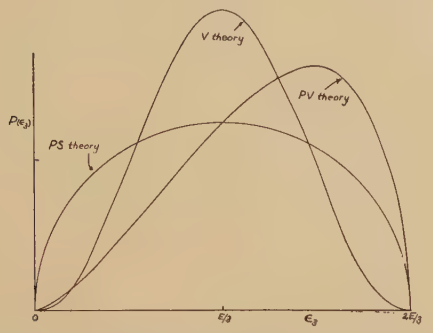

The energy distribution of the unlike π-meson in τ-meson decay for several τ-meson spin values.

Fig. 4

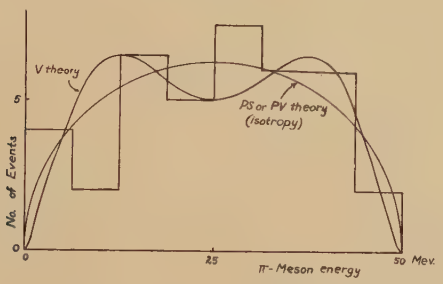

(*a*)

Energy distribution for all π-mesons from τ-meson decay: comparison with histogram for 13 events.

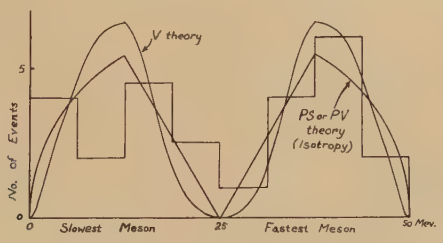

(*b*)

Energy distribution of the slowest and fastest π-meson in τ-meson decay. Experimental histogram based on 13 events.

also Danysz *et al.* 1953). However, Brueckner and Watson (1952) have remarked that the existence of a strong attractive interaction between π-mesons could provide an alternative explanation for these correlations and have pointed out that, in any case, the study of correlation effects near the threshold for multiple meson production would provide quantitative evidence on the nature of the meson–meson interaction. A similar point of view has already lead to some information on the neutron–neutron interaction (Watson and Stuart 1951) from the distortion of the γ-ray spectrum emitted in the capture of π^--mesons by deuterium due to the neutron–neutron correlations resulting from their interaction.

In τ-meson decay, three π-mesons are produced with low kinetic energy and the existence of strong attractive meson–meson interactions might be expected to distort the distribution of decay patterns in a characteristic way. The kinetic energy of the relative motion of two mesons (1 and 2, say) is given by

$$\Delta=(\mathbf{p}_1-\mathbf{p}_2)^2/4M=E-3\epsilon_3/2,$$

so that, since the interaction is most effective between mesons of low relative momentum, this effect would favour a configuration in which the third meson has energy near to the maximum $2E/3$. The corresponding angle between the paths of the interacting mesons is about $\sqrt{(3\Delta)}/5$, or less, i.e. about 30° for $\Delta\sim 2$ Mev (a value for Δ which is typical of the cosmic ray data at very much higher total energies). The parameters (λ, θ) of these configurations have values close to $\lambda=1$, $\theta=\pi/2$, so that the distribution of the decay events would then crowd towards the corner B of fig. 1.

Following the discussion of Watson (1951), the matrix element leading to a state in which two mesons have small relative momentum k has a k-dependence essentially given by a factor $(\sin\delta)/k$, when it is supposed that meson–meson scattering is strong for small k in only one partial wave (assumed here, for simplicity, to be the s-wave) of phase-shift δ. If, to illustrate the effects quantitatively, it is supposed that the basic process is otherwise isotropic and that only unlike mesons attract strongly, the matrix element is essentially $C(\sin\delta_{13}/k_{13})(\sin\delta_{23}/k_{23})$, and

$$F(\epsilon_1, \epsilon_2\,;\,\epsilon_3)=C^2/(\alpha^2+(\mathbf{p}_1-\mathbf{p}_3)^2)(\alpha^2+(\mathbf{p}_2-\mathbf{p}_3)^2), \quad . \quad . \quad (5.1)$$

if it is supposed further that $k\cot\delta=-\alpha=-h/a$, a being the zero-energy scattering length. With $\mu=\alpha^2/2ME$, the corresponding symmetrized function is then

$$\phi(\lambda,\theta)=C^2(1+\mu)/M^2E^2(\mu(3+2\mu)^2+3(1+\mu)(1-\lambda)+(1-\lambda^{3/2}\sin\theta))$$
$$\simeq C^2/M^2E^2(9\mu+3(1-\lambda)+1-\lambda^{3/2}\sin\theta), \quad . \quad . \quad . \quad (5.2)$$

since the values of μ of interest are small. If the interaction effect is strong for relative energies of up to $\sim\Delta$, then $\mu\sim 2\Delta/E$, which is 0·05 for $\Delta=2$ Mev. The expression (5.2) will not be a good approximation for points not close to B since both k_{13} and k_{23} will then be large and the

approximations leading to (5.1) are not valid. Even for a point close to B, one of the three corresponding configurations will have both k_{13} and k_{23} large, but the error thus made will be small compared with the large increase in the probability of the other two configurations. Hence if the τ-meson is pseudoscalar and there is an attractive interaction between mesons comparable with that necessary to explain the correlations in cosmic ray stars, a considerable fraction of the τ-decay events should lie quite close to B. The present data (fig. 2) shows no evidence for any very strong effect of this kind.

The vector meson deserves separate consideration since its matrix element favours configurations in which the relative momentum of each meson pair is high. For this case,

$$\left.\begin{aligned} F(\epsilon_1, \epsilon_2 ; \epsilon_3) &= \frac{[\epsilon_3(2E-3\epsilon_3)-(\epsilon_1-\epsilon_2)^2](\epsilon_1-\epsilon_2)^2}{\left(\frac{\alpha^2}{2M}+2E-3\epsilon_1\right)\left(\frac{\alpha^2}{2M}+2E-3\epsilon_2\right)}, \\ \phi(\lambda,\theta) &= 4(1-\lambda)(\lambda+\tfrac{1}{2}\eta)/(9\mu+3(1-\lambda)+(1-\eta)), \end{aligned}\right\} . \quad (5.3)$$

assuming μ is small. This expression remains bounded as $\mu \to 0$; though the meson–meson interaction increases the probability of an event near to B, the effect does not crowd a high proportion of events into this corner. Away from this corner, (5.3) shows a considerable θ-dependence, which depends, however, on the incorrect assumptions underlying (5.1) when k_{13}, k_{23} are large ; a genuine θ-dependence will, of course, occur near the outer edge of AOB. The present limited data of τ-meson decay does not conflict with the hypothesis of a strong meson–meson attraction in the case of a vector τ-meson (or of a (2+) or (3−) τ-meson). It should finally be noted that in all cases, the upper half of the region AOB should suffer very little distortion as a result of this interaction effect.

§ 6. Conclusions

The data available at present on the decay of the τ-meson offers no significant evidence for any lack of isotropy in the decay process nor for any distortion of the decay patterns as would be characteristic of a strong attraction between π-mesons. On the other hand, the data does not at present exclude the possibility that the τ-meson is a vector particle, in which case the absence of evidence for any correlations characteristic of strong π–π attraction would not be significant, their effect not being particularly marked in the vector theory. However, theories giving quite different matrix elements have been found to lead finally to very similar results, so that a comparison with the evidence would not be sensitive to the τ-meson spin and parity. This insensitivity results from the need for averaging over three mesons whose energies are limited by energy and momentum conservation—a knowledge of the energy distributions for the unlike meson alone would provide a more sensitive indication of the meson spin. In this respect, the τ-meson decay contrasts

sharply with the decay event $\mu \rightarrow e + 2\nu$ in which less quantitative data is available from each event but in which the electron spectrum has a fair dependence on quite detailed μ-meson properties. If it should prove possible to analyse τ-meson decay events in more detail (e.g. if the τ-mesons which decay were all of positive charge, as is conceivable, identification of the π^--meson in each event would suffice) a more direct comparison with the functions $F(\epsilon_1, \epsilon_2 ; \epsilon_3)$ will become possible and a more sensitive analysis of the data be feasible. At that stage a more detailed study of these functions will be justified.

In conclusion, I am pleased to thank Dr. E. P. George, Dr. P. Hodgson, Dr. M. G. K. Menon and particularly Dr. W. O. Lock for information concerning the experimental data on τ-mesons and to thank Professor R. E. Peierls for his encouragement and advice during this study.

References

Armenteros, R., Barker, K. H., Butler, C. C., Cachon, A., and Chapman, A. H., 1951, *Nature, Lond.*, **167,** 501.

Barker, K. H., 1953, *Proc. Roy. Soc.* A, in press.

Brown, R., Camerini, U., Fowler, P. H., Muirhead, H., Powell, C. F., and Ritson, D. M., 1949, *Nature, Lond.*, **163,** 82.

Brueckner, K. A., and Watson, K. M., 1952, *Phys. Rev.*, **87,** 621.

Dalitz, R. H., 1953, *Proc. Phys. Soc.*, in press.

Daniel, R. R., Davies, J. H., Mulvey, J. H., and Perkins, D. H., 1952, *Phil. Mag.*, **43,** 753.

Danysz, M., Lock, W. O., and Yekutieli, G., 1952, *Nature, Lond.*, **169,** 364.

Danysz, M., Harris, G. G., Juritz, J. W., and Lock, W. O., 1953, *Proc. Roy. Soc.* A, in press.

Menon, M. G. K., and O'Ceallaigh, C., 1953, *Proc. Roy. Soc.* A, in press.

Rochester, D., and Butler, C. C., 1953, *Reports on Progress in Physics*, **16,** (London : Physical Society), p. 364.

Thompson, R. W., Buskirk, A. V., Etter, L. R., Karzmark, C. J., and Rediker, R. H., 1953, *Phys. Rev.*, **90,** 329.

Watson, K. M., 1953, *Phys. Rev.*, **88,** 1163.

Watson, K. M., and Stuart, R. N., 1951, *Phys. Rev.*, **82,** 738.

CXIII. *Low Intensity Lines in the Spectrum of the Gamma-Rays from* $^{7}Li(p\gamma)^{8}Be(\alpha)^{4}He$

By E. K. Inall and A. J. F. Boyle
Research School of Physical Sciences, Australian National University, Canberra*

[Received June 25, 1953]

Abstract

Evidence for a γ-ray line at about 12·5 Mev, in the $^{7}Li(p\gamma)$ spectrum has been put forward recently by several workers. Although the measurements differ amongst themselves it appears that a line is present to about 10% of the intensity of the well known 17·6 Mev component. Experiments in this laboratory have shown that, in addition to the broad 14·8 Mev line, there are other transitions from the 17·6 Mev state of ^{8}Be to lower even states. The results were obtained by observing the emitted γ-ray coincidence with one of the α-particles resulting from the breakup of the even state. The measured α-particle ranges show that transitions occur to ^{8}Be levels at 4·09, $5·31\pm0·06$ and $7·51\pm0·06$ Mev. The corresponding γ-rays have energies of 13·54 Mev, $12·32\pm0·06$ and $10·12\pm0·06$ Mev and intensities of 2%, 2% and 0·5% of the total intensity. Backgrounds of soft x-radiation from the target backing, and energetic α-particles from the reaction $^{7}Li(p\alpha)^{4}He$ complicated the experiment necessitating the performance of check experiments to ensure correct interpretation of the results. In particular the time of flight of the α-particles was used to give a rough indication of their energy and demonstrate the reliability of the coincidence counting.

§ 1. Previous Observations by Other Workers

The gamma-ray spectrum from the reaction $^{7}Li(p\gamma)^{8}Be$ was studied by Walker and McDaniel (1948) using an electron pair gamma-ray spectrometer. They found two lines, a narrow one at 17·6 Mev and a broad one, 2 Mev wide, at 14·8 Mev, with an intensity ratio of 2 to 1 when the bombarding proton energy was 460 kev. No other component was detected. Three particle stars from the reaction $^{12}C(\gamma, 3\alpha)$ produced by the radiation from $^{7}Li(p\gamma)$ have been observed by Nabholz, Stoll and Wäffler (1951) and by Goward and Wilkins (1952). The former reported evidence for a line at 12·6 Mev with an intensity of about one tenth of the 17·6 Mev line, while Goward and Wilkins reported the energy to be 12·3 Mev and the intensity one half that of the 17·6 Mev component. Recently, Titterton (1953) used the radiation from this reaction to induce the disintegration $^{7}Li(\gamma t)^{4}He$ and the results of the experiment gave evidence for a line of 12·5 Mev energy with intensity about one twentieth of the 17·6 Mev line.

* Communicated by Professor E. W. Titterton.

McDaniel has stated in a private communication that a line at 12·5 MEV having a width less than 1 MEV would have been observed if the intensity were one tenth of the one at 17·6 MEV. If the width were 2 MEV about twice that intensity would have been required for detection.

Burcham and Freeman (1950) have shown that the 14·8 MEV component is produced by a transition to the 3 MEV level in ^{8}Be which then disintegrates into two alpha-particles. The following gamma–alpha coincidence experiments were carried out to determine whether weaker gamma-ray lines are present, and if so, to which levels of the ^{8}Be nucleus the transitions occur.

§ 2. APPARATUS

The target chamber and counters were arranged as shown in fig. 1.

Fig. 1

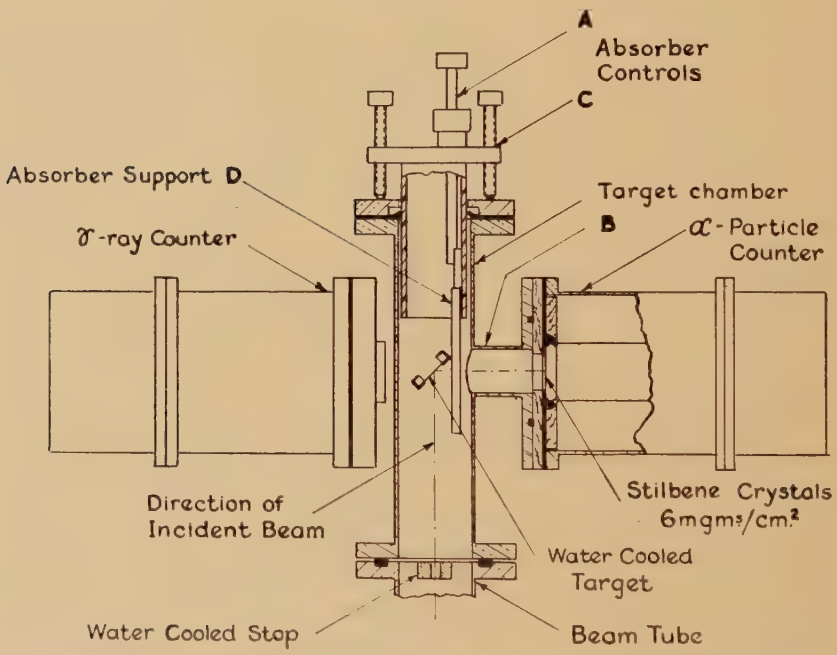

The arrangement of the target chamber, absorber supports and counters.

The alpha-particles were detected by a scintillation counter in which the scintillator was a layer of stilbene, 6 mg/cm² thick evaporated on to a glass slide. This was attached to the end window of the photo-multiplier tube which itself formed the vacuum wall across the tube B. Aluminium foil of 0·66 cm air equivalent prevented light from the target and low energy particles from entering the crystal. The solid angle of acceptance of the counter was $4\pi/138$ sterad, the crystal being 4·4 cm from the centre of the target.

The scintillator in the γ-ray counter was a NaI crystal 1 cm thick by 2 cm square placed with its centre 4 cm from the target in the plane of the beam and the α-counter. Aluminium absorber foils of graded thickness were mounted on frames D, supported from the two plungers A and C which could move into the end of the target chamber through Wilson seals. These foils could be interposed between the target and the alpha counter, so that the air equivalent of the total thickness of absorber between the target and counter could be varied from 0·66 cm to 7 cm in steps of about 0·1 cm.

Fig. 2

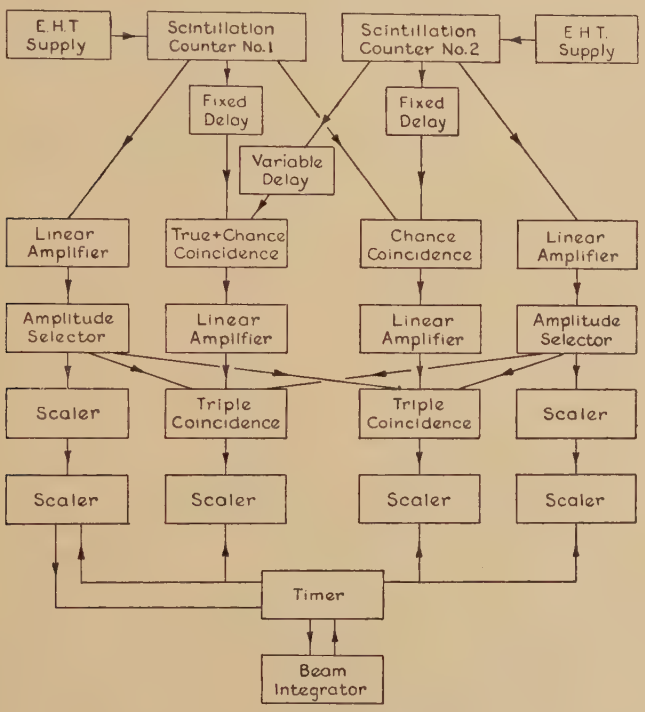

Block diagram of recording units.

A block diagram of the recording equipment is shown in fig. 2. The fast coincidence circuit was similar to that described by Bay (1951). The pulses into the coincidence circuit were clipped to 6×10^{-9} sec using a shorted transmission line, space charge limiting in the multiplier ensuring that the pulses reached their limiting value within this time.

§ 3. Experiment

Separated ^{7}Li targets of 350 $\mu g/cm^2$ superficial weight deposited on a silver backing were bombarded with a beam of 450 kev protons.

The bias of the discriminator in the α-counter were set so as to reject the large number of small pulses due to x-rays from the target and the

timing unit was arranged to stop the scaling circuits after 10^5 γ-ray counts had been recorded.

The coincidence counts recorded in this interval are plotted in fig. 3 against a value for the equivalent range which includes the range in the crystal required to produce a pulse of sufficient amplitude to be detected. α-particles from polonium were used to calibrate this scale.

The minimum absorber which could be used was 0·9 cm air equivalent because with less absorber, pulses due to the soft x-rays and protons scattered from contaminants on the target caused excessive currents in the photo-multiplier tube. The chance coincidence counts were about one-tenth of the true coincidences. It was necessary to check the balance of the fact coincidence circuit frequently, since the pulses producing the

Fig. 3

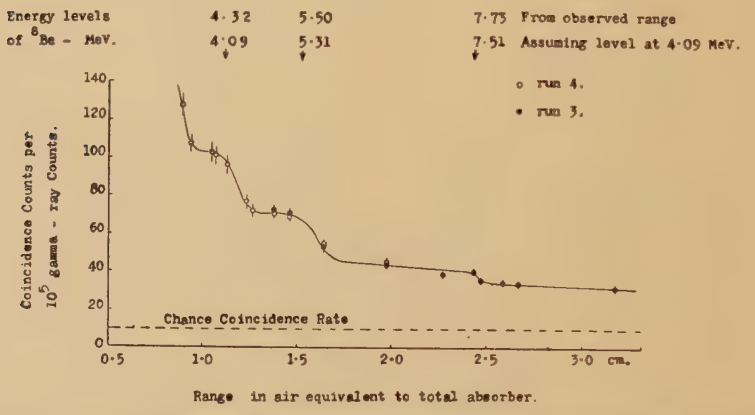

Showing the range of the alpha-particles detected in coincidence with a gamma-ray.

coincidences were small compared with the background pulses and, therefore, small pulses from the coincidence circuit had to be counted, although a slight misbalance could give such an output from a single large background pulse. Each point on the curve is the average of four observations of 100 seconds duration, during which time 10^5 gamma-rays and some $1{\cdot}5 \times 10^6$ alpha-particles were counted. About 95% of the alpha-particles were produced by the reaction $^7\mathrm{Li}(\mathrm{p}\alpha)^4\mathrm{He}$ and had a range of about 9 cm. Hence the alpha counting rate and therefore the chance coincidence rate changed but little over the range of fig. 3. In spite of the checks on the fast coincidence circuit there was a spread in the coincidence counts for any particular absorber.

Counts were therefore taken for a sequence of absorbers and this was reversed and repeated several times. Snedecor's F test applied to the many readings taken at each point showed that the standard deviation of the readings was not significantly greater than that expected from a Poisson distribution.

§ 4. Energy Levels of ^{8}Be.

Three groups of alpha-particles, having ranges of 1·19 cm, 1·60 cm, and 2·50 cm were detected in coincidence with a gamma-ray. These could only have been produced by a cascade reaction of the type

$$^{7}Li+{}^{1}H\rightarrow{}^{8}Be^{*}\rightarrow{}^{8}Be^{+}+\gamma+Q_1, \quad . \quad . \quad . \quad . \quad . \quad (1)$$

$$^{8}Be^{+}\rightarrow{}^{4}He+{}^{4}He+Q_2. \quad . \quad . \quad . \quad . \quad . \quad . \quad . \quad (2)$$

Devons and Hine (1949) have confirmed the expected lifetime of about 10^{-19} seconds for the 17·63 Mev level of ^{8}Be, formed by the resonant capture of the proton. Therefore, in these experiments, before the ^{8}Be disintegrated as shown in (2) it was in motion due to the combined effect of the momentum of the incident proton, plus the recoil from the emitted gamma-ray. Since in the experiment the gamma-ray was detected in the opposite direction to the alpha-particle, the resultant motion of the nuclei which produced coincidence counts was uniquely determined. In order to calculate the levels of ^{8}Be involved, the measured energy of the alpha-particles was converted to the equivalent energy in the centre-of-mass

Fig. 4

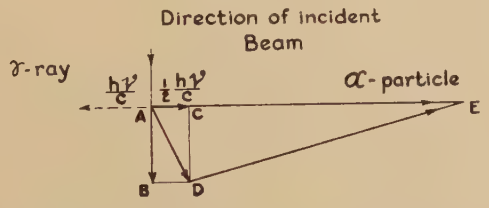

The momentum diagram for an alpha-particle detected at 90° to the direction of the beam and at 180° to the direction of emission of the associated gamma-ray.

system. The gamma-ray energy was then equal to the difference between the energy of the ^{8}Be level from which the α-particles arose and the 17·63 Mev of the compound nucleus. Thus the energy conversions were simplified by assuming the energy of the level to be twice the measured energy of the alphas and so obtaining a value of the gamma-ray energy which was sufficiently accurate to calculate the recoil. The momentum diagram, fig. 4, represents the momenta for one of the alpha-particles before and after disintegration. The recoil energy received from the proton was 0·055 Mev. The momentum gained from the proton by one of the alpha-particles in the combined nucleus was represented by AB and was proportional to $\frac{1}{2}\sqrt{55}$. The recoil momentum from the emission of the gamma-ray was represented by AC (about $\frac{1}{2}\sqrt{10}$), and the resultant momentum by AD. Then if AE was the momentum of the alpha-particle detected, DE was the momentum of the particle in the centre-of-mass system.

In table 1 the measured range of the alpha-particles is shown. The range-energy relations found by Bethe (1950) were used to obtain the energy

values shown in column 2. These include an extra 40 kev to compensate for loss in the target. The energy in the centre-of-mass system is also listed.

The energy released, Q_2, in the dissociation of the ^{8}Be nucleus with an excitation energy E above the ground state is

$$Q_2 = E + 0{\cdot}09 \text{ MeV},$$

the 0·09 MeV being the energy difference between the ground state of ^{8}Be and two free alpha-particles (Ajzenberg and Lauritsen 1952). Allowance was made for this when calculating the excitation energies shown in the table.

Table 1

Measured range (cm)	Energy of alpha-particles. Lab. system (MeV)	Energy of alpha-particles. C. of M. system (MeV)	Corresponding excitation energy of ^{8}Be (MeV)
1·19 ± 0·1	2·36 ± 0·16	2·20	4·32 ± 0·32
1·60 ± 0·1	2·96 ± 0·14	2·79	5·50 ± 0·28
2·50 ± 0·1	4·40 ± 0·10	3·91	7·73 ± 0·2

The accuracy of measurement of the excitation energy was sufficient to identify the source of the 1·19 cm and the 2·50 cm groups as the 4·09 MeV and 7·5 MeV levels of ^{8}Be. The 1·60 cm group confirms the existence of a level which was suggested by Titterton *et al.* (Calcraft and Titterton 1951, Brinkworth and Titterton 1951, Titterton 1953). The greatest uncertainty in the value of the excitation energy, and consequently the energy of the associated gamma-ray, is due to the difficulty in determining the zero for the range measurements. The relative ranges of the groups are about four times more accurate. For this reason the energy values quoted in table 2 were based on the value 4·09 ± 0·018 MeV determined by Salmon (1951) for the energy of the level of ^{8}Be which apparently disintegrated into the alpha-particles observed with a range of 1·19 cm.

Table 2. Corrected Energy Values

Corrected range (cm)	Energy of particle (MeV)	Corresponding excitation of ^{8}Be (MeV)	Gamma-ray energy (MeV)
1·12	2·24	4·09 (assumed)	13·54
1·53 ± 0·02	2·87 ± 0·03	5·31 ± 0·06	12·32 ± 0·06
2·39 ± 0·02	3·95 ± 0·02	7·51 ± 0·06	10·12 ± 0·06

Using this calibration the alpha-particles from the well-known level at 2·9 MeV would have been centred at 0·86 cm range in fig. 3, a fact which suggests the cause of the rise observed in the coincidence counts when the thinnest absorbers were used.

§ 5. Intensity of Gamma-Radiation

The number of coincidence counts C detected from n transitions each be of which produces a gamma-ray and two alpha-particles would be

$$C=\epsilon_{\gamma}\times 2\epsilon_{\alpha}\times n$$

where ϵ_{γ}=the absolute efficiency of the gamma-ray counter, assumed to constant for gamma-rays in the energy range 10 to 18 Mev and

$$\epsilon_{\alpha}=\text{absolute efficiency of the alpha-counter}$$
$$=1/138.$$

If the n transitions were accompanied by N gamma-radiating events, the number of counts N_{γ} in the gamma-ray counter would be

$$N_{\gamma}=(N+n)\,\epsilon_{\gamma}.$$

The fraction $n/(N+n)=C/(2\epsilon_{\alpha}\,N_{\gamma})$ then expresses the intensity of the weak gamma-ray component relative to the total. Table 3 lists the intensities, expressed as a percentage, calculated in this way from the data of fig. 3.

Table 3

Energy of radiation (Mev)	Intensity (%)
13·54	$2{\cdot}0\pm0{\cdot}3$
12·2	$1{\cdot}9\pm0{\cdot}3$
10·1	$0{\cdot}5\pm0{\cdot}1$

The values quoted for the intensity and the accuracy depend upon the assumption that all the transitions to the levels in ^{8}Be which emitted products into the cone of acceptance of the counters, were detected as coincidence events. Although this is likely to be true it is not possible to be sure of it. It is very unlikely that the intensities could be as much as twice those observed, unless the angular correlations were markedly anisotropic.

§ 6. Operation of the Fast Coincidence Circuit

Because such a small fraction of the counts in each of the detectors was registered as coincident events, it was necessary to ensure that these could not have been produced by faulty operation of the coincidence circuits.

Figure 5 shows the results of three tests which were applied. The coincidence rate is plotted against the delay produced by extra cables inserted in the γ-counter channel.

Curve (*a*) was obtained with a ^{60}Co source placed between the counters and gives a value for the delay caused by the cable used in the α-channel being longer than that used in the γ-channel, namely 11 mμs.

Curve (*b*) was obtained for the γ-rays and α-particles from the reaction under study. The 5 mμs displacement of the peak of (*b*) with respect to (*a*) compares well with the value 4·4 mμs calculated as the time required by a 2·5 MeV α-particle to travel to the crystal. The asymmetry of the curve, it being wider to the left of the peak, would be due to the shorter time of flight of the more energetic α-particles.

Leaving the alpha-counter in place, the gamma counter was removed from its position near the target chamber and a ^{60}Co source was placed near to it to make the ^{60}Co gamma-counting rate equal to that produced by the gamma-rays from the ^{7}Li(pγ)^{8}Be reaction. The E.H.T. supply to the photo-tube was then increased until the output pulses were of the same amplitude as those produced by the gamma-rays from the ^{8}Be.

Fig. 5

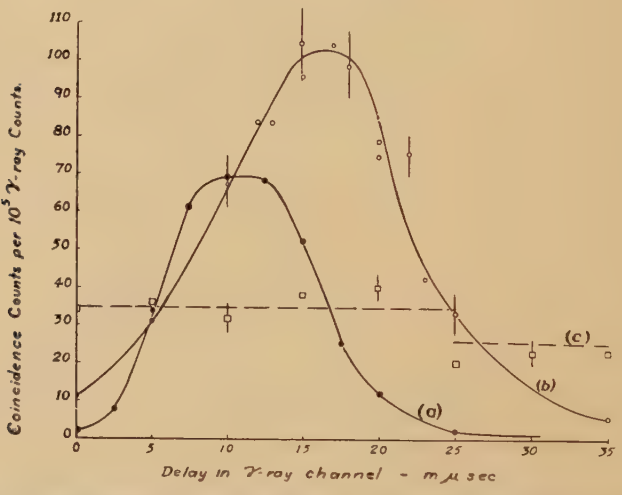

The change in coincidence counts produced by varying the delay in the gamma-ray channel, with a fixed delay of 11 ms in the alpha-particle channel.

Curve (*a*) for gamma–gamma coincidences of gamma-rays from ^{60}Co,
(*b*) for alpha–gamma coincidences of radiation from ^{8}Be*,
(*c*) for alpha–gamma coincidences of gamma-rays from ^{60}Co and alpha-particles from ^{8}Be*.

The amplitude of the pulses and the number entering the coincidence circuit were then substantially the same as for the main experiment. In this case no more than the expected chance coincidences were observed (curve (*c*) fig. 5) although there was a small reduction in the rate for delays greater than 25 mμs, probably due to unexpected losses introduced by the 25 mμs delay cable.

These experiments taken together confirm that the coincidences observed from ^{8}Be were due to alpha-particles and gamma-rays from the target and not to some spurious effect in the circuits.

§ 7. The Alpha-Particle Spectrum and the Pulse Amplitude Selection

Having identified the γ–α transitions by coincidence measurements the pulse amplitude selector was set to record only those pulses within a limited amplitude range so that the α-counter pulses produced by the 9 MEV particles from the reaction $^{7}Li(p\alpha)^{4}He$ were rejected. The absorption curve obtained is shown in fig. 6. It was not possible to resolve the α-particle groups from the ^{8}Be levels because of the background from the pile-up of X-ray pulses and pulses produced by protons scattered from target contamination. This background varied from point to point across the surface of the target so that reproduceable counts could not be recorded. According to the coincidence counts, about 5000 of the 23,000 counts shown at 1·0 cm in fig. 6 would have come from the disintegration of the excited ^{8}Be nuclei produced by the γ-ray transitions.

Fig. 6

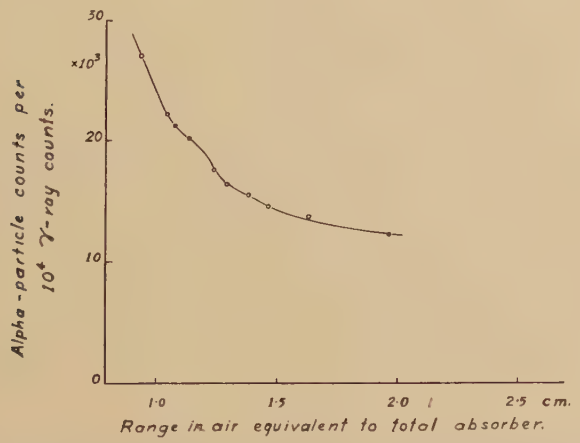

Pulses from the alpha-particle counter within the amplitude limits of 25 to 165 volts. On this scale the amplitude of the pulses due to the alpha-particles from $^{7}Li(p\alpha)^{4}He$ was 360 volts.

§ 8. Discussion of Results

The work of Walker and McDaniel with the pair spectrometer would not have revealed the presence of lines occurring with an intensity as low as those reported here. On the other hand in the photo-disintegration experiments discussed above, the 13·54 and 12·32 MEV lines would be difficult to resolve and could be expected to appear as a broad line at about 12·8 MEV. The total intensity would have been estimated as 7% of the 17·6 MEV line. These figures are in reasonable agreement with the values 12·6 MEV and 10% found by Nabholz *et al.*, and 12·5 MEV and 5% quoted by Titterton. They are, however, in marked disagreement with the high intensity (50%) reported by Goward and Wilkins. However,

the relative intensities would be expected to depend upon the beam energy and the angle between the direction of observation. Measurements have been made at a beam energy of 700 kev and others with an angle of 120° between the counters. Each confirm that the relative intensities do change but not enough to explain the result of Goward and Wilkins. Measurement of the γ–α angular correlations should make it possible to determine the angular momentum quantum numbers for the levels concerned and enable a test to be made of the alpha-particle model for ^{8}Be.

Acknowledgments

We wish to express our thanks to Professor M. L. Oliphant for the facilities used in the investigations ; to Professor E. W. Titterton who suggested the experiment and has contributed much in helpful discussion ; to W. van Barneveld and S. Sincock who built the target chamber and counters ; to Mr. N. F. Bowkett for help in operating the accelerating equipment.

References

Ajzenberg, F., and Lauritsen, T., 1952, *Rev. Mod. Phys.*, **24,** 321.
Bay, Z., 1951, *Rev. Sci. Instrum.*, **22,** 397.
Bethe, H. A., 1950, *Rev. Mod. Phys.*, **22,** 213.
Brinkworth, M. J., and Titterton, E. W., 1951, *Phil. Mag.*, **42,** 952.
Burcham, W. E., and Freeman, Joan M., 1950, *Phil. Mag.*, **41,** 921.
Calcraft, M. E., and Titterton, E. W., 1951, *Phil. Mag.*, **42,** 666.
Devons, S., and Hine, M. G. N., 1949, *Proc. Roy. Soc.* A, **199,** 56.
Goward, F. K., and Wilkins, J. J., 1952, *A.E.R.E.* G/M 127.
Nabholz, H., Stoll, R., and Wäffler, H., 1951, *Phys. Rev.*, **82,** 963.
Salmon, A. J., 1952, private communication.
Titterton, E. W., 1953, *Aust. J. Science*, **16,** 174.
Walker, R. L., and McDaniel, B. D., 1948, *Phys. Rev.*, **74,** 315.

CXIV. *Cosmic Rays at* 60 m.w.e. *Underground III : The Anomalous Scattering of* μ*-Mesons*

By M. L. T. Kannangara
The Physical Laboratories, The University, Manchester*
and
G. S. Shrikantia
Physics Department, Imperial College, London†

[Received April 25, 1953]

Abstract

Large-angle scatterings which have been found on 126·6 m of the tracks of relativistic particles in Ilford G5 plates exposed at a depth of 60 m.w.e. underground, are analysed, and are shown to be scatterings of μ-mesons. A cross section of $(2{\cdot}3\pm1)\times10^{-28}$ cm^2/nucleon is derived for scatterings greater than 7° by μ-mesons with $p\beta>100$ mev/c in the cosmic radiation at 60 m.w.e., and a cross section of $(3{\cdot}4\pm1{\cdot}5)\times10^{-27}$ cm^2/nucleon for a similar scattering by μ-mesons with $p\beta$ in the region (100–600) mev/c. These cross sections are shown to be rather too high to be explained in terms of a pure Coulomb scattering at a finite nucleus. Agreement between theory and experiment can be achieved, however, on the assumption of a point charge nucleus. Various mechanisms are examined for a possible explanation of the effect without success, and it is concluded that the scatterings probably represent a weak nuclear interaction of μ-mesons.

§ 1. Introduction

It is well known that a slow μ-meson has only a very weak interaction with matter. Wheeler (1949) has shown that the μ-meson is capable of travelling distances of the order of 200 cm in nuclear matter before being captured. However, during the past thirteen years, evidence has been presented by various authors for the scattering of μ-mesons as they passed through metal plates, in a manner which could not be explained in terms of Coulomb forces and a finite nucleus (Wilson 1940, Code 1941, Sinha 1945, Shutt 1946, Sahiar 1951, George and Trent 1951, Amaldi and Fidecaro 1950, Whitemore and Shutt 1952, Leontic and Wolfendale 1953). The experiment described in I of the present series of papers provided a good opportunity to investigate this problem further using the photographic plate technique. As shown in I, the observations refer to 126·6 m

* On leave from the University of Ceylon.
† Communicated by Dr. G. D. Rochester.

of straight minimum ionization track occurring in Ilford G5 plates, coated, exposed, and processed at a depth of 60 m.w.e. underground. In I and II, the knock-on electrons, tridents, electron pairs, and stars found during the scanning of this length of track were analysed. In the present paper, the large-angle scatterings are described and discussed.

§ 2. Experimental Results

A large angle scattering is observed as the sudden deflection of a straight track at a point (see I, fig. 2 (*d*)). A list of all such events recorded is given in table 1, where α° is the spatial deflection. No significant energy change is noticed at the deflection.

Table 1

Event No.	Track before deflection		Track after deflection		Deflection α°
	Length mm	$p\beta$ Mev/c	Length mm	$p\beta$ Mev/c	
1	4	110 ± 20	15	190 ± 35	$5{\cdot}7\pm0{\cdot}1$
2	36	275 ± 20	16	280 ± 30	$7{\cdot}4\pm0{\cdot}2$
3	13	550 ± 60	1·2	>300	$8{\cdot}0\pm0{\cdot}5$
4	16	130 ± 28	9	100 ± 20	$8{\cdot}1\pm0{\cdot}5$
5	7·2	120 ± 30	1·5	~100	$9{\cdot}0\pm0{\cdot}1$
6	5	210 ± 40	16	140 ± 20	$9{\cdot}1\pm0{\cdot}2$
7	20	340 ± 50	11	210 ± 25	$10{\cdot}8\pm0{\cdot}5$
8	17	160 ± 25	1·2	~100	$34{\cdot}4\pm0{\cdot}1$

All the tracks were grain counted on both sides of the deflection, and none of the counts were significantly different from counts on high-energy electron pairs on the same plate. The results of the grain-counting are shown in fig. 1. The plates were not developed sufficiently uniformly to distinguish between ' plateau ' and minimum grain density.

§ 3. Identity of the Particles

From fig. 1, it is clear that of the known particles, the tracks could have been caused by π-mesons, μ-mesons or electrons only. It will be shown that π-mesons and electrons are very unlikely to have caused the events.

As a result of a scan of 27 m of π-meson track, with $p\beta$ in the range (150–200) Mev/c, Bernardini *et al.* (1951) gave a mean free path of about 25 cm in G5 emulsion for the production of stars. inelastic scatterings (where the grain density changes by a factor of more than three) and stoppings in the emulsion (cf. Lock 1952). None of these events which are characteristic of π-mesons have been observed in the present experiment. Again, from the underground star rate given by George and Evans (1951), it can be shown that the percentage of π-meson tracks in the relativistic radiation at 60 m.w.e. is only 0·05% (George, private communication).

Thus, of the total track length followed, viz. 126·6 m, only 6 cm would be expected to be due to π-mesons. Hence it is extremely unlikely that the large angle scatterings are due to π-mesons.

It was estimated in II that about 70 cm of the track length examined is due to electrons with energy greater than 100 MeV. It might appear at first sight that the large angle deflections could be caused by ' Bremsstrahlung ' from these electrons. However, a 100 MeV electron is already a highly relativistic particle, and a deflection of the order of 7° is unlikely from such a process unless the electron were to lose almost its entire energy. If the events are to be explained in terms of some other form of electron interaction, then the cross section for such a process would have to be almost twice the geometric cross section and no such interaction is known.

Fig. 1

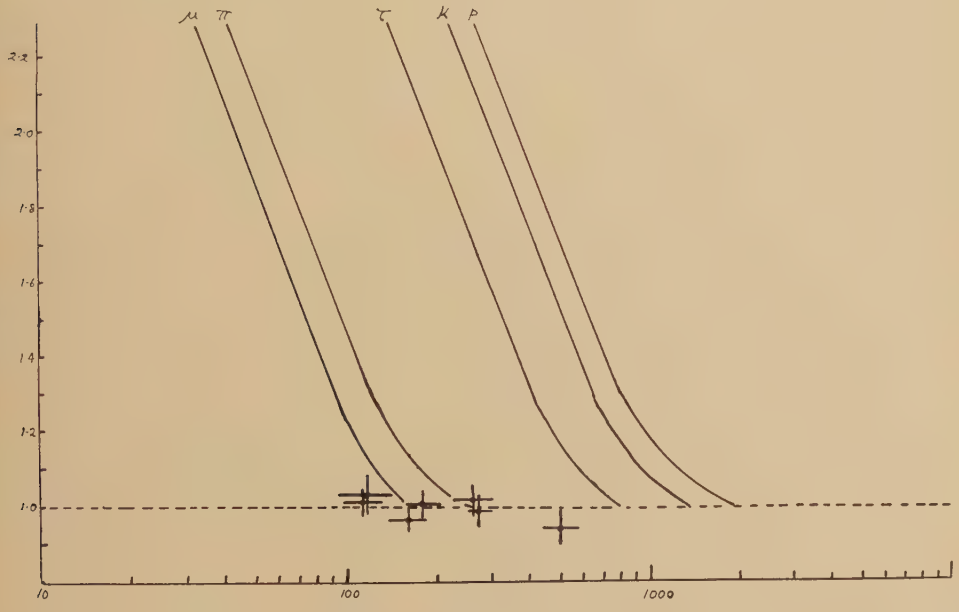

Grain density as a function of $p\beta$.

The tracks will therefore be assumed to be due to μ-mesons. The possibility that the events are caused by the decay of μ-mesons can be dismissed at once, since the time taken by a relativistic particle to travel 126·6 m is about $4{\cdot}5\times10^{-7}$ sec, which is shorter than the lifetime of μ-mesons even without time dilatation.

§ 4. Momentum Transfer

The momentum transfer involved in the events described in table 1 is given in table 2, together with the corresponding energy transfer to a proton, and the range of such a proton in Ilford G5 emulsion.

Since no recoil track was observed in any of the events, it is clear from table 2 that at least four of the deflections could not have been at hydrogen nuclei.

Table 2

Event No.	Momentum transfer MeV/c	Energy transfer to a proton MeV	Range of proton in Ilford G5 emulsion in μ
1	10	0·07	<1
2	34	0·6	7
3	70	2·6	60
4	12	0·08	<1
5	12	0·08	<1
6	24	0·2	1·5
7	46	1·1	17
8	66	2·3	50

§ 5. Scanning Efficiency

It is important to examine the geometrical factors which influence the finding of these events. It is clear that relatively small deflections will be largely missed, whereas large deflections will almost certainly be detected. If the primary track remains flat in the field of view before and after the deflection, it is estimated that a deflection of less than 3° would not be detected at all, and that the scattering would have to be greater than 4° before the event is observed with high probability. This is the most favourable case for detection. The most unfavourable case arises when the track deflects in a plane at right angles to the surface of the emulsion. In this case the only way of detecting the deflection is to notice the sudden change in the flatness of the track being followed. Now a track is followed in the first place because it appears flat in the field of view. From the track length distributions (I, fig. 1), it is seen that the number of tracks followed drops sharply when the track length drops below 5 mm. Thus it is reasonable to assume that if a track which is flat at first suffers a sudden deflection in a plane at right angles to the surface of the emulsion, so as to cause it to move subsequent to the deflection with an inclination corresponding to a track of length less than 5 mm, then the deflection would have a large probability of being observed. Clearly, a deflection which causes a track moving towards the surface (say) to turn back towards the glass would usually be detected quite easily. Most of the deflections that actually occur will lie between the extreme cases described above.

A track of 5 mm length has a steepness of about 6° with respect to the surface of an unprocessed 400 μ or 600 μ emulsion. It follows then that deflections less than 6° would have an appreciable chance of being missed, whereas deflections larger than about 7° should be detected with high

efficiency. Hence in evaluating cross sections, only deflections greater than 7° will be considered.

§ 6. Effective Track Length

When a track suffers a large deflection, it ceases in general to be flat in the emulsion. The consequent shortening of the track results in a smaller probability of its being followed. This effect is largely compensated for by tracks being scattered into the emulsion. The effective track length can therefore be taken as the length actually followed—i.e. 126·6 m. It is unlikely that this estimate is in error by more than 25%.

§ 7. The Experimental Cross Section for Large-Angle Scatterings

A mean free path of 18 m of Ilford G5 emulsion is deduced for a deflection greater than 7° by a μ-meson with $p\beta$ greater than 100 mev/c in the cosmic radiation at 60 m.w.e. This corresponds to a cross section $\sigma(\alpha>7°)=(2{\cdot}3\pm1)\times10^{-28}$ cm²/nucleon. However, since all the events recorded are associated with low energy tracks having $p\beta$ less than 600 mev/c, a cross section referring to μ-mesons of these energies gives a better picture of the situation. According to the μ-meson energy spectrum at 60 m.w.e. given by I, eqn. (4), the fraction of tracks with $p\beta$ in the region (100–600) mev/c is about one fifteenth. A cross section $\sigma(\alpha>7°)=(3{\cdot}4\pm1{\cdot}5)\times10^{-27}$ cm²/nucleon is then obtained for a deflection greater than 7° in G5 emulsion by μ-mesons with $p\beta$ between 100 and 600 mev/c.

§ 8. The Expected Number of Large-Angle Scatterings from a Pure Coulomb Interaction

If $\chi(\theta)\,d\theta$ cm²/nucleus is the differential cross section for the scattering of a fast charged particle (charge ze and momentum p) through an angle θ in the range $d\theta$ by a nucleus of charge Ze, then if the charge on the nucleus is concentrated at a point, the well known Rutherford formula applies:

$$\chi(\theta)d\theta=\frac{2\pi Z^2z^2e^4}{p^2\beta^2c^2}\frac{d(\sin\theta/2)}{\sin^3\theta/2}. \quad . \quad . \quad . \quad . \quad . \quad . \quad . \quad (1)$$

The integral cross section for a deflection greater than $\alpha°$ is given by

$$I(\alpha)=\int_{\alpha}^{180°}\chi(\theta)d\theta=\frac{\pi Z^2z^2e^4}{p^2\beta^2c^2}\left[\frac{1}{\sin^2\alpha/2}-1\right]. \quad . \quad . \quad . \quad (2\,a)$$

If p is in mev/c and $\alpha=7°$, eqn. (2 *a*) becomes

$$I(7°)=1{\cdot}74\times10^{-23}(Z^2/p^2\beta^2)\text{ cm}^2\text{/nucleus}. \quad . \quad . \quad . \quad (2\,b)$$

It may be noted that for Ilford G5 emulsion $\overline{Z^2}=405$ and the average number of nucleons per nucleus=27.

The finite size of the nucleus was taken into account by Williams (1939) by assuming the nuclear charge to be distributed uniformly over a sphere of radius $r_z=1{\cdot}5\times10^{-13}A^{\frac{1}{3}}$ cm (the classical nuclear radius). Williams showed that the Coulomb potential inside the nucleus could then be represented by

$$V(R)=Ze/R[1-\exp(-2R/r_z)].$$

Using this potential distribution, it was shown that for a finite nucleus, the Rutherford formula becomes

$$\chi(\theta)d\theta = \frac{2\pi Z^2 z^2 e^4}{p^2\beta^2 c^2} \frac{d(\sin\theta/2)}{\sin^3\theta/2} \cdot K, \quad \ldots\ldots \quad (3)$$

where

$$K = \left\{1 - \frac{1}{1+(\theta_{\max}/\theta)^2}\right\}^2 \quad \text{and} \quad \theta_{\max} = \frac{2\hbar}{pr_z}.$$

The variation of K with $\theta/\theta_{\max}$ is shown in table 3.

Using eqns. (2 *b*) and (3), the differential energy spectrum of the μ-meson flux at 60 m.w.e. given in I eqn. (3), and also the composition of Ilford G5 emulsion, the expected number of large angle scatterings greater than 7° can be calculated.

Table 3

$\theta/\theta_{\max}$	K	$\theta/\theta_{\max}$	K
0·3	0·84	1·5	0·09
0·5	0·64	2·0	0·04
1·0	0·25	3·0	0·01

Since only tracks which appeared to be at minimum grain density were followed, only mesons with $p\beta$ greater than 100 MeV/c (or kinetic energy greater than 50 MeV) are of interest. The μ-meson flux has therefore been divided into energy bands each extending over a range of 100 MeV from 50 MeV upwards, and the expected number of large angle scatterings calculated from each of these energy bands. The results are given in table 4. It is found that scattering at silver and bromine nuclei of the emulsion provide practically the entire cross section for the scattering. In fig. 2, $\theta_{\max}$ is plotted against $p\beta$ for silver and bromine nuclei.

It has been shown by Williams (1939) that the effect of a finite nucleus becomes apparent at scattering angles greater than h/pr_z (i.e. $\theta_{\max}/2$).

In the present experiment, five events were observed with $\alpha > h/pr_z$. These are the points above the dashed line in fig. 2. The expected number of large-angle scatterings falling into this category is 5·5 for a point charge nucleus and 1·5 for a finite nucleus. A similar calculation can be made for scattering angles greater than $2h/pr_z$. In this case, the expected number for a point charge nucleus is 2·1, and 0·12 for a finite nucleus. The observed number of events was 2. These results are summarized in table 5.

It can be shown, Regener (1951), that the probability that the events are solely due to Rutherford scattering at a finite nucleus of the Williams' type (with $r_z = 1{\cdot}5 \times 10^{-13} A^{-\frac{1}{3}}$), is less than 5%. If the assumed value of r_z is too large by 25%, the probability is increased from 5% to 16%.

Defining an anomalous scattering as one which cannot be explained in terms of Rutherford scattering at a finite nucleus, a cross section

σ(anomalous)$=(1{\cdot}5\pm1)\times10^{-27}$ cm^2/nucleon is deduced for μ-mesons with $p\beta$ between (100–600) MeV/c.

Table 4

Range of K.E. MeV	Corresponding range of $p\beta$ MeV/c	Observed number of scatterings $>7°$	Expected number of scatterings $>7°$	
			Point charge nucleus	Finite nucleus
50–150	90–220	4	6	3
150–250	220–340	2	1·6	0·5
250–350	340–450	0	0·8	0·1
350–450	450–560	1	0·5	0·05
450–550	560–650	0	0·35	0·02
550–650	650–750	0	0·25	—
650–750	750–850	0	0·2	—
750–850	850–950	0	0·15	—
850–950	950–1050	0	0·1	—
Total		7	10	3·7

Fig. 2

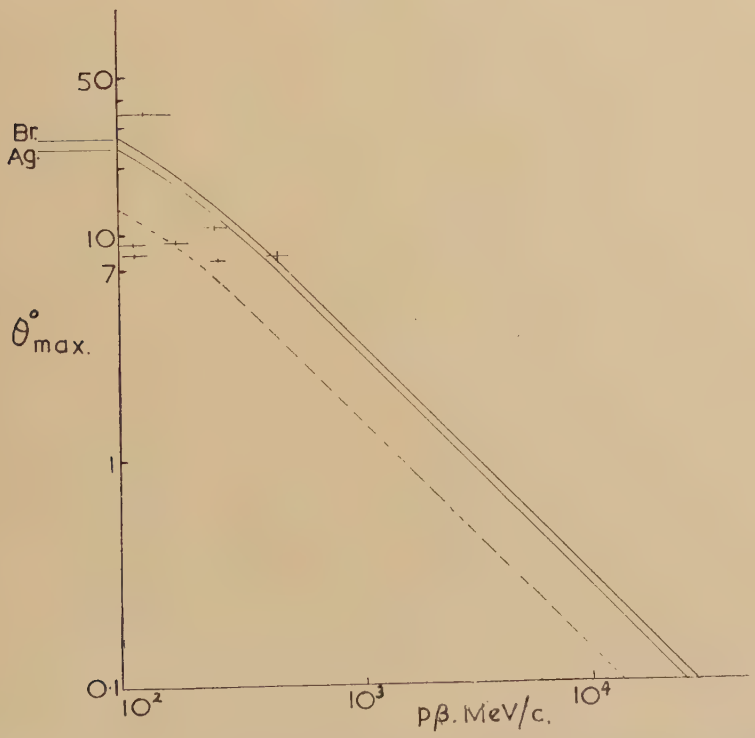

θ_{max} and $\theta_{max}/2$ (full and dashed lines respectively), as a function of $p\beta$ for bromine and silver nuclei.

§ 9. Results of Other Workers

Recent cloud-chamber experiments by Whitemore and Shutt (1952) and by Leontic and Wolfendale (1953) indicate clearly the tendency for the large angle scattering of μ-mesons in lead to fit the calculations better when no cut-off is applied for finite nuclear size. The earlier work on this subject is summarized in the paper of Leontic and Wolfendale (1953). If this picture of a point charge nucleus has any significance, the cross section per nucleon for a large angle scattering should be proportional to Z and hence should be lower in a light material. Between lead and Ilford G5 emulsion the expected difference in the cross section per nucleon is only a factor two, and the statistical accuracy of the experimental results is not

Table 5

Range of scattering angle	Observed No. of events	Expected number	
		Point charge nucleus	Finite nucleus
$>7°$	7	10	3·7
$>7°$ and $>\hbar/pr_z$	5	5·5	1·5
$>7°$ and $>2\hbar/pr_z$	2	2·2	0·12

sufficient to make this difference significant. Recently Walker (1953), working with μ-mesons of energy greater than 1·5 Bev at sea-level, has failed to observe a single deflection greater than 5° at a one inch carbon plate after 21 500 traversals. He concluded that the cross section for scattering greater than 5° in carbon is less than 2×10^{-29} cm^2/nucleon. The expected value for carbon for a point nucleus is 10^{-29} cm^2/nucleon. For lead one would expect a cross section of the order of

$$5\times10^{-29}\ \text{cm}^2/\text{nucleon}$$

for a deflection greater than 5° by μ-mesons in the stated energy range. Thus Walker's results appear to give a slight indication that the scattering is Z dependent per nucleon (or Z^2 per nucleus).

§ 10. Possible Explanations of the Anomalous Scattering

In the analysis presented in § 8, the effect of a finite nucleus was calculated by considering the nuclear charge Ze to be spread uniformly over the volume of the nucleus. Such a model can strictly be used only when the de Broglie wavelength of the incident particle is longer than the mean distance of protons inside the nucleus. When this wavelength is of the same order of magnitude or shorter than such a distance, as it is in the case with the particles under consideration, the nuclear protons have to be considered as individual centres of Coulomb forces distributed inside the nucleus. One has therefore to consider the effects of coherent and incoherent scattering within a nucleus : in the former case the nuclear

protons are not excited, whereas in the case of incoherent scattering the nuclear protons undergo a transition from the ground state to an excited state.

A simple approach to the problem of coherent scattering within a nucleus could be made by first giving each of the charged nucleons in a complex nucleus the same status as a point charge proton. Then using eqn. (2 *b*) and the fact that the number of charged nucleons per cm^3 of G5 emulsion is approximately $1{\cdot}8N_0$ (where N_0 is Avogadro's number), it can be shown that the expected number of large angle scatterings greater than 7° in the present experiment is only 0·3, a value at least 10 times smaller than the observed number of anomalous events. It is difficult to visualize a plural scattering mechanism within a nucleus which would increase the cross section by such a large factor.

The effects of incoherent scattering have been considered in some detail by Amaldi *et al.* (1950 a, b) for light nuclei only. The problem was shown to be similar to that of the scattering of an electron of a few kev energy or x-rays by an atom. In particular, Amaldi *et al.* considered the scattering of 200 Mev and 600 Mev μ-mesons at lithium and carbon nuclei, using two possible extreme values of the electromagnetic radius of the proton. They deduced cross sections for large-angle scatterings which were of the same order of magnitude as those calculated on a point charge picture. However, the incoherent scattering cross section is only Z dependent per nucleus. Thus if the cross sections of Amaldi *et al.* can be extrapolated to heavy nuclei such as silver and lead, the cross sections for incoherent scattering would be expected to be considerably smaller than the corresponding cross sections for Rutherford scattering worked out on a point charge model. Such an extrapolation has been made by Whitemore and Shutt (1952), who estimate that for lead the cross section drops to one-tenth the value calculated for a point nucleus when r_0, the electromagnetic radius of the proton, is taken as $2{\cdot}1\times10^{-14}$ cm, and to one-hundredth the value for a point nucleus when r_0 is taken to be $1{\cdot}4\times10^{-13}$ cm.

It would therefore appear that the explanation of the phenomenon is not to be found in terms of coherent or incoherent Coulomb scattering within a nucleus.

Another possible explanation of the effect is in terms of a photo-nuclear interaction between the ' virtual ' photons of the electromagnetic field of the incident μ-meson and the short-range nuclear forces. George and Evans (1950) explained the stars produced by fast μ-mesons underground in terms of such an interaction. They deduced a cross section, σ, for an energy transfer greater than ϵ of the form $\sigma=K\sigma_{h\nu}[\log_e(E/\epsilon)]^2$ cm^2/nucleon, where E is the energy of the incident μ-meson, K is a constant, and $\sigma_{h\nu}$ is the cross section for nuclear disintegration by a high-energy photon. Substituting $E=14$ Bev for the average energy of μ-mesons at 60 m.w.e., $\sigma=10^{-28}$ cm^2/nucleon from the experimental work of Miller (1951) and $\epsilon=150$ Mev as the energy required to produce a 3-prong star, they obtained a cross section $\sigma=4\times10^{-30}$ cm^2/nucleon. In the present experiment,

the average energy of the μ-mesons under consideration is about 200 MeV, and the energy transfer to a nucleon is about 2 MeV. Thus (E/ϵ) remains the same as for George's calculations. However, the experimental cross section for anomalous scattering is $\sigma \sim 1{\cdot}5 \times 10^{-27}$ cm^2/nucleon. Hence to bring experiment and theory into agreement σ_{hr} would have to be increased to about 3×10^{-26} cm^2/nucleon for small energy transfers of the order of 1 or 2 MeV, as against 10^{-28} cm^2/nucleon for larger energy transfers of the order of 150 MeV. There is no evidence whether such an assumption is reasonable or not. This mechanism is Z-dependent per nucleus, so that if experiments with light and heavy elements were to support a Z^2-dependence, this process would be excluded.

§ 11. Conclusion

The large-angle scatterings of μ-mesons are shown to be consistent with theory if the scattering nuclei are imagined as point charges. Since such a picture is contrary to present theories of the structure of the nucleus, the agreement seems to be accidental. It is possible that the scatterings represent a new type of nuclear interaction.

Acknowledgments

This investigation was carried out under the direction of Dr. G. D. Rochester, whose valuable advice is deeply appreciated. The authors thank Dr. A. W. Wolfendale and Mr. B. Leontic for communicating their results prior to publication. The authors' thanks are also due to Dr. G. N. Fowler and the members of the photographic emulsion group at Manchester for helpful cooperation and discussion. Mr. P. H. Fowler and Dr. M. G. K. Menon of Bristol University have made valuable comments on the paper.

References

Amaldi, E., and Fidecaro, G., 1950, *Nuovo Cim.*, **7,** 535.
Amaldi, E., Fidecaro, G., and Mariani, F., 1950 a, *Nuovo Cim.*, **7,** 553 ; 1950 b, *Ibid.*, **7,** 757.
Bernadini, G., Booth, E. T., Lederman, L., and Tinlot, J. H., 1951, *Phys. Rev.*, **82,** 105.
Code, L., 1941, *Phys. Rev.*, **59,** 229.
George, E. P., and Evans, J., 1950, *Proc. Phys. Soc.* A, **63,** 1248.
George, E. P., and Trent, P. T., 1949, *Nature, Lond.*, **164,** 838.
Leontic, B., and Wolfendale, A. W., 1953, *Phil. Mag.*, **44,** 1101.
Lock, W. O., 1952, *Ph.D. Thesis*, Bristol University.
Miller, R. D., 1951, *Phys. Rev.*, **82,** 260.
Regener, H. V., 1951, *Phys. Rev.*, **84,** 164.
Sahiar, A. B., 1951, *Proc. Indian Acad. Sci.*, **34,** No. 3A, 201.
Shutt, R. P., 1946, *Phys. Rev.*, **69,** 261.
Sinha, K., 1945, *Phys. Rev.*, **68,** 153.
Walker, W. D., 1953, private communication.
Wheeler, J. A., 1949, *Rev. Mod. Phys.*, **21,** 133.
Whitemore, W. L., and Shutt, R. P., 1952, *Phys. Rev.*, **88,** 1312.
Williams, E. J., 1939, *Proc. Roy. Soc.* A, **169,** 531.
Wilson, J. G., 1940, *Proc. Roy. Soc.* A, **174,** 73.

CXV. *The Anomalous Scattering of μ-Mesons in Lead*

By B. Leontic and A. W. Wolfendale
The Physical Laboratories, The University, Manchester*

[Received April 25, 1953]

Abstract

A multi-plate cloud chamber has been operated at sea-level under a thick lead absorber and the scattering of penetrating particles—presumably μ-mesons—has been investigated. In common with the results of other workers, a component of scattering has been found which is not consistent with the distribution expected from simple Coulomb scattering from a nucleus in which the charge is distributed uniformly throughout the volume ('solid' nucleus). We find that the magnitude of this anomalous component is similar to that expected from the Coulomb interaction with a nucleus of effective radius much smaller than that of the 'solid' nucleus. Since it is very unlikely that the electrostatic charge of the nucleus can be considered to be concentrated at the centre of the nucleus, we conclude that the anomaly is probably due to a short range non-electric interaction between μ-mesons and nucleons.

§ 1. Introduction

The interaction of very slow μ-mesons with matter has been studied by a number of workers and has been found to be very weak (Conversi *et al.* 1945, 1947, etc.). In the present work the interaction of fast μ-mesons with lead nuclei is found to be relatively large.

Data on the scattering of μ-mesons in lead is analysed statistically and the magnitude of a scattering component, additional to that expected from simple Coulomb scattering from a solid nucleus, is determined. The results of other workers are analysed using the scattering distribution found by us and are found to be mainly in agreement.

The scattering distribution should give evidence for the particle-structure of the nucleus or the short range forces between μ-mesons and nucleons.

§ 2. Experimental Arrangement

The experiment was carried out in the laboratory at sea-level using a cloud chamber of illuminated volume $40 \times 25 \times 25$ cm^3 containing six 2 cm lead plates (fig. 1). The chamber was illuminated through a rear window by two flash discharge tubes placed at the foci of two parabolic mirrors, and stereoscopic photographs were taken by twin cameras, the axis of photography making an angle of about 20° with the direction of

* Communicated by Dr. G. D. Rochester.

illumination. The expansion for the chamber was produced by the symmetrical lateral movement of two rubber diaphragms on opposite sides of the chamber. Electromagnetic release valves, connected in series, controlled the movement of the diaphragms ; the delay between the passage of a particle through the chamber and the completion of the expansion was only 8 m sec, ensuring reasonably fine tracks.

A narrow lead filter 100 cm in height was situated above the chamber and particles which had traversed the filter were selected by the counter telescope A B C. The telescope was situated wholly above the chamber in order to give no geometrical bias for events occurring inside the chamber. An upper limit to the number of primary and secondary protons and π-mesons reaching the chamber has been calculated for an absorber of this thickness (Wolfendale 1953), and is quite negligible.

Fig. 1

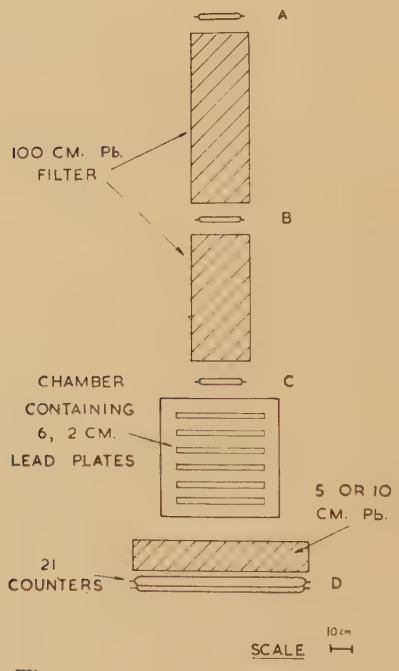

The experimental arrangement.

For part of the experiment an absorber Σ was present underneath the chamber, and below it there was a double tray of counters. This tray was connected to an indicator lamp by way of the appropriate circuits so that the further penetration of mesons appearing in the chamber could be determined.

For the analysis single tracks were selected whose positions indicated that the particles had penetrated the filter and were in fact the particles responsible for the expansions.

§ 3. Experimental Results

2969 photographs were taken, each showing at least one particle penetrating all the plates. The projected angles of scattering of selected particles in some of the lead plates were measured using a microscope fitted with a goniometer eyepiece. On account of track distortion above the top and below the bottom plates only the deflections in the centre four plates were measured. Measurements were limited to cases where the root mean square deflection for the four traversals was greater than

Table 1

θ_0	No.	θ_0	No.
2–3°	69	8–9°	3
3–4°	44	9–10°	2
4–5°	18	10–11°	0
5–6°	12	11–12°	1
6–7°	16	12–13°	3
7–8°	6		
		Total	174

2°, since scattering angles appreciably less than this magnitude were uncertain due to distortion. The selection of tracks to be measured was made by eye and a number of tracks were probably missed having root mean square projected deflections $\theta_0 > 2°$. However, it will be shown later that this inefficiency is not important. The frequency distribution for θ_0 is given in table 1.

§ 4. Analysis of the Experimental Results

4.1. *Data with the Chamber and Indicator Tray*

In order to detect any anomalous scattering, the Coulomb scattering spectrum must be known and this can be calculated if the momentum spectrum is known from independent observations. This, however, is not the case and it is not possible to derive a Coulomb scattering spectrum by simple methods from the observed scatterings of table 1, since they are few in number. Consequently no attempt has been made to derive the magnitude of the anomalous scattering in this way from the complete data.

625 photographs were taken in which the single meson seen in the chamber penetrated a further 5 or 10 cm Pb, and discharged a counter in the tray D below the chamber. Six photographs showed large-angle scattering of more than 10° in one of the centre four plates, and in each case the momentum of the meson after the interaction was >250 MeV/c (from the known minimum range). In this momentum region the multiple Coulomb scattering has a fairly low average value, compared with the occasional large scatterings which may or may not be anomalous. It is therefore possible to infer an approximate multiple Coulomb scattering spectrum from our measurements, and on the assumption that this is Gaussian (Williams 1939, and others) we can compute the number

of large scatterings to be expected and compare it with the observed number.

The effect of occasional large single scattering will, in general, be superposed on the multiple scattering distribution. This single scattering follows a power law in θ, and if the nucleus has a finite size it will be cut off at a maximum angle given by

$$\theta_{s,\max} \sim \frac{\lambda\!\!\!^{-}}{d} \text{ (Williams 1939, Olbert 1952)} \quad . \quad . \quad . \quad . \quad (1)$$

where $2\pi\lambda\!\!\!^{-}$ is the De Broglie wavelength of the meson and $d = 0{\cdot}5\, r_0 A^{1/3}$ is the ' radius ' of the nucleus. A is the atomic weight of the element and r_0 is the classical electron radius. The true root mean square projected deflection θ_{RMS} due to multiple scattering in an absorber of thickness t is given by

$$\theta_{\text{RMS}} = \frac{14{\cdot}8}{p\beta}\sqrt{t} \text{ radians (Rossi and Greisen 1941, and others)} \quad . \quad (2)$$

where p is in Mev/c and t is in radiation lengths (1 radiation length in lead $= 0{\cdot}52$ cm).

From eqns. (1) and (2) we find

$$\frac{\theta_{s,\max}}{\theta_{\text{RMS}}} = \frac{2{\cdot}0}{\sqrt{t}} \quad . \quad . \quad . \quad . \quad . \quad . \quad . \quad . \quad . \quad (3)$$

For a 2 cm lead plate the maximum angle for single scattering is nearly the same as the RMS angle of multiple scattering and the contribution of single scattering to the distribution is very small. (In general, when the cut off is not considered, the single scattering ' tail ' is only important for deflections greater than about 3 θ_{RMS}.) The resultant scattering distribution in this experiment should, therefore, be approximately Gaussian.

On the multiple Coulomb scattering distribution we expect only about one scattering having a deflection greater than 10° and five events remain as ' anomalous '. This yields a cross section for anomalous scattering for angles greater than 10° with our particular spectrum

$$\sigma_{>10^\circ} \sim (1{\cdot}5 \pm 0{\cdot}7)\ 10^{-28}\ \text{cm}^2/\text{nucleon}.$$

Table 2 gives the deflections, minimum ranges and corresponding minimum momenta of the particles scattered through more than 10°, together with the calculated probabilities that they form part of the multiple Coulomb scattering distribution (MCS).

It will be noticed that the number of events decreases rapidly as the deflection θ increases so that the cross section for $\theta > 20°$, say, is possibly an order of magnitude less than the corresponding cross section for $\theta > 10°$.

4.2. *Statistical Analysis*

An alternative and more satisfactory treatment of the data has been carried out using all the measured tracks and considering the relative

magnitudes of the four deflection measurements made on each particle traversing the cloud chamber. The analysis is statistical in character and the method was suggested by Professor M. S. Bartlett.

Table 2

Event No.	Deflection θ degrees	Min. range in cm Pb	Min. momentum in MeV/c	Probability of deflection being due to MCS %
1	18	13	285	0·4
2	11	18	345	10
3	12·5	18	345	3
4	11	11	250	40
5	10	14	305	20
6	11	13	285	20

The main problem in the interpretation of the results consists in determining to what extent the anomalous component (non-Gaussian or Gaussian of different magnitude) contributes in producing occasional large-angle deflections.

We first consider the case where no anomalous component exists, the scattering being simple Gaussian.

Let θ_0^2=mean square angle from the four observations on a single particle ;

θ_m^2=maximum square angle.

We define then $g=\theta_m^2/4\,\theta_0^2$.

Cochran (1941) has discussed the distribution of g and has given as the probability distribution of g

$$P_G(g)=\frac{8}{\pi}g^{1/2}(1-g)^{1/2} \text{ for } g \geqslant \tfrac{1}{2}. \quad . \quad . \quad . \quad . \quad . \quad (4)$$

The number distribution is then

$$N_G(g)=N_0 P_G(g),$$

where N_0 is the total number of events (for $g>0$).

The advantage of this method of analysis is that g is independent of the true mean square and also of the observed mean square (for Gaussian observations).

It is found that the distribution is independent of selection of θ_0^2 so that rejecting small values of θ_0^2 will not affect appreciably the anomalous samples since these show up as large angles.

The values of g have been calculated for the tracks having $\theta_0>2^\circ$ and the experimental distribution is given in fig. 2. The theoretical distribution calculated from eqn. (4), normalized to the same number of particles having $g>0$, is drawn for comparison. To determine the effect of track distortion the distribution of g for $\theta_0>4^\circ$ has also been determined and

normalized to the same number of particles. This is also given in fig. 2. The form of the distribution is very similar to that for $\theta_0 > 2°$. It can be assumed therefore that the distortion has little effect on the shape of the distribution for either category, since we expect the distortion effects for $\theta_0 > 4°$ to be quite negligible.

The discrepancy between the expected and experimental distributions is large particularly in the region of high g and the statistical χ^2 test shows that the two distributions are significantly different, so that an anomalous effect clearly exists.

Fig. 2

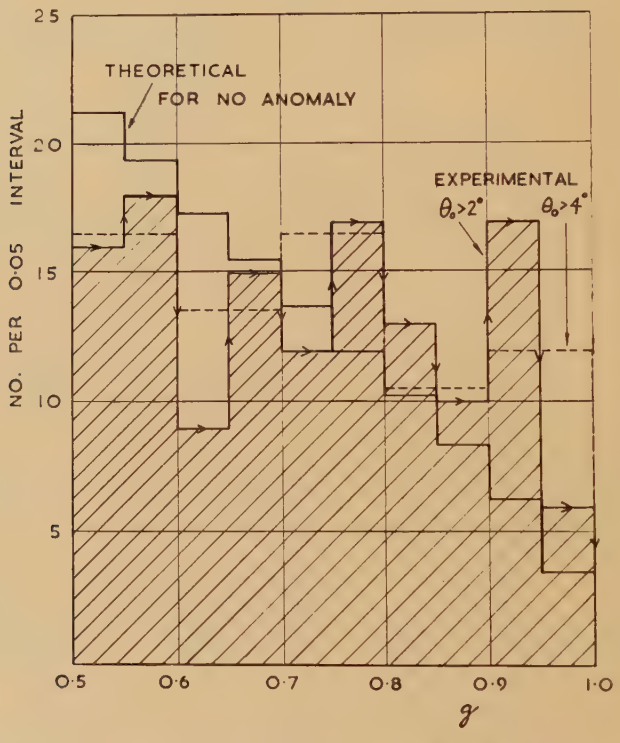

Comparison of the experimental distribution of 'g' with the theoretical distribution for multiple Coulomb scattering only.

The probability of anomalous scattering can be estimated on the following assumptions :

(*a*) the chance ϵ of an anomalous deflection is small, so that the probability of more than one such deflection in four observations is negligible ;

(*b*) the distribution of the anomalous scattering is Gaussian with a larger standard deviation σ_H which bears a constant ratio to the normal Gaussian distribution σ_G for particles of different momenta.

$$\frac{\sigma_H^2}{\sigma_G^2} = \frac{1}{\mu}.$$

The latter assumption means that the probability for anomalous scattering varies with momentum in an identical manner to that of multiple and single scattering. Since the excess of events having large values of g occurs for all measured values of θ_0, i.e. for all momenta less than about 1 Bev/c, assumption (b) is at least approximately true.

Assume further that an anomalous deflection provides the maximum reading (this is only strictly true in the limit as $\mu \to 0$). The distribution of g with one anomalous observation in each set of four deflections can be determined.

This has been evaluated by Bartlett as

$$P_H(g)=\frac{\frac{2}{\pi}\sqrt{\left[\left(\frac{1}{g}-1\right).\frac{1}{\mu}\right]}}{\left\{1+\left(\frac{1}{g}-1\right)\frac{1}{\mu}\right\}^2 g^2\mu} \quad . \quad . \quad . \quad . \quad . \quad . \quad . \quad (5)$$

The chance of one anomaly in a set of four is 4ϵ and so the resultant probability distribution of g is

$$P(g)=(1-4\epsilon)P_G(g)+4\epsilon P_H(g)$$

and the number distribution

$$N(g)=N_0P(g).$$

By varying the parameters ϵ and μ, the curve of best fit (minimum χ^2) to the experimental distribution (from fig. 2, $\theta_0>2°$) has been found and is given in fig. 3.

The optimum values of the parameters are

$$\epsilon=0{\cdot}083,$$
$$\mu=0{\cdot}07.$$

Since the optimum value of ϵ is small, assumption (a) is valid. A large number of pairs of ϵ and μ were tried and χ^2 determined for each pair. A set of pairs that gave a constant χ^2 corresponding to a 90% chance of the true value lying within the set, were taken and the limiting distributions determined.

We identify the multiple Coulomb scattering with the normal Gaussian distribution. The distributions are given in fig. 4. The abscissa $\theta/\theta_{\text{RMS}}$ is independent of the momentum of the particles for single scattering so that the probability distributions for a point nucleus (i.e. omitting the cut off mentioned on p. 1103) can also be plotted. Of the single scattering distributions given in fig. 4, one is that calculated by Williams (1939) and the other is the result of Snyder and Scott's (1949) more detailed theoretical investigation.

Our experimental distribution shows that the large-angle scattering observed for particles having $\theta_0>2°$, i.e. momenta less than about 1 Bev/c, is definitely in excess of the Coulomb scattering for a solid nucleus and of magnitude similar to that for a point nucleus. Our curve of best fit lies rather above that calculated for single scattering from a point nucleus, but this is not necessarily important because our experimental points are raised by the inclusion of small distortions.

The effective radius of the lead nucleus for this scattering may be of the order of 1/10 of the value given by the usual relation $r=0{\cdot}50\ r_0A^{1/3}$ and still give results consistent with our experiment within the statistical errors.

Examples of anomalous scattering are shown in Plates 44 and 45.

Fig. 3

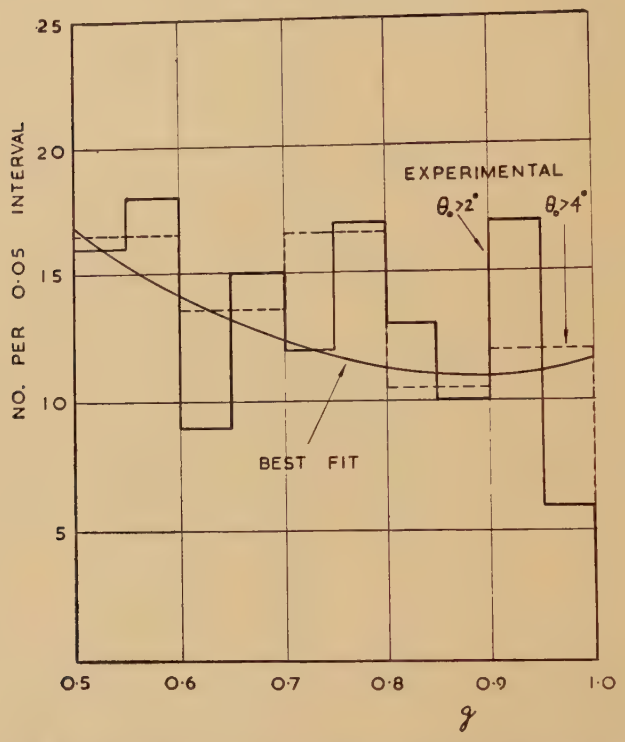

Comparison of the experimental distributions of 'g' with the 'best-fit' distribution, considering both multiple Coulomb scattering and anomalous scattering.

§ 5. Determination of the Cross Section for Anomalous Scattering

If the so-called anomalous scattering is treated as a type of single Coulomb scattering, then the cross section will in general depend on the particular particle spectrum and the minimum angle of scattering accepted as anomalous. The cross section would in that case fall off rapidly with increasing angle of scatter, whereas if the scattering is due to short range nuclear interactions where the angle of emergence of a particle after interaction is probably symmetric in the centre of mass system, the fall off should be less rapid (Amaldi and Fidecaro 1950).

From the best fitting curve (fig. 3) we can deduce the cross section for anomalous scattering as a function of the ratio of the minimum angle

accepted as anomalous to the RMS angle of multiple Coulomb scattering. The cross section can also be determined as a function of the minimum momentum transfer in the anomalous scattering event, from the following considerations.

Fig. 4

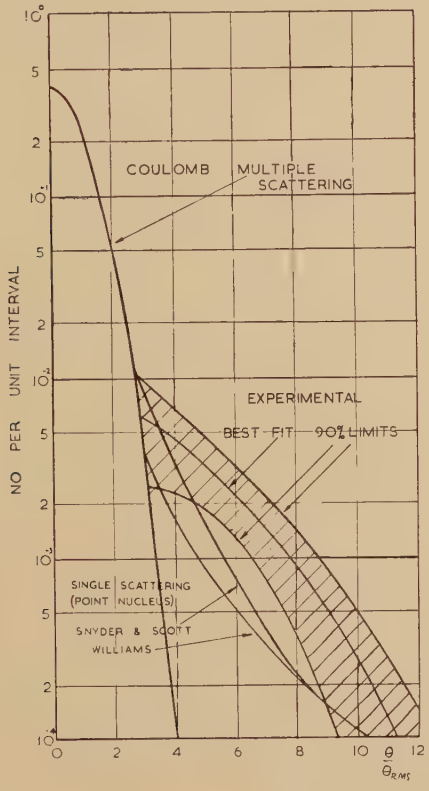

Coulomb scattering distributions for 'solid' and 'point' nuclei compared with the distribution giving the 'best-fit' to the experimental results.

Consider a particle of momentum p (MeV/c) being scattered anomalously through a small angle θ. The momentum transfer for small deflections is approximately

$$p = p\theta = p\theta_{\mathrm{RMS}} \frac{\theta}{\theta_{\mathrm{RMS}}} = 29{\cdot}0 \frac{\theta}{\theta_{\mathrm{RMS}}}$$

from the equation

$$\theta_{\mathrm{RMS}} = \frac{14{\cdot}8}{p\beta} \sqrt{t}$$

assuming that $\beta \sim 1$.

Therefore the momentum transfer is a function of $\theta/\theta_{\mathrm{RMS}}$ and hence of the cross section. The approximate values are given in table 3.

Table 3

θ/θ_{RMS}	Cross section (cm^2/nucleon) in Pb for deflections $>\theta$	Approximate momentum transfer MeV/c
3	$2{\cdot}3\times10^{-27}$	85
6	$5{\cdot}7\times10^{-28}$	170
9	$6{\cdot}9\times10^{-29}$	255
12	$4{\cdot}4\times10^{-30}$	340

§ 6. Comparison with Other Observations

The results of other experiments on anomalous scattering (AS) are given in table 4 where the cross sections (σ) found are in most cases compared with the values expected from our results. It will be noticed that most of the results are consistent with our interpretation.

§ 7. Discussion and Conclusion

It has been shown that most of the experimental results on μ-mesons scattering are consistent with the point nucleus hypothesis. Considerations of binding energy, nuclear stability, magnetic moment, etc., show, however, that the individual nucleons in a nucleus are not in fact concentrated at a point but are distributed fairly uniformly over the nuclear volume. The effective radius of the nucleus for short range forces has been determined from neutron cross sections by De Juren and Knable (1950) and others. It is reasonable to assume that the effective radius for Coulomb interactions is of similar magnitude, and in fact the scattering of moderately fast electrons by nuclei (Lyman *et al.* 1951) shows that the nucleus can be represented by a sphere of uniform electrostatic charge density having a radius about 20% smaller than the value determined from the neutron interaction cross sections.

It appears then that the similarity between the experimental results and those expected for the single Coulomb scattering from a point nucleus is quite fortuitous and that the anomaly is due to incoherent Coulomb interactions or to short range non-electric interactions.

It is interesting to note here that the calculation of the coherent and incoherent Coulomb scattering of μ-mesons by light nuclei, carried out by Amaldi *et al.* (1950), gives scattering distributions similar to those expected from coherent scattering by point nuclei. Whittemore and Shutt have estimated very approximately the maximum contribution from this incoherent scattering in the case of lead to be $<10\%$ of the observed effect so that if the calculations are correct it seems likely that a large fraction of the anomalous scattering is due to non-Coulomb short range forces. Further information on the forces responsible for the anomaly might be given by the sign dependence of the scattering. Whittemore and Shutt find no difference within rather large statistical errors and it is important that this aspect should be examined in greater detail.

Reference	Method	Scattering material	Meson-spectrum	Minimum angle for AS	σ for AS $\times 10^{-28}$ cm^2/ nucleon	Comparison with value expected form our results
Wilson (1940)	Magnet-cloud-chamber	Lead, Copper and Gold	Measured	3 events for θ events expec scattering gi	$>5\ \bar{\theta}$ against 0·25 ted for solid nucleus ving AS$\sim$1·5 %	$\sim$2 %
Code (1941)	Magnet-cloud-chamber	Tungsten	Measured	$\theta > 3{\cdot}3\ \theta_{\text{RMS}}$	$\sim$9	$\sigma \sim 20$
Shutt* (1942, 1946)	Cloud-chamber under filter	Lead	Complete	9°	2–4	$\sigma \sim 1{\cdot}5$ for rather harder spectrum.
			$E > 500$ MeV	9°	4–6	Expect smaller σ than for complete spectrum.
Sinha* (1945)	Cloud-chamber	Lead	Total energy $\sim$ 200 MeV	All angles	$\sim$200	$\sigma \sim 40$–60
Amaldi and Fidecaro (1950)	Counter-hodo-scope	Iron	$200 < KE < 320$ MeV	20°	0·8 (99 % chance of $< \sigma$)	Experimental conditions too dissimilar for good comparison. However obviously expect $\sigma \ll 1{\cdot}5$ (table 2).
			$320 < KE$ MeV	20°	0·04	
George and Trent (1951)	Counter-hodo-scope	Lead	Complete	Most $> 10°$	$\sim$2	$\sigma \sim 1{\cdot}5$ for harder spectrum.
Sahiar (1951)	Cloud-chamber	Lead	Complete	12°	$\lesssim 4$	As above. (Detailed analysis showed that distribution of deflections consistent with our results although statistics are weak.)
Whittemore and Shutt (1952)	Magnet-cloud-chamber	Lead	Measured $0{\cdot}3 < pc < 3$ BeV	Results consist expected fo scattering fr	ent with distribution r single Coulomb om point.	Similar conclusion.
George, Redding and Trent (1953)	Cloud-chamber underground	Lead	Complete	15°	$\sim$2	Similar magnitude.
Kannangara and Shrikantia (1953)	Nuclear emulsion	Silver, bromine, etc.	$100 < p\beta < 600$ MeV/c	7°	$\sim$15	Results consistent with single scattering from point nucleus.
Walker (1953)	Magnet-cloud-chamber	Carbon	$pc > 1{\cdot}5$ BeV	5°	$< 0{\cdot}2$	Not inconsistent with point nucleus hypothesis.

* These authors find that the AS component cannot be explained by Coulomb forces.

Acknowledgments

The authors wish to thank Professor P. M. S. Blackett, F.R.S., for his interest in the experiment, and Dr. H. J. J. Braddick for his help and encouragement. We also wish to thank Dr. G. D. Rochester and Dr. M. L. T. Kannangara for the benefit of several useful discussions and the communication of results prior to publication. Professor M. S. Bartlett suggested the statistical analysis and gave us helpful guidance. One of us (B.L.) is indebted to the Institute of Physics of the University of Zagreb for the provision of a maintenance grant.

References

Amaldi, E., and Fidecaro, G., 1950, *Nuovo Cim.*, **7,** 535.
Amaldi, E., Fidecaro, G., and Mariana, F., 1950, *Nuovo Cim.*, **7,** 553.
Cochran, W. G., 1941, *Ann. Eugen.*, **11,** 47.
Code, F. L., 1941, *Phys. Rev.*, **59,** 229.
Conversi, M. E., Pancini, E., and Piccioni, O., 1945, *Phys. Rev.*, **68,** 232; 1947, *Ibid.*, **71,** 209.
De Juren, J., and Knable, N., 1950, *Phys. Rev.*, **77,** 606.
George, E. P., and Trent, P. T., 1951, *Proc. Phys. Soc.* A, **64,** 1134.
George, E. P., Redding, J. L., and Trent, P. T., 1953, *Proc. Phys. Soc.* (in the press).
Kannangara, M. L. T., and Shrikantia, G. S., 1953, *Phil. Mag.*, **44,** 1091.
Lyman, E. M., Hanson, A. O., and Scott, M. B., 1951, *Phys. Rev.*, **84,** 626.
Olbert, S., 1952, *Phys. Rev.*, **87,** 319.
Rossi, B., and Greisen, K., 1941, *Rev. Mod. Phys.*, **13,** 240.
Sahiar, A., 1951, *Proc. Indian Acad. Sci., Bangalore*, **34,** 201.
Shutt, R. P., 1942, *Phys. Rev.*, **61,** 6; 1946, *Ibid.*, **69,** 26.
Sinha, M. A., 1945, *Phys. Rev.*, **68,** 153.
Snyder, H. S., and Scott. W. T., 1949, *Phys. Rev.*, **76,** 220.
Walker, W. D., 1953, unpublished.
Whittemore, W. L., and Shutt, R. P., 1952, *Phys. Rev.*, **88,** 1312.
Williams, E. J., 1939, *Proc. Roy. Soc.*, **169,** 531.
Wilson, J. G., 1940, *Proc. Roy. Soc.* A, **174,** 73.
Wolfendale, A. W., 1953, *Ph.D. Thesis*, Manchester.

CXVI. *Nuclear Disintegrations caused by* 50–125 MeV *Protons : I*

By P. E. Hodgson
Imperial College of Science and Technology, London, S.W.7*

[Received June 23, 1953]

Summary

The results of measurements on nuclear disintegrations caused by 50–125 MeV protons in photographic emulsion are given. The relative numbers and the angular and energy distributions of the secondary alpha-particles and protons have been found and the collision mean free path for protons in emulsion deduced.

§1. Introduction

In this paper the results of an investigation of the nuclear disintegrations or ' stars ' produced in photographic emulsion by 50–125 MeV protons are presented. They refer to the mixture of elements constituting photographic emulsion, and are consequently difficult to interpret theoretically. In a subsequent paper an attempt to separate the disintegrations into those in the light elements in the emulsion (carbon, nitrogen and oxygen) and those in the heavy (silver and bromine) will be made. Apart from a few general remarks, all theoretical discussion of the results presented here is postponed until that paper.

§2. Experimental Procedure

Ilford C2 Nuclear Research emulsion, 200 microns thick, was exposed to the external proton beam of the Harwell cyclotron. The beam passed through blocks of aluminium of various thicknesses, which reduced its energy from an initial value of 147 MeV to 50, 75, 100 and 125 MeV respectively for the different exposures. The thicknesses of these blocks were calculated using the range–energy curves of Smith (1947) for protons in aluminium. The protons entered the emulsion at an angle of about three degrees and consequently, on the average, they passed through a considerable thickness of emulsion before collision. The average energies of the protons at collision were found from the inclinations of their paths and the rates of energy loss in emulsion to be 45, 68, 94 and 122 MeV respectively. The total spread of the proton energies was about 6 MeV.

The emulsion was sufficiently well developed for the tracks of the incident protons to be visible but the tracks of secondary protons of over 30 MeV could not be found with certainty as they are generally inclined

* Communicated by the Author.

to the plane of the emulsion. The relation between grain density and rate of energy loss was obtained from the tracks of incident protons and from those of stray protons ending in the emulsion. It is shown in fig. 1.

Fig. 1

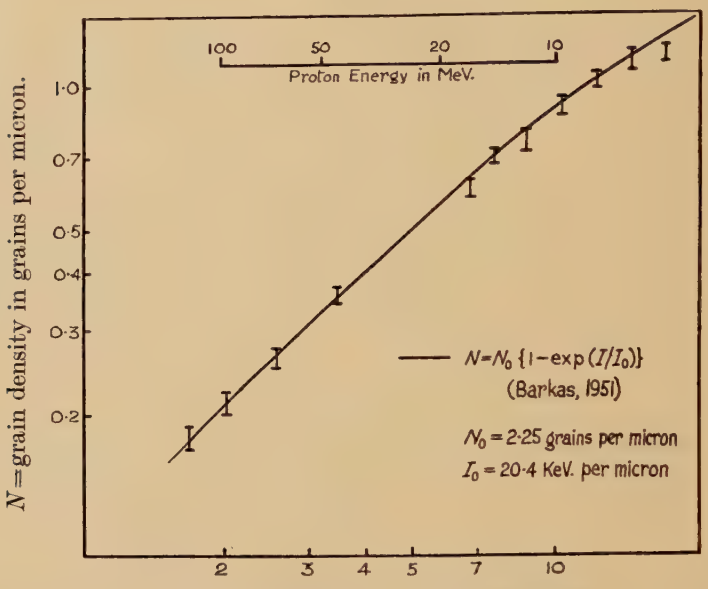

I=rate of energy loss in KeV per micron.

Grain density as a function of rate of energy loss for C2 emulsion.

The emulsion was scanned at high magnification with an oil-immersion objective, and two hundred events found for each energy of incident proton. Events due to collisions between incident protons and hydrogen nuclei in the emulsion were excluded.

§3. The Size Distribution

The distributions of star sizes are given in table 1 for the four energies of incident protons.

Table 1

Proton energy	Number of tracks						
	1	2	3	4	5	6	7
45	38	53	53	49	7	–	–
68	46	63	56	23	10	2	–
94	15	68	70	30	13	4	–
122	18	61	51	44	21	4	1

The mean size M and the standard deviation W of these distributions was calculated for the events with two or more tracks. One-track events

were excluded as the difficulty of finding them makes their frequencies uncertain. These values of M and W are compared with the results of other observers in figs. 2 (a) and (b), and show good agreement.

Fig. 2

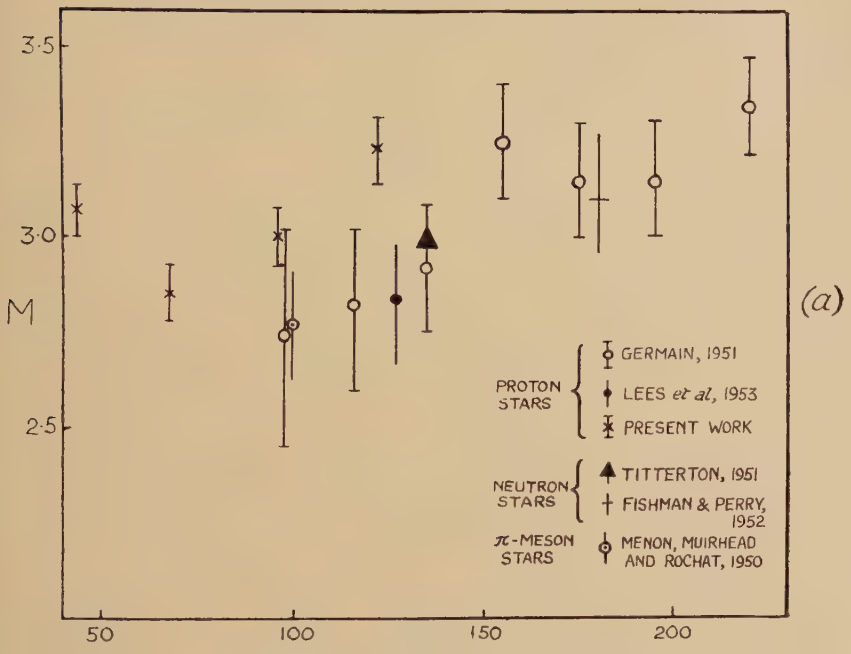

Energy of incident particle in MEV.

Mean star size as a function of energy of incident particle.

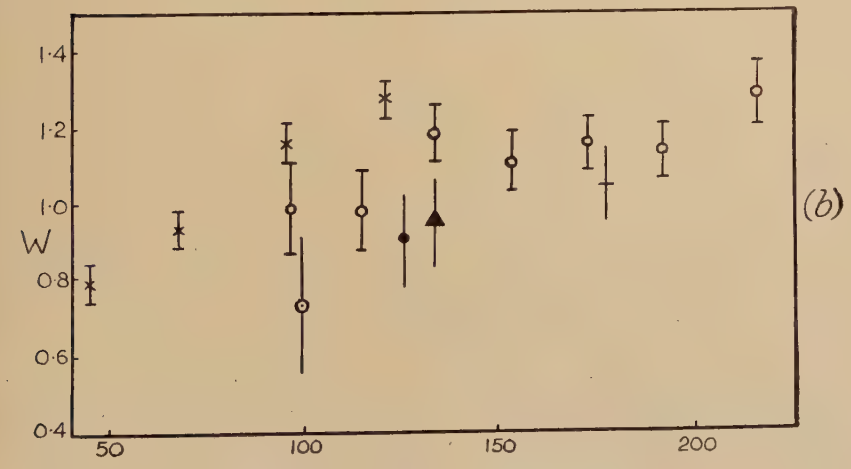

Energy of incident particle in MEV.

Width of size distribution as a function of energy of incident particle.

§4. Energy Distribution of the Secondary Particles

The ranges of all the secondary particles emitted from the nuclear disintegrations and ending in the emulsion were measured, and their

Fig. 3

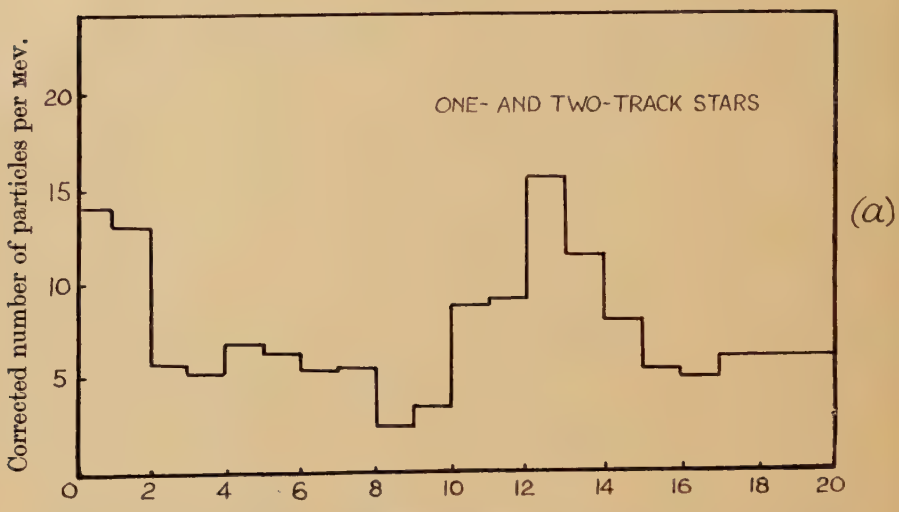

Energy distribution of alpha-particles from one- and two-track stars.

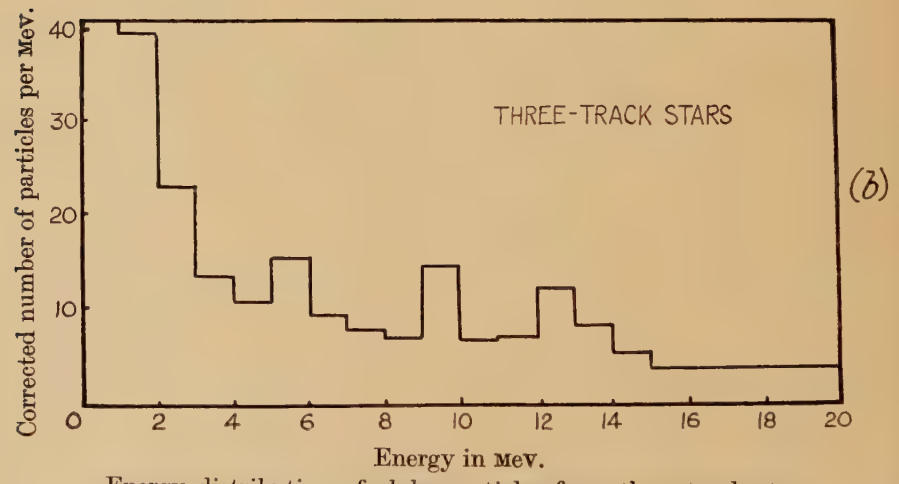

Energy distribution of alpha-particles from three-track stars.

energies found from the range–energy relations. The tracks of alpha-particles were separated from those of protons by inspection. It was not possible to discriminate between protons, deuterons and tritons and so all singly-charged particles were grouped together. Similarly, particles of charge greater than two were grouped with the alpha-particles.

The energy distributions of the alpha-particles are shown in fig. 3 for stars of different sizes for all energies of incident protons. They are grouped in this way rather than as a function of incident proton energy

Fig. 3

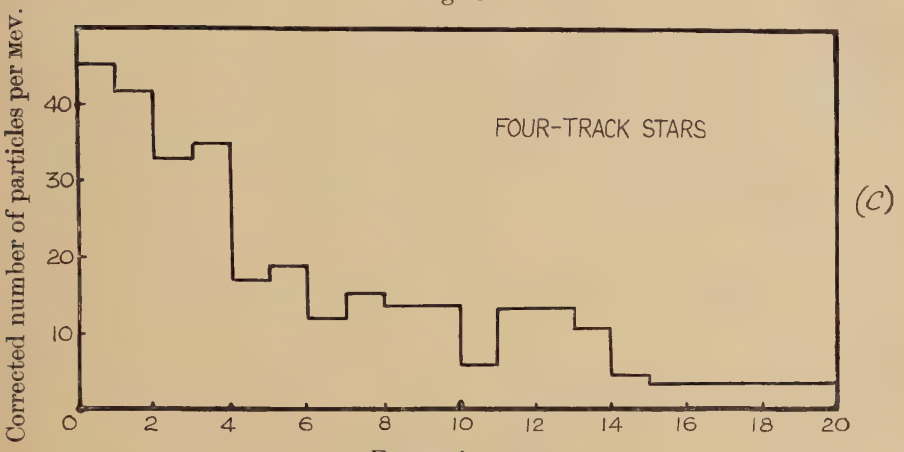

Energy distribution of alpha-particles from four-track stars.

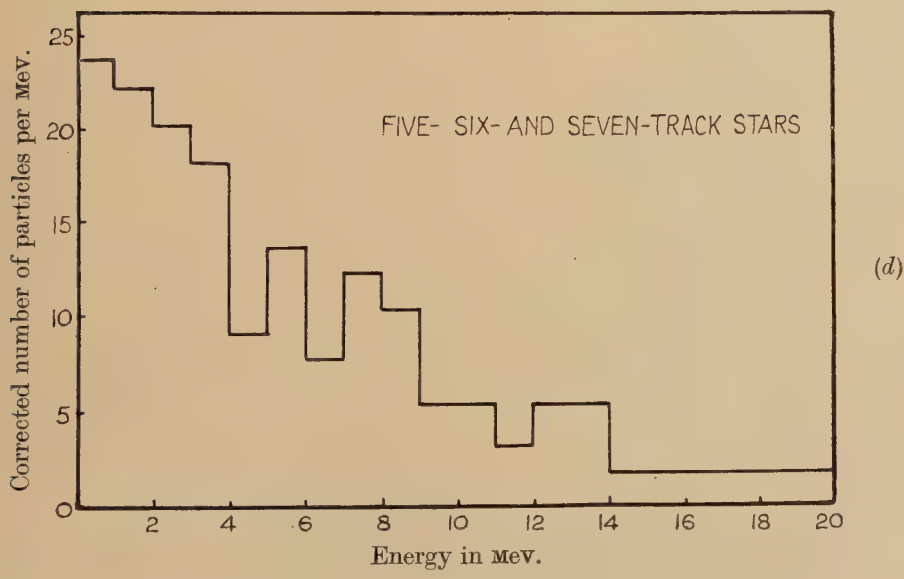

Energy distribution of alpha-particles from five- six- and seven-track stars.

because it was found that the distributions of alpha-particles from stars of various sizes were significantly different from each other while those from stars due to protons of different energies were not. A peak at about 10–15 MeV, which may be interpreted as due to alpha-particles emitted

from the heavy nuclei silver and bromine, is visible in the distribution corresponding to one and two track stars, but not in the others. It is likely that nearly all of the alpha-particles of less than about 9 MeV are emitted from the light elements of the emulsion. If this is so, then fig. 3 shows their energy distributions, apart from superimposed distributions due to alpha-particles from the heavy elements, which are an appreciable fraction of the whole only for the one and two track stars.

The energy distribution of the secondary protons of less than 10 MeV were found to be rather insensitive both to star size and to energy of incident protons. The results for all stars were therefore added together to give the distribution shown in fig. 4.

Fig. 4

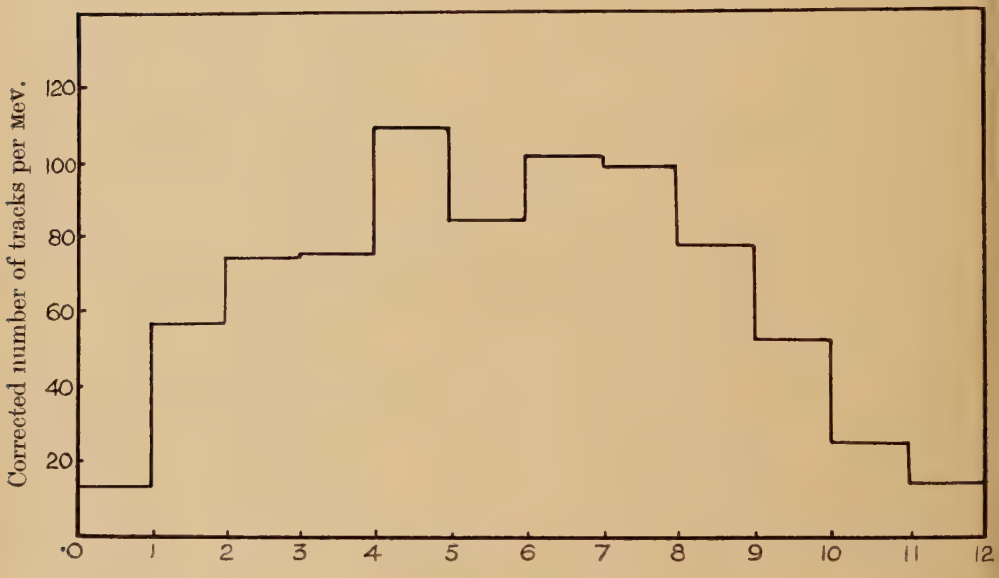

Energy distribution of protons from stars of all sizes.

The usual corrections for particles passing out of the emulsion were made in all cases.

§ 5. The Angular Distribution of the Emitted Particles and the Relative Numbers of Alpha-Particles and Protons

A convenient measure of the angular distribution of the emitted particles is the forward fraction F, which is defined as the fraction of all the emitted particles which go in the forward direction in the laboratory system. This was found as a function of star size for all particles together, and then for the alpha-particles and protons separately and is given in table 2. The fraction P_α of all the emitted particles having charge two or more is also given in the table.

These results are in agreement with those of Seed (1952) who found a forward fraction of 0·79 for all emitted particles from stars produced by 100 MEV protons.

P_α increases sharply from a value 0·28 for one and two-track stars to about 0·55 for three- to seven-track stars. This may be interpreted in the light of previous investigations of the disintegrations caused by cosmic radiation, in which it was shown that P_α for stars in the light elements was about 0·50 and in the heavy about 0·25, if the one and two-track stars are mainly due to disintegration of the heavy elements while all larger stars are mainly due to the light elements. This conclusion is similar to that reached by Lees, Morrison, Muirhead and Rosser (1953) from an examination of disintegrations caused by 130 MEV protons.

Table 2

Star size	F Alpha-particles	F Protons	F All particles	P_α
1	0·77±0·22	0·79±0·13	0·79±0·11	0·28±0·04
2	0·72±0·10	0·62±0·06	0·65±0·05	0·28±0·03
3	0·69±0·07	0·59±0·06	0·63±0·05	0·52±0·04
4	0·71±0·06	0·62±0·07	0·67±0·05	0·61±0·05
5, 6, 7	0·75±0·09	0·76±0·10	0·75±0·06	0·52±0·06

The values of F do not, however, show a corresponding discontinuity, which indicates that the forward collimation of particles from the heavy elements is not markedly different from those from the light elements. This conflicts with the concept of evaporation from heavy nuclei which are moving slowly forward under the impact of the primary particle for, if this were so, the particles from the heavy nuclei would show only a slight forward collimation. It is in agreement with the results of Bernadini, Booth and Lindenbaum (1952) who concluded, from an examination of disintegrations produced by 350 MEV protons, that even the low energy particles from excited heavy nuclei are to a great extent the result of a nuclear cascade and not of an evaporation process.

All tracks shorter than four microns, which are mainly due to the recoil of the residues of heavy nuclei, and also tracks of protons of over 30 MEV, were excluded when F and P_α were computed as the difficulty of finding them makes their frequencies uncertain. These tracks are strongly collimated in the forward direction.

§ 6. The Collision Mean Free Path of Protons in Emulsion

The relative values of the collision mean free paths for production of events of two or more tracks by protons in emulsion were found from the numbers of events of two or more tracks per unit volume of emulsion

and the relative beam currents in the four exposures. These were converted to absolute values by counting the number of tracks of incident protons in the 45 MeV exposure. This could not be done for the other exposures owing to the difficulty of finding all the tracks of high energy protons.

The results are shown in fig. 5 as a function of incident proton energy. The values found in the present experiment are rather lower than those of Germain. This is possibly because more short tracks due to recoil

Fig. 5

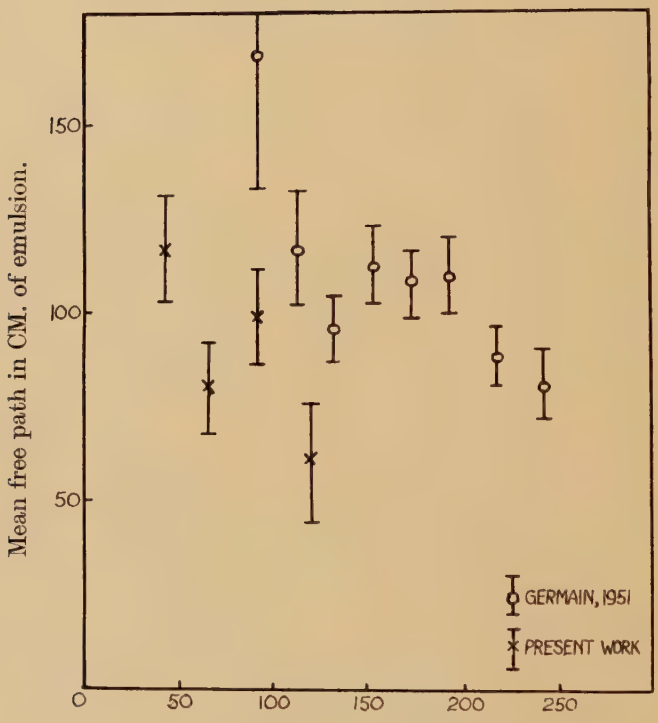

Mean free path for protons in emulsion producing events of two or more tracks.

fragments were observed in the fine grain C2 emulsion used here than in the G5 emulsion used by Germain. As a result, more events are counted as two-track stars, resulting in a lower mean free path.

Lees *et al.* (1953) have pointed out that mean free paths found by ' area ' scanning tend to be considerably longer than those found by the more accurate ' track ' scanning and they attribute this to the difficulty of making properly overlapping scans when using high power objectives with very small fields of view. This effect also could account for some of the discrepancy between the present results and those of Germain.

ACKNOWLEDGMENTS

I would like to thank the Director of the Atomic Energy Research Establishment, Harwell, for permission to work there, Dr. D. M. Skyrme, Dr. J. M. Cassels and the Harwell cyclotron operators for assistance during the exposures, Dr. A. J. Herz for developing the plates, and the Department of Scientific and Industrial Research for a Senior Research Award.

REFERENCES

BARKAS, W. H., 1951, *Colloque sur la Sensibilite des Cristaux et des Emulsions Photographiques* (Paris), p. 316.
BERNARDINI, G., BOOTH, E. T., and LINDENBAUM, S. J., 1952, *Phys. Rev.*, **85,** 826.
FISHMAN, H., and PERRY, A. M., 1952, *Phys. Rev.*, **86,** 167.
GERMAIN, L. S., 1951, *Phys. Rev.*, **82,** 596.
LEES, C. F., MORRISON, G. C., MUIRHEAD, H., and ROSSER, W. G. V., 1953, *Phil. Mag.*, **44,** 304.
MENON, M. G. K., MUIRHEAD, H., and ROCHAT, O., 1950, *Phil. Mag.*, **41,** 583.
SEED, R. G., 1952, *Phys. Rev.*, **87,** 182.
SMITH, J. H., 1947, *Phys. Rev.*, **71,** 32.
TITTERTON, E. W., 1951, *Phil. Mag.*, **42,** 109.

CXVII. *A Stochastic Problem Relating to Counters*

By Alladi Ramakrishnan and P. M. Mathews
Department of Physics, University of Madras*

[Received May 18, 1953]

Summary

The probability distribution function $\pi(n, t)$ of the number of registered events n in a time interval t for a counter in the case when the registered and unregistered events are followed by different dead times, is derived by using the method of product densities formulated recently by one of us (R.).

§ 1. Statement of the Problem

A counter is supposed to register random events such that the probability of an event in any small interval of time of length Δt (Δt is an infinitesimal quantity) independently of previous events is $\alpha\Delta t+O(\Delta t)^2$, or simply Δt (provided we choose the unit of time suitably). The probability that exactly n events occur during a time interval of length t is given by the Poisson law $e^{-t}(t^n/n!)$. Due to resolving time, the counter is unable to register all events. It is customary to treat two cases :—

Type I.—After each registration the counter is locked for a constant time a. An event is registered if and only if no registration has taken place during a time a preceding it.

Type II.—The counter registers an event if and only if no event has occurred during the preceding time interval of length, a. Here an event occurring at a moment when the counter is locked prolongs the inoperative period. In theory the counter can remain locked indefinitely.

In a more general type of counter we assume the registered and unregistered events are followed by two different ' dead times ', a and b respectively.

The problem is to determine $\pi(n, t)$, the probability that n events are registered in time t. While this has been solved in the case of counters type I and type II (Feller 1948), the authors have not seen any derivation of $\pi(n, t)$ in the case of a general type counter, though this problem was discussed by Klemens (1948). In this paper we shall derive an exact expression for $\pi(n, t)$ by using a technique developed recently by one of us (R.). We shall first formulate the method in a general manner and apply it to the problem of counters.

* Communicated by the Authors.

§ 2. The Formulation of the Method.

Recently one of us (R.) has formulated* a ' theory of product densities ' in connection with stochastic problems where we have to deal with a stochastic variable representing the number of ' particles ' distributed in a continuous infinity of states characterized by a parameter. The word ' particle ' was used merely to facilitate the understanding of the problem, but the method developed is quite general and can be used in a wide variety of problems involving the statistical distribution of a discrete number of ' particles ' or ' entities ' in a continuous infinity of states.

Consider events occurring along the time axis. We can define product-densities of events along the time axis. Let the product density of degree n of events be $f_n(t_1, t_2, \ldots, t_n)$. Then according to the theory of product densities $f_n(t_1, t_2, \ldots, t_n)\, dt_1, dt_2, \ldots dt_n$ represents the probability that an event occurs in the interval between t_1 and t_1+dt_1, one event between t_2 and $t_2+dt_2, \ldots$, and one between t_n and t_n+dt_n irrespective of the occurrence of events elsewhere. Let us assume we deal with a class of product densities defined by

$$f_n(t_1, t_2, \ldots, t_n)=f_1(t_1)f_1(t_2-t_1)\ldots f_1(t_n-t_{n-1}), \quad \ldots \quad (1)$$

provided $t_1, t_2, \ldots, t_n$ are ordered $(t_1<t_2<t_3<\ldots<t_n)$† where f_1 is the product density of degree one. This represents a class of stochastic processes examples of which are easily found. For instance

1. Poisson events (a trivial example),
2. Electron counter problems,
3. ' Renewal ' problems,

can be cited as illustrative of such processes.

If $\pi(n, t)$ represents the probability that n events have occurred in time t, what happens between t and $t+dt$ is not only dependent on the fact that n events have occurred in time t but upon the ' prehistory '—i.e., when the last event happened. Hence the usual method of expressing $\pi(n, t+dt)$ in terms of $\pi(n, t)$ is unsuitable for such problems. We shall show that the product density technique or the method of regeneration points yields the required results.

A. Product Density Approach

Let $G(u, t)$ be the generating function corresponding to $\pi(n, t)$ and by a result proved in a previous paper ‡

---

* For a complete formulation of the theory, see Alladi Ramakrishnan, 1950, *Proc. Camb. Phil. Soc.*, **46**, 595 ; 1952, *Ibid.*, **48**, 451.

† If $t_1, t_2, \ldots, t_n$ are not ordered, f_n still exists. f_n is a product density and hence is symmetrical in the variables $t_1, t_2, \ldots, t_n$. We can therefore order them and then apply (1).

‡ Alladi Ramakrishnan, 1952, *Proc. Camb. Phil. Soc.*, **48**, 451.

$$\frac{\partial^n G(u,t)}{\partial t^n} = \int_0^t dt_n \int_0^t dt_{n-1} \cdots \int_0^t f_n(t_1, t_2, \ldots, t_n)\, dt_1.$$

Since f_n is symmetrical in $t_1, t_2, \ldots, t_n$ we can write the above as

$$n! \int_0^t dt_n \int_0^{t_n} dt_{n-1} \int_0^{t_{n-1}} dt_{n-2} \cdots \int_0^{t_2} f_n(t_1, t_2, \ldots, t_n)\, dt_1$$

$$= n! \int_0^t dt_n \int_0^{t_n} dt_{n-1} \cdots \int_0^{t_2} f_1(t_1) f_1(t_2 - t_1) \cdots f_1(t_n - t_{n-1})\, dt_1. \quad . \quad (2)$$

Let the Laplace Transform* (L.T.) with respect to the variable t of the function $f_1(t)$ be $\psi(s) = \int_0^\infty e^{-st} f_1(t)\, dt$.

Then since $$\left[\frac{\partial G(u,t)}{\partial u}\right]_{u=1} = \int_0^t f_1(\tau)\, d\tau,$$

the L.T. of $$\left[\frac{\partial G(u,t)}{\partial u}\right]_{u=1} \text{ is } \frac{\psi(s)}{s} \quad . \quad . \quad . \quad . \quad . \quad . \quad . \quad . \quad . \quad (3)$$

and of $$\left[\frac{\partial^n G(u,t)}{\partial u^n}\right]_{u=1} \text{ is } n! \frac{[\psi(s)]^n}{s!} . \quad . \quad . \quad . \quad . \quad . \quad . \quad . \quad (4)$$

If $g(u, s)$ be the L.T. of $G(u, t)$

$$g(u,s) = \frac{1}{s} \cdot \frac{1}{1-(u-1)\,\psi(s)} . \quad . \quad . \quad . \quad . \quad . \quad . \quad (5)$$

If $p(n, s)$ is the L.T. of $\pi(n, t)$

$$p(n,s) = \frac{1}{s} \frac{[\psi(s)]^n}{[1+\psi(s)]^{n+1}} . \quad . \quad . \quad . \quad . \quad . \quad . \quad . \quad (6)$$

In any stochastic problem of this type we must determine either $\psi(s)$ or $f_1(t)$.

B. Approach by the 'Method of Regeneration Points'

Let us consider the above class of stochastic processes from the point of view of the method of regeneration points. The relation (1) between the product densities of degree 1 and n is equivalent to stating that if we are given that an event occurred at $t=0$, the probability that an event occurs between t and $t+dt$ (whether or not an event occurred between 0 and t) is determined by the function $f_1(t)\, dt$ and is independent of what happened before $t=0$. It also follows that, given an event happened at $t=0$, the probability that the *next* event happens between t and $t+dt$ is also independent of what happened before $t=0$. The probability can be expressed by the function $(-\partial\phi(t)/\partial t)dt$ where $\phi(t)$ represents the probability that no event occurs between 0 and t given that an event occurred at $t=0$. Usually $\phi(t)$ can be expressed as $\exp\left[-\int_0^t \alpha(\tau)\, d\tau\right]$ where $\alpha(\tau)\, d\tau$ has the obvious meaning of the probability that an event occurs between τ and $\tau+d\tau$ *given that* no event occurred between 0 and τ and that an event

* In this paper, L.T. means Laplace Transform.

occurred at $t=0$. According to the method of regeneration points we at once write the integral equation

$$\pi(n, t)=-\int_0^t \pi(n-1, t-\tau)\,\phi'(\tau)\,d\tau+\delta(n)\,\phi(t), \quad . \quad . \quad . \quad (7)$$

where $\phi'(\tau)=\partial\phi(\tau)/\delta\tau$ and $\delta(n)=1$ for $n=0$ and zero otherwise . . . (8)

$$G(u, t)=-\int_0^t u\,G(u, t-\tau)\,\phi'(\tau)\,d\tau+\phi(t),$$

$$g(u, s)=-g(u, s)(s\sigma(s)-1)\,u+\sigma(s), \quad . \quad . \quad . \quad . \quad . \quad . \quad . \quad . \quad . \quad (9)$$

where $\sigma(s)$ is the L.T. of $\phi(t)$

$$g(u, s)=\frac{\sigma(s)}{1+u(s\sigma(s)-1)}. \quad . \quad . \quad . \quad . \quad . \quad . \quad . \quad (10)$$

Also $$\left[\frac{\partial g(u, s)}{\partial u}\right]_{u=1}=\frac{\psi(s)}{s}=\frac{1}{s}\cdot\frac{1-s\sigma(s)}{s\sigma(s)} \quad . \quad . \quad . \quad . \quad . \quad (11)$$

or $$\sigma(s)=\frac{1}{s}\cdot\frac{1}{1+\psi(s)}. \quad . \quad . \quad . \quad . \quad . \quad . \quad . \quad (12)$$

Thus $$g(u, s)=\frac{1}{1-(u-1)(1+\psi(s))}, \quad . \quad . \quad . \quad . \quad (13)$$

a result derived by the product density method.

Thus $p(n, s)$ the L.T. of $\pi(n, t)$ is

$$\frac{1}{s}\cdot\frac{[\psi(s)]^n}{[1+\psi(s)]^{n+1}}=\sigma(s)\,(1-s\sigma(s))^n. \quad . \quad . \quad . \quad . \quad . \quad (14)$$

In any stochastic problem we must determine $\sigma(s)$ or $\psi(s)$ i.e., $\phi(t)$ or $f_1(t)$ in order to obtain $p(n, s)$, i.e., $\pi(n, t)$. We shall now apply the above results to the problem relating to counters.

§ 3. The Solution of the Counter Problem

In the following discussion we assume (i) that the initial condition is specified as follows: At $t=0$ an event is registered. We require the probability $\pi(n, t)$ that n events are registered in time t. Omitting the initial event

$$\pi(n, t)=0 \text{ at } t=0 \text{ for } n\neq 0,$$

$$\pi(0, 0)=1,$$

(ii) that $\phi(t)$ represents the probability that no event is registered in time t,

(iii) that $f_1(t)$ represents the product density of degree one of registered events.

For type I counter it is more easy to compute $\phi(t)$ rather than $f_1(t)$.

$$\phi(t)=e^{-(t-a)} \text{ for } t>a$$

$$\phi(t)=1 \qquad \text{for } t<a$$

L.T. of $\phi(t)$ is

$$\sigma(s)=\frac{1}{s}-\frac{e^{-as}}{s(s+1)}. \quad . \quad . \quad . \quad . \quad . \quad . \quad . \quad . \quad . \quad . \quad (15)$$

L.T. of $\pi(n, t)$, the probability that n registrations occur in time t is

$$\sigma(s)(1-\sigma(s)\,.\,s)^n = \frac{e^{-nas}}{(s+1)^n}\left[\frac{1}{s} - \frac{e^{-as}}{s(s+1)}\right]$$
$$= \frac{1}{s}\left[\frac{e^{-nas}}{(s+1)^n} - \frac{e^{(n+1)as}}{(s+1)^{n+1}}\right],$$

Thus $$\frac{\partial\pi(n, t)}{\partial t} = H(t-na)\, e^{-(t-na)}\frac{(t-na)^{n-1}}{(n-1)!} - H(t-(n+1)a)\, e^{-(t-(n+1)a)} \times \frac{(t-(n+1)a)^n}{n!}$$

$$\pi(n, t) = \int_0^{t-na} \frac{e^{-t}t^{n-1}}{(n-1)!}\,dt - \int_0^{t-(n+1)a} \frac{e^{-t}t^n}{n!}\,dt, \quad . \ . \ . \ . \ . \quad (16)$$

where H is the Heaviside unit function, i.e.,

$$H(x)=1 \text{ if } x>0, \quad H(x)=0 \text{ if } x<0.$$

For the counter of type II it is easy to calculate $f_1(t)$ the product density of the first degree relating to registered events.

$$f_1(t)\,dt = H(t-a)\, e^{-a}\,dt, \quad . \ . \ . \ . \ . \ . \ . \ . \quad (17)$$

where H is the Heaviside unit function. The above expression results from arguing that an event is recorded when it is not preceded by an event in time interval a and is not also preceded by the event occurring at $t=0$ within a time interval a. Thus

$$\psi(s) \text{ the L.T. of } f_1(t) = \frac{1}{s\, e^{a(s+1)}}. \quad . \ . \ . \ . \ . \ . \quad (18)$$

And this yields

$$G(u, t) = 1 + \frac{(u-1)\, e^{-a}\,(t-a)}{1!} + \ldots\ldots + \frac{(u-1)^N\, e^{-Na}\,(t-Na)^N}{N!} \quad . \quad (19)$$

where N is a number such that $(N+1)\,a>t>Na$

$$\pi(n, t) = \sum_{m=n}^{m=N} (-1)^{m-n} \binom{m}{n} \frac{e^{-ma}}{m!}\,(t-ma)^m \quad . \ . \ . \ . \quad (20)$$

a result derived in a previous paper.*

We can now derive the L.T. of $\pi(n, t)$ when it represents the probability of n registrations occurring in time t for a *more general type of counter* in which the registered and unregistered events are followed by two different ' dead times ', a and b respectively. We proceed as follows :

At $t=0$ an event is registered ; we ask : what is the probability $\phi(t)$ that no event is registered up to time t ? Let us assume $a>b$. We can write $\phi(t)$ as

$$\phi(t) = \{H(t)-H(t-(a-b))\} + \phi^{II}(t-(a-b))\, H(t-(a-b)). \quad . \quad (21)$$

The first part expresses the condition that no event is registered for $t<a-b$. $\phi(t)=1$ for $t<a-b$.

---

* Alladi Ramakrishnan, 1951, *J. Roy. Stat. Soc.* B, **13**, 131.

$\phi^{II}(t-(a-b))$ represents the probability that no event is registered in time $(t-(a-b))$ on the hypothetical assumption that we are dealing with a counter of type II with dead time b. As has been previously mentioned, for type II counter we do not usually compute $\phi^{II}(t)$ but only $f_1^{II}(t)$, the product density of registered events of a type II counter with dead time b. But the L.T.'s of $\phi^{II}(t)$ and $f_1^{II}(t)$ are connected by the relation (12). Thus

$$\text{L.T. of } \phi(t)=\text{L.T. of } \{H(t)-H(t-(a-b))\} + \text{L.T. of } \{\phi^{II}(t-(a-b))\} \quad . \quad . \quad . \quad . \quad . \quad . \quad (22)$$

We know that the L.T. of $f_1^{II}(t)$ is

$$\frac{1}{s\, e^{b(s+1)}}.$$

Thus we have L.T. of $f_1(t)$ the product density of registered events of the generalized type of counter given by

$$\psi(s)=\frac{1}{s\, e^{as+b}+e^{(a-b)s}-1}. \quad . \quad . \quad . \quad . \quad . \quad . \quad (23)$$

Put $b=0$ we get counter type I.

Put $a=b$ we get counter type II.

Put $a=b=0$ we get a Poisson distribution for $\pi(n, t)$ characteristic of an ideal counter.

The same result is obtained for $b>a$ following exactly the same arguments.

We have, for the L.T. of $\pi(n, t)$ for general a and b, the expression

$$\frac{1}{s}\frac{[\psi(s)]^n}{[1+\psi(s)]^{n+1}}=\frac{1}{s}(s\, e^{as+b}+e^{(a-b)s})^{-(n+1)}\,(s\, e^{as+b}+e^{(a-b)s}-1). \quad . \quad (24)$$

Taking the inverse

$$\pi(n, t)=\frac{1}{2\pi i}\int_{\sigma-i\infty}^{\sigma+i\infty}\left[\frac{1}{s}(s\, e^{as+b}+e^{(a-b)s})^{-n}-\frac{1}{s}(s\, e^{as+b}+e^{(a-b)s})^{-(n+1)}\right]e^{st}ds. \quad . \quad . \quad . \quad (25)$$

$$\text{Since } \frac{1}{s}(s\, e^{as+b}+e^{(a-b)s})^{-n}=\frac{1}{s}(s\, e^{as+b})^{-n}\left\{1+\frac{e^{-b(s+1)}}{s}\right\}^{-n}$$

$$=\frac{1}{s}(s\, e^{as+b})^{-n}\sum_{r=0}^{\infty}(-1)^r\binom{n+r-1}{r}\frac{e^{-rb(s+1)}}{s^r},$$

$$\pi(n, t)=\frac{1}{2\pi i}\int_{\sigma-i\infty}^{\sigma+i\infty}\sum_{r=0}^{\infty}ds\left\{e^{-(n+r)b}(-1)^r\binom{n+r-1}{r}\frac{e^{s(t-na-rb)}}{s^{n+r+1}}-e^{-(n+r+1)b}\right.$$

$$\left.\times(-1)^r\binom{n+r}{r}\frac{e^{s(t-(n+1)a-rb)}}{s^{n+r+2}}\right\}. \quad . \quad . \quad . \quad . \quad . \quad . \quad . \quad . \quad . \quad . \quad (26)$$

Remembering that

$$\frac{1}{2\pi i}\int_{\sigma-i\infty}^{\sigma+i\infty}\frac{e^{sz}}{s^n}ds=\frac{z^{n-1}}{(n-1)!}\text{ for } z>0, \text{ and zero for } z<0, \quad . \quad . \quad (27)$$

we get

$$\pi(n, t)=\sum_{r=0}^{N_1}(-1)^r\binom{n+r-1}{r}\frac{(t-na-rb)^{n+r}}{(n+r)!}e^{-b(n+r)}$$

$$-\sum_{r=0}^{N_2}(-1)^r\binom{n+r}{r}\frac{(t-(n+1)a-rb)^{n+r+1}}{(n+r+1)!}e^{-b(n+r+1)} \quad . \quad . \quad (28)$$

where N_1, N_2 are integers such that

$$\frac{t-na}{b}-1<N_1<\frac{t-na}{b} \text{ and } \frac{t-(n+1)a}{b}-1<N_2<\frac{t-(n+1)a}{b}.$$

Particular cases of the above solution for $b=0$, and for $a=b$ agree with those already given.

When $a\neq 0$, $b\neq 0$, we note that $\pi(n, t)$ is given by a finite series ; also $\pi(n, t)\equiv 0$ if $na>t$. Hence the moments of n are calculated from the definition

$$\overline{n^r}=\sum_{r=0}^{\infty} n^r\pi(n, t)=\sum_{r=0}^{N} n^r\pi(n, t) \quad \text{where } N$$

is an integer such that $(N+1)a>t>Na$. . . . . (29)

References

Feller, W., 1948, *Courant Anniversary Volume*, 105–115.
Klemens, P. G., 1948, *Phil. Mag.*, **39**, 656.

CXVIII. *The Onset of Convection by Thermal Instability in Spherical Shells—(A Correction)*

By S. Chandrasekhar, F.R.S.
Yerkes Observatory, University of Chicago*

[Received July 6, 1953]

In a paper (Chandrasekhar 1953) recently published in this Magazine, the author has considered the criterion for the onset of convection by thermal instability in spherical shells and has described a variational procedure for solving the underlying characteristic value problem. Unfortunately in the numerical evaluation of the final results an error has occurred due to the oversight that $\mathscr{C}'_{l+1/2}(\alpha_j)$ and $\mathscr{C}'_{l+1/2}(\alpha_j\eta)$ which occur in equations (21), (22) and the subsequent ones are not the same as those defined in equations (14) and (15) : actually in equations (21) and (22) (and in all later ones) $\mathscr{C}'_{l+1/2}(\alpha_j)$ and $\mathscr{C}'_{l+1/2}(\alpha_j\eta)$ are $1/\alpha_j$ times the values given in equations (14) and (15).

Table 1. The Characteristic Numbers C_l for Various Values of l and η

l	$\eta=0{\cdot}2$	$\eta=0{\cdot}4$	$\eta=0{\cdot}5$	$\eta=0{\cdot}6$	$\eta=0{\cdot}8$
1	$4{\cdot}999\times10^3$	$1{\cdot}682\times10^4$	$4{\cdot}188\times10^4$	$1{\cdot}403\times10^5$	$7{\cdot}789\times10^6$
2	$5{\cdot}696\times10^3$	$1{\cdot}091\times10^4$	$2{\cdot}181\times10^4$	$6{\cdot}133\times10^4$	$2{\cdot}753\times10^6$
3	$8{\cdot}881\times10^3$	$1{\cdot}196\times10^4$	$1{\cdot}924\times10^4$	$4{\cdot}424\times10^4$	$1{\cdot}500\times10^6$
4	$1{\cdot}400\times10^4$	$1{\cdot}585\times10^4$	$2{\cdot}146\times10^4$	$4{\cdot}076\times10^4$	$1{\cdot}005\times10^6$
5	$2{\cdot}121\times10^4$	$2{\cdot}227\times10^4$	$2{\cdot}673\times10^4$	$4{\cdot}313\times10^4$	$7{\cdot}656\times10^5$
6		$3{\cdot}143\times10^4$	$3{\cdot}492\times10^4$	$4{\cdot}945\times10^4$	$6{\cdot}368\times10^5$
7		$4{\cdot}365\times10^4$	$4{\cdot}629\times10^4$	$5{\cdot}933\times10^4$	$5{\cdot}651\times10^5$
8			$6{\cdot}125\times10^4$	$7{\cdot}292\times10^4$	$5{\cdot}270\times10^5$
9			$8{\cdot}027\times10^4$	$9{\cdot}057\times10^4$	$5{\cdot}109\times10^5$
10			$1{\cdot}039\times10^5$	$1{\cdot}128\times10^5$	$5{\cdot}104\times10^5$
11			$1{\cdot}325\times10^5$	$1{\cdot}401\times10^5$	$5{\cdot}223\times10^5$
12			$1{\cdot}669\times10^5$	$1{\cdot}732\times10^5$	$5{\cdot}448\times10^5$
13			$2{\cdot}074\times10^5$	$2{\cdot}126\times10^5$	$5{\cdot}767\times10^5$
14			$2{\cdot}549\times10^5$	$2{\cdot}590\times10^5$	$6{\cdot}178\times10^5$
15			$3{\cdot}099\times10^5$	$3{\cdot}131\times10^5$	$6{\cdot}678\times10^5$

The corrected values of C_l are given in table 1 ; this table replaces table 1 of the paper to which reference has been made. The dependence of C_l on l and η is illustrated in fig. 1 ; it will be noticed that this figure does not have the unsatisfactory feature of the figure based on the erroneous calculations : the curves for the different η's do not cross but lie systematically one above the other.

The principal conclusions of the paper are not affected by this correction.

* Communicated by the Author.

Fig. 1

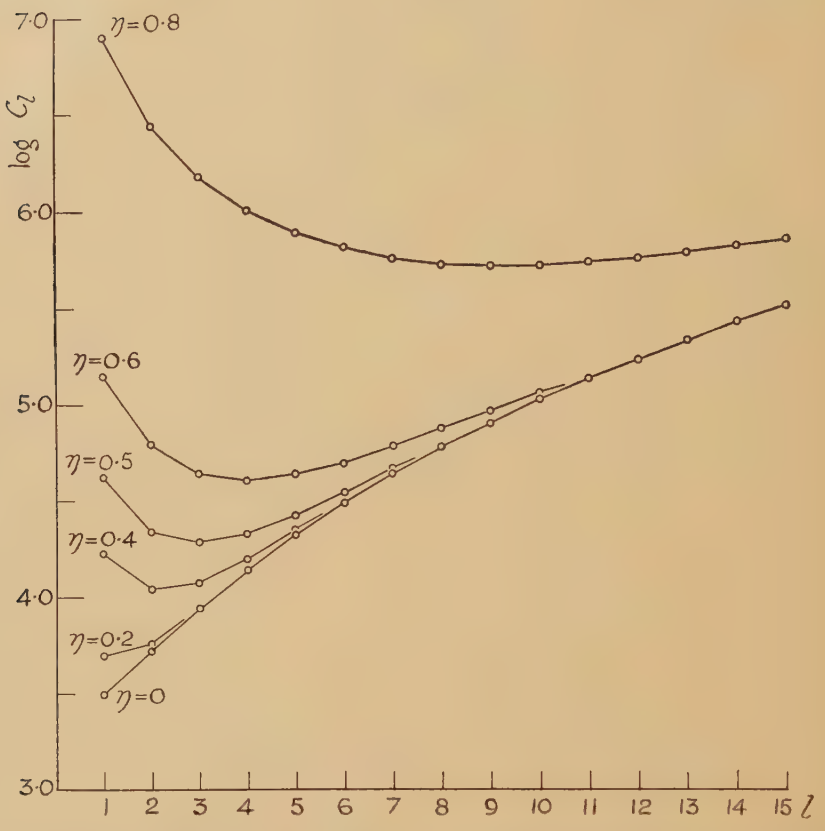

The criterion (C_l) for the onset of convection in the mantle as a spherical harmonic disturbance of order l for various thicknesses of the mantle. The different curves are distinguished by the values of the fraction (η) of the radius of the sphere occupied by the inviscid core.

Reference

Chandrasekhar, S., 1953; *Phil. Mag.* [7], **44**, 233.

CXIX. *Spallation of Vanadium, Manganese, and Cobalt with* 187 MeV *Protons*

By S. G. Rudstam
The Gustaf Werner Institute for Nuclear Chemistry, University of Uppsala, Uppsala, Sweden*

[Received June 17, 1953]

Summary

This paper describes measurements of the yield of various spallation products from vanadium, manganese, and cobalt. From the experiments it is concluded that in the spallation of medium weight elements with high energy protons, the total cross section per mass number decreases almost exponentially with increase in the difference between the actual mass number and the mass number of the target nucleus. It is also concluded that for a given mass number the cross sections of the isobars are approximately represented by a Gaussian distribution.

§ 1. Introduction

A reaction in which a high energy particle hits a nucleus and knocks out a number of low mass particles from the nucleus is called a spallation reaction. If the residual nucleus is radioactive, it is often possible to measure its yield and so determine the cross section for the spallation reaction, which gives this residual nucleus. The purpose of the present investigation was to determine the cross section distribution, i.e. how the total reaction cross section was distributed among the product nuclides.

Previous spallation investigations of medium weight elements have been carried out for arsenic with 180 MeV deuterons (Hopkins and Cunningham 1948), copper with 340 MeV protons, 180 MeV deuterons, and 380 MeV alpha particles (Batzel, Miller and Seaborg 1951, Miller, Thompson and Cunningham 1948), copper with 400 MeV neutrons (Marquez 1952), cobalt with 240 MeV protons (Wagner and Wiig 1952), iron with 340 MeV protons (Rudstam, Stevenson and Folger 1952).

Ideally a spallation investigation should be carried out with a single isotope target. For this reason vanadium, manganese and cobalt were chosen as target materials for the present experiments, although the vanadium target contained 0·25% of ^{50}V.

* Communicated by T. Svedberg.

§ 2. Experimental

(*a*) *Procedure*

The target materials were analysed chemically (V, Mn, Co) and spectroscopically (V). The analyses did not show any impurities likely to interfere with the measurements.

Table 1

Element	Main purification method	Weighed as
Cr	Extraction of perchromic acid with diethyl ether.	$BaCrO_4$
V	Precipitation with cupferron. Extraction with cupferron and chloroform.	V_2O_5
Ti	Precipitations with potassium iodate and with cupferron.	TiO_2
Sc	Extraction from 50% potassium thiocyanate solution with diethyl ether.	Sc_2O_3
Ca	Precipitation with oxalic acid.. Destruction of the oxalate and hydroxide-scavenge.	$CaC_2O_4 . H_2O$
K	Hydroxide-, sulphide-, and oxalate-scavenges. Precipitation with perchloric acid.	$KClO_4$
Cl	Distillation of hydrogen chloride. Precipitation of silver chloride.	AgCl
S	Precipitation of barium sulphate, which was dissolved in a saturated potassium carbonate solution.	$BaSO_4$
P	Precipitations with molybdic acid and with magnesia mixture.	$Mg_2P_2O_7$
Si	Carrier : ammonium fluosilicate. Precipitation of silicic acid with boric acid. Dissolution in alkali.	SiO_2
Mg	Precipitation with diammonium ortho-phosphate.	$Mg_2P_2O_7$
Na	Hydroxide-, sulphide-, and oxalate-scavenges. Precipitation with zink uranyl acetate. Precipitation of sodium chloride with alcohol saturated with hydrogen chloride.	NaCl

The targets were bombarded with 187 Mev protons in the circulating beam of the Uppsala synchrocyclotron. After irradiation the target was dissolved in nitric acid containing carriers for the elements to be studied

in the experiment. The carriers were then separated and purified very carefully, and finally precipitated in a form suitable for gravimetric analysis. The precipitate was spread as uniformly as possible on a weighed aluminium or platinum dish (diameter 13 mm) and then dried or ignited. The dish was weighed again and mounted on a small aluminium holder for particle counting.

An end-window Geiger–Müller counter in an ordinary lead house set-up was used for counting the activity present.

The separation and purification methods used are indicated in table 1.

(*b*) *Bombardments*

A summary of the bombardments is given in table 2.

Table 2

Bombardment No.	Duration of bombardment (min)	Elements isolated
V 1	57	Cr, V, Ti
V 2	80	Cl
V 3	60	Cr, Ti, Ca, K
V 4	61	V, Sc, Cl, S, P, Si
V 5	52	K, S
V 6	20	V, Ti, Sc, Si
V 7	31	Cr, V, Sc, P, Na
V 8	9	V, Ti, Mg
V 9	5	V
V 10	60	V, Ca, Cl, S, P, Na
V 11	10	V
V 12	10	V, Cl
Mn 1	143	Ti, Ca, Cl, P
Mn 2	61	Ti, K
Mn 3	65	Ti, Sc, Ca, K, S
Mn 4	76	Cr, P, Si
Co 1	60	Cr, V, Ti, Sc, K, P, Si

In most of the vanadium bombardments the nuclide ^{48}V was used as a monitor. The absolute cross section of this monitor was determined by comparing the yield of it with the yield of ^{24}Na from an aluminium foil covering the same area as the target. The cross section for the reaction ^{27}Al (p, 3pn)^{24}Na was taken to be 10·8 millibarn (Stevenson and Folger). The nuclide ^{45}Ti was chosen as a monitor in the manganese bombardments.

§ 3. Results

The cross sections were computed from the measured data in the usual way. Corrections had to be applied to the counting rates for coincidence losses, background activity, geometrical differences, absorption in the window and in the air between the sample and the window, backscattering, self-absorption and self-scattering, counting efficiency,

chemical yield, and decay (Burtt 1949). The correction factors for the backscattering were obtained from the papers by Burtt (1949) and by Yaffe and Justus (1949). A smaller correction factor was used for positrons than for electrons (Seliger 1952). The correction factors for self-absorption and self-scattering were estimated from the work of Nervik and Stevenson (1952).

Owing to the great number of corrections which had to be applied, very accurate results were not to be expected. The measured cross sections were estimated to be accurate to 50%.

The cross sections for the spallation of vanadium, manganese, and cobalt are listed in the tables 3, 4 and 5 respectively. The cross sections in table 3 and table 4 are, with few exceptions weighted means of 2–4 determinations.

Table 3. Spallation of Vanadium

Nuclide	Cross section (mb)	Nuclide	Cross section (mb)
^{49}Cr	1·8	^{43}K	2·5
^{48}Cr	0·23*	^{42}K	3·9
^{48}V	28	^{39}Cl	0·30
^{47}V	5·7	^{38}Cl	0·74
^{45}Ti	6·1	^{34}Cl	0·031
^{48}Sc	4·8	^{35}S	0·61
^{47}Sc	10	^{33}P	0·32
^{46}Sc	20	^{32}P	0·34
^{44}Sc^{m}	8·4	^{31}Si	0·18
^{43}Sc+^{44}Sc	13	^{27}Mg	0·028
^{47}Ca	0·11	^{24}Na	0·030
^{45}Ca	3·6	^{22}Na	0·07†

* Computed from the amount of ^{48}V formed.
† Uncertain since the activity of ^{22}Na was low.

It is difficult to separate the chlorine isotopes by particle counting since their half-lives are nearly the same. The cross sections of the chlorine isotopes given in table 3 have been kindly submitted to me by Mr. E. Arbman of this institute, who used a betaspectrometer for the determinations.

§ 4. Discussion

Devoting the first part of the discussion to the determination of the cross section distribution for vanadium, it is clear that this can be described if two terms are known, namely (*a*) the total cross section per mass number ($=\sigma_s(M)$) and (*b*) the cross section as a function of the atomic number ($=\sigma(M, Z)$) for a given mass number.

$$\sigma_s(M)=\sum_Z \sigma(M, Z).$$

In order to determine $\sigma_s(M)$ it is necessary to make certain approximations. Every mass number in the actual region of the nuclide chart contains at least one stable isobar, for which the cross section has to be estimated. To be able to carry out these approximations it is assumed that the cross sections are independent of the individual properties of the product nuclides. This is reasonable when the energy of the bombarding particles is high. Then it is to be expected that the cross sections of

Table 4. Spallation of Manganese

Nuclide	Cross section relative to ^{45}Ti	Nuclide	Cross section relative to ^{47}Sc
^{49}Cr	2·2	^{48}Sc	0·6
^{45}Ti	1	^{47}Sc	1
^{47}Ca	0·007	^{46}Sc	2·0
^{45}Ca	0·25	^{44}Sc^{m}	1·2
^{43}K	0·21	^{43}Sc + ^{44}Sc	1·3
^{42}K	0·39		
^{39}Cl	0·008		
^{34}Cl + ^{38}Cl	0·013		
^{32}P	0·034		
^{31}Si	0·027		

Table 5. Spallation of Cobalt

Nuclide	Cross section relative to ^{49}Cr	Nuclide	Cross section relative to ^{47}Sc
^{49}Cr	1	^{48}Sc	0·35
^{48}V	1·2	^{47}Sc	1
^{45}Ti	0·45	^{46}Sc	4·1
^{42}K	0·16	^{44}Sc^{m}	1·7
^{32}P	0·025	^{43}Sc + ^{44}Sc	1·7
^{31}Si	0·010		

nuclides belonging to the same isodiaphere should vary monotonically, i.e. decrease monotonically with increasing distance from the target nucleus. That this is really the case will be evident from fig. 1, which is a plot of the cross sections of all the investigated nuclides as a function of the mass number. Curves are drawn through nuclides belonging to the same isodiaphere and the isotopic number I is noted. It is clear from the figure that the cross sections vary in a quite regular way. It should be possible to obtain a fairly good approximation of the cross section for any nuclide by interpolating or extrapolating in the curve with the same value of I as the nuclide in question.

The total cross section $\sigma_s(M)$ of a certain mass number can now be estimated in the following way. Suppose the mass number to be studied is 34. The cross section of ^{34}Cl (and of all the neutron deficient isobars) has been measured. The cross section of ^{34}S and of all the neutron efficient isobars can be extrapolated from the curve with $I=2$ in fig. 1. The sum of these cross sections should give $\sigma_s(34)$. In this way the

Fig. 1

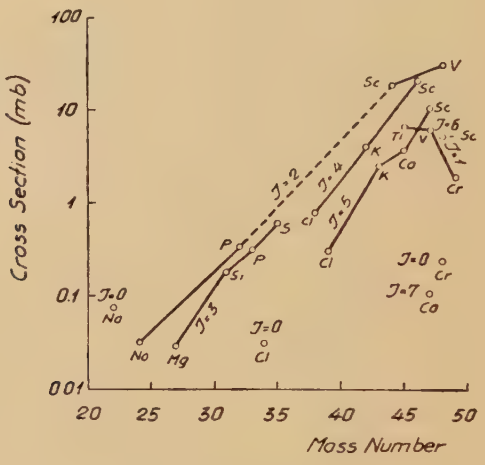

Fig. 2

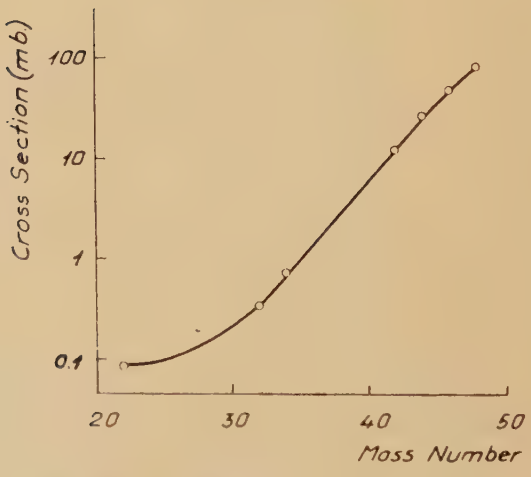

curve in fig. 2 has been constructed. This figure gives $\sigma_s(M)$ in a logarithmic scale as a function of M. The decrease of the cross section with decreasing mass number is seen to be nearly exponential between $M=48$ and $M=32$.

It now remains to determine the variation of the cross section with the atomic number for a given mass number. Consider the mass number 47. The cross sections of ^{47}V, ^{47}Sc, and ^{47}Ca have been measured.

Figure 2 gives $\sigma_s(47)$ so that the cross section of ^{47}Ti can be obtained by subtraction. The same procedure can be undertaken for the mass numbers 43, 45, and 48. The variation of the logarithm of the cross section as a function of the atomic number for these four mass numbers is shown in fig. 3.

It is true that some of the measured cross sections include the cross sections of parent nuclides. However, it is evident from fig. 3 that the daughter nucleus generally has a much larger cross section than its parent, the cross section curves of fig. 3 having their maxima close to the stability line. For that reason the measured cross section of a nuclide does not differ much from the primary yield of that nuclide.

Fig. 3

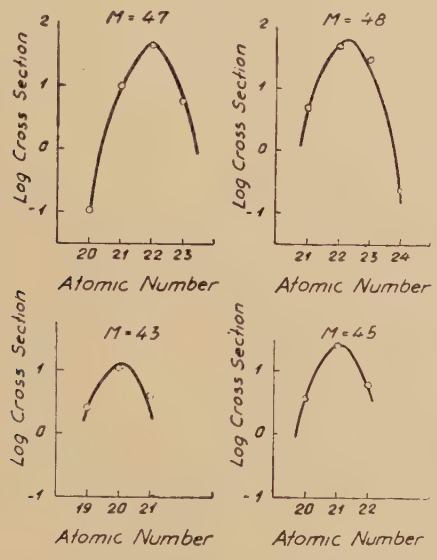

The experimental points in fig. 3 can be fitted rather well to parabolas as is shown in the figure. These parabolas can be written :

$$\log \sigma(M, Z) - \log \sigma(M, Z_0) = -p(Z - Z_0)^2 \quad . \quad . \quad . \quad . \quad (1)$$

(p, $\sigma(M, Z_0)$, and Z_0 are constants).

This means that the distribution of the cross sections of isobars with the same mass number is approximately a Gaussian one :

$$\sigma(M, Z) = \sigma(M, Z_0) \exp\left[-(p/\log e)(Z - Z_0)^2\right]. \quad . \quad . \quad (2)$$

All the parabolas in fig. 3 have been constructed with the same value of p, namely $p = 0{\cdot}78$, which gave a fairly good fit to the experimental points. The Gaussian distribution (2) has a variance of 0·53 atomic number units, if the value 0·78 is chosen for p.

In the following estimations of cross sections the distribution (2) with p equal to 0·78 was arbitrarily extended down to the mass number 22.

Now, it would be possible to compute the cross section of a given nuclide from the eqn. (2) if $\sigma(M, Z_0)$ and $Z_0(M)$ were known as functions

of M. From the parabolas in fig. 3 the following values of $Z_0(M)$ and $\sigma(M, Z_0)$ can be obtained (table 6).

Table 6

M	Z_0	$\sigma(M, Z_0)$ (mb)
43	20·1	13·5
45	21·1	26
47	21·9	47
48	22·3	60

$Z_0(M)$ is plotted as a function of M in fig. 4. The points lie close to a straight line which passes through the origin. From this figure $Z_0(M)$ can be estimated for any mass number.

Fig. 4

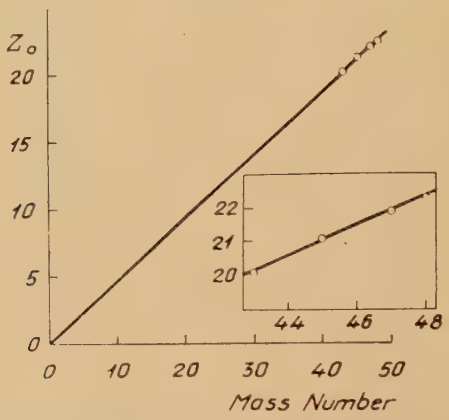

The distribution (2), integrated from the smallest permitted value of Z to the largest, would give a rough estimate of $\sigma_s(M)$. The limits of the integration can be extended from $-\infty$ to $+\infty$ without introducing serious errors since small and large values of Z give negligible contributions to the integral

$$\sigma_s(M) = \sum_Z \sigma(M, Z) \sim \int_{-\infty}^{\infty} \sigma(M, Z_0) \exp\left[-(p/\log e)(Z-Z_0)^2\right] dZ$$
$$= \sigma(M, Z_0)\, I,$$

(I is equal to 1·32 for $p=0{\cdot}78$).

Since I is independent of the mass number, $\sigma(M, Z_0)$ is approximately proportional to $\sigma_s(M)$. A plot of $\sigma(M, Z_0)$ as a function of $\sigma_s(M)$ should then give a straight line through the origin with a slope equal to 1/1·32. Figure 5 shows that this is so.

From the figs. 2 and 5 $\sigma(M, Z_0)$ can now be computed as a function of M (fig. 6).

The eqn. (2) and figs. 4 and 6 describe completely the cross section distribution for spallation of vanadium.

The measured cross sections are compared in table 7 with the cross sections calculated from eqn. (2) and the figs. 4 and 6. In the fourth column of the table the difference between computed and measured cross sections is given as a percentage of the latter.

The agreement is fair. This is of course to be expected since many of the measured cross sections of table 7 were used for the construction of the figs. 4 and 6 and for the determination of p in eqn. (2).*

Fig. 5

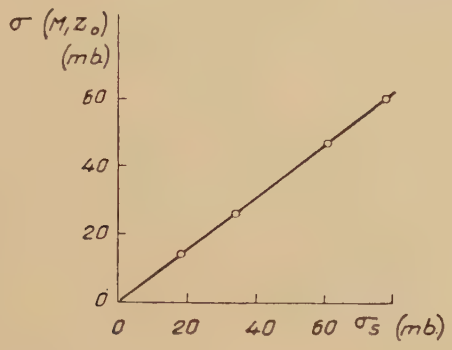

Fig. 6

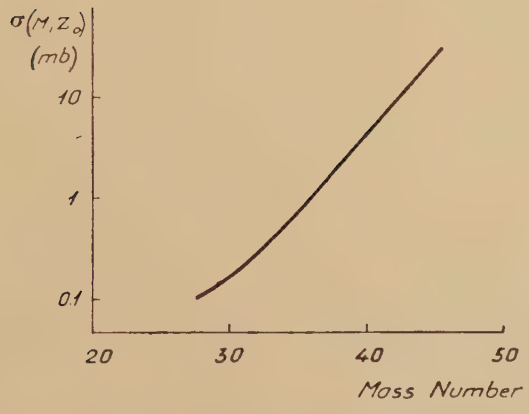

The methods of calculation indicated can now be used to estimate the cross sections of the spallation products of manganese and cobalt. Assuming that the cross section distribution is the same as for vanadium, eqn. (2) is again used. The straight line in fig. 4 passes through the points (0 ; 0) and (23·8 ; 51). (Target nucleus : $^{51}_{23}$V.) The corresponding lines for manganese and cobalt are now assumed to pass through the

* *Note added in proof.*—The cross sections of the spallation products of vanadium can be described by the formula :

$$\sigma(M, Z) = \exp\,[0{\cdot}358M - 12{\cdot}82 - 1{\cdot}80(Z - 0{\cdot}466M)^2]\ mb.$$

This formula can be used down to ^{27}Mg and gives cross sections not very different from the calculated cross sections in table 7.

Table 7

Nuclide	Measured cross section (mb)	Calculated cross section (mb)	Difference (%)
^{48}Cr	0·23	0·26	+13
^{48}V	28	22	−21
^{47}V	5·7	5·7	0
^{45}Ti	6·1	4·3	−30
^{48}Sc	4·8	3·5	−27
^{47}Sc	10	10	0
^{46}Sc	20	25	+20
^{44}Sc+^{44}Sc^{m}	17	11	−35
^{43}Sc	4·0	3·0	−25
^{47}Ca	0·11	0·06	−45
^{45}Ca	3·6	4·7	+30
^{43}K	2·5	1·8	−28
^{42}K	3·9	6·6	+72
^{39}Cl	0·30	0·24	−20
^{38}Cl	0·74	0·85	+15
^{34}Cl	0·031	0·043	+39
^{35}S	0·61	0·59	− 3
^{33}P	0·32	0·28	−13
^{32}P	0·34	0·27	−21
^{31}Si	0·18	0·15	−17
^{27}Mg	0·028	0·047	+68
^{24}Na	0·030	0·062	+106
^{22}Na	0·072	0·025	−65

Table 8

Nuclide	Measured cross section σ/σ ^{45}Ti	Calculated cross section σ/σ ^{45}Ti	Difference (%)
^{49}Cr	2·2	3·0	+36
^{47}Ca	0·007	0·006	−14
^{45}Ca	0·25	0·51	+108
^{43}K	0·21	0·18	−14
^{42}K	0·39	0·63	+62
^{32}P	0·034	0·074	+117
^{31}Si	0·027	0·037	+37
	σ/σ ^{47}Sc	σ/σ ^{47}Sc	
^{48}Sc	0·6	0·2	−67
^{46}Sc	2·0	2·6	+30
^{44}Sc+^{44}Sc^{m}		1·8	
^{43}Sc		0·5	
^{43}Sc+^{44}Sc+^{44}Sc^{m}	2·5	2·3	−8

points (0 ; 0) and (25·8 ; 55) and (0 ; 0) and (27·8 ; 59) respectively. The curve in fig. 6 is used except that the abscissa is increased by four mass units for manganese and eight mass units for cobalt.

The measured and computed cross sections for the spallation of manganese and cobalt are shown in tables 8 and 9 respectively.

The agreement between measured and calculated cross sections is quite good. From this it can be concluded that the cross section distribution for spallation of vanadium, manganese, and cobalt with high energy protons is rather well characterized by an exponential decrease of the total yield per mass number with increasing distance from the mass number of the target nucleus and by a Gaussian distribution for a given mass number.

Table 9

Nuclide	Measured cross section σ/σ ^{49}Cr	Calculated cross section σ/σ ^{49}Cr	Difference (%)
^{48}V	1·2	2·2	+83
^{45}Ti	0·45	0·32	−29
^{42}K	0·16	0·10	−38
^{32}P	0·025	0·043	+72
^{31}Si	0·010	0·022	+120
	σ/σ ^{47}Sc	σ/σ ^{47}Sc	
^{48}Sc	0·35	0·15	−57
^{46}Sc	4·1	3·5	−17
^{44}Sc+^{44}Sc^{m}		3·5	
^{43}Sc		1·1	
^{43}Sc+^{44}Sc+^{44}Sc^{m}	3·4	4·6	+35

ACKNOWLEDGMENTS

I wish to express my thanks to Professor T. Svedberg for his continued interest in this work, and to Professor S. Claesson, Mr. H. Tyrén, and Mr. A. E. Taylor for helpful discussions. I also wish to thank the staff of the Uppsala synchrocyclotron for carrying out the bombardments.

REFERENCES

BATZEL, R. E., MILLER, D. R., and SEABORG, G. T., 1951, *Phys. Rev.*, **84,** 671.
BURTT, B. P., 1949, *Nucleonics*, **5,** August 28.
HOPKINS, H. H., and CUNNINGHAM, B. B., 1948, *Phys. Rev.*, **73,** 1406.
MARQUES, L., 1952, *Phys. Rev.*, **88,** 225.
MILLER, D. R., THOMPSON, R. C., and CUNNINGHAM, B. B., 1948, *Phys. Rev.*, **74,** 347.
NERVIK, W. E., and STEVENSON, P. C., 1952, *Nucleonics*, **10,** March 18.
RUDSTAM, G., STEVENSON, P. C., and FOLGER, R. L., 1952, *Phys. Rev.*, **87,** 358.
SELIGER, H. H., 1952, *Phys. Rev.*, **88,** 408.
STEVENSON, P. C., and FOLGER, R. L., unpublished work.
WAGNER, G., and WIIG, E. O., 1952, *J. Amer. Chem. Soc.*, **74,** 1101.
YAFFE, L., and JUSTUS, K. M., 1949, *J. Chem. Soc.*, **1949,** S 341.

CXX. *Electron Microscopic Observations of* 111 *Faces of* ZnS *Crystals*

By W. Dekeyser, S. Amelinckx, E. Votava and G. Vandermeerssche

Lab. voor Kristalkunde, Rozier, 6, Centrum voor Electronenmicroscopie, Plateaustraat, 22, Gent, Belgium*

[Received July 6, 1953]

The object of this communication is to draw attention on two features, one concerning growth fronts, the other slip lines, which were observed by electronmicroscopic examination of replicas of two (111) faces of a large and macroscopically nearly perfect ZnS crystal.

A previous optical and interferometric study (Votava, Amelinckx and Dekeyser 1953), the results of which will be published elsewhere, had revealed that the topography of these faces was very complex. They present, next to growth fronts and slip lines, areas exhibiting a complex substructure, delimiting closed or nearly closed areas of the order of 0·001 mm^2, which themselves are further subdivided into similar, but much smaller regions.

The observation of these details was made possible, or at least greatly increased, by the slight natural corrosion of the crystal, which proved also to bring out clearly details on the electronmicrographs.

It is assumed that the crystal, originating from Jugoslavia, has grown at rather high temperature (hydrothermally or from the vapour phase) and that rather great internal stresses developed owing to temperature fluctuations and impurity content during the final stages of growth and after growth had ceased. The replicas were methylmethacrylate—SiO obtained in the usual way, and then shadowed with palladium. The photographs are negatives, black is shadow.

Figure 1 (Pl. 46, figs. 1 and 2) represents lines which are interpreted as growth fronts. This assumption is based on two arguments: (i) their main aspect is identical with lines on other electron-micrographs of the same face (not reproduced here), and where we are dealing unambiguously with growth fronts, as could be deduced from interference with obstacles and dislocations; (ii) they present features, which will be commented upon, and which have also been observed, on a different scale, on spiral growth fronts on (0001) faces of some carborundum crystals (Amelinckx 1952).

These features consist of lines such as AB which are confined between two (rarely more) successive growth fronts, making a nearly constant angle with them. The lines between consecutive pairs of fronts form a

---

* Communicated by the Authors.

geometrical pattern. In idealized form, this pattern looks like an array of quadrangles on the sides of which limited transverse lines are drawn.

As the segments AB are situated between two growth fronts, it would seem likely to consider them as misfit lines separating, in a same front, parts which have a different composition (polytypes). We also can accept that such a discontinuity can be ' washed ' away by a following front. But we cannot explain by this hypothesis the pattern following which these lines are aranged as a whole.

On the other side, if we consider the lines AB connected with features in the interior of the crystal, one can difficultly see why they should be confined between growth fronts. So, we find it better to delay any interpretation, and to stress that the similar observations on carborundum indicate that we are dealing here with something which is not accidental, at least for substances with this type of lattice.

Figure 2 represents sets of lines which are different from the growth fronts described so far. Figure 3 (Pl. 47, figs. 3 and 4) is an enlargement of part of it. They have been interpreted as slip lines because : (i) the corrosion along them occurs in a special way ; (ii) their spacing is irregular and their height variable (as deduced from the shadow).

Spots like A are hills on the replica, they correspond to etchpits in the crystal. As can readily be deduced, the corrosion was confined along the slip lines ; etch channels, most of which are more or less resolved in isolated pits, are seen to alternate with areas where nothing happened. This discontinuity can be very well seen along lines as BC.

If we accept that etchpits develop most easily at points where screw dislocations emerge (Gevers, Amelinckx and Dekeyser 1952, Horn 1952, Gevers 1952, 1953), we deduce that the lines are defined by the emergence of groups of such dislocations, resulting from the action, in the same (or nearly the same) plane of successive Frank and Read generators. On some occasion they act in a different set of (111) planes (DE) (cross slip). This picture corresponds rather well with the ideas put forward by Mott (1952).

The spacing of the lines is rather small, $\frac{1}{3}\,\mu$ as a mean. Some are closer together, and for these something like a fine structure may be present (GF). This points towards deformation at temperatures well above ' room temperature '.

Figure 4 originates from a different (111) face, things are more complicated here : slip has taken place on two different sets of planes. The discontinuity of the shadow shows here very strikingly the rows and grouping of etchpits. Some segments are more or less bent. The nature of intersection is that one line seems to stop as the transverse one is approached, and to start again on the other side (A, A′) sometimes with a slight deviation.

The concentration of dislocations is here extremely great, the opposite situation being the case of a well annealed single Al-crystal considered by Amelinckx (1953).

Acknowledgments

We are greatly indebted to Prof. J. Orcel, director of the Muséum d'Histoire Naturelle, Paris, for loan of the specimen.

This work is part of a research programme (C.E.S.) supported by I.R.S.I.A. (Brussels).

One of us (E.V.) thanks the Union Carbon and Carbide for a research fellowship.

References

Amelinckx, S., 1952, *Thesis*, Ghent ; 1953, submitted for publication.
Gevers, R., Amelinckx, S., and Dekeyser, W., 1952, *Naturwiss.*, **19**, 448.
Gevers, R., 1952, *Nature, Lond.*, **171**, 171 ; 1953, in the press.
Horn, F. H., 1952, *Phil. Mag.*, **43**, 1210.
Mott, N. F., 1952, *Phil. Mag.*, **43**, 1151.
Votava, E., Amelinckx, S., and Dekeyser, W., 1953, to be published.

CXXI. *Experiments on the Deposition of Iodine* 131 *Vapour onto Surfaces from an Airstream*

By A. C. Chamberlain
Atomic Energy Research Establishment, Harwell*

[Received May 7, 1953]

Abstract

Experiments are described on the deposition of ' carrier-free ' Iodine 131 vapour from a moving airstream onto surfaces. With copper and filter paper surfaces and at low or moderate Reynolds numbers, the deposition is controlled by aerodynamical factors, and the analogy with heat transfer by forced convection holds. The detailed deposition pattern produced by an obstacle on a flat plate is shown by a radioautograph.

§ 1. Introduction

The purpose of these experiments was to show that the deposition of a carrier-free radioactive vapour of iodine from air streams onto certain surfaces is controlled by diffusion across the laminar layer of air flow over the surfaces, and is governed by the same laws as the diffusion of heat in forced convection.

Pasquill (1943), with plane surfaces of saturated paper, and Ranz and Marshall (1952) with droplets of water and other liquids, have shown that evaporation from saturated surfaces can be predicted by diffusion theory, and the same should be true of deposition of a vapour on a surface, provided that the physical or chemical conditions at the surface are such that the vapour pressure just above it is zero, so that the surface acts as a ' perfect sink '.

The use of ' carrier-free ' radioactive isotopes makes this condition easily realizeable, since it is possible to work with less than a monomolecular layer of activity on the surface. Clean copper, and filter paper surfaces have been found to act as perfect sinks for the deposition of ' carrier-free ' ^{131}I vapour, at the activity levels used in these experiments.

The use of radioactive tracers in this way has a possible practical application, since by making a radioautograph of the deposited activity very fine detail can be seen of the variation of deposition with the characteristics of the boundary layer.

---

* Communicated by the Author.

§ 2. Method

2.1. *Source of* ^{131}I *Vapour*

Iodine 131, prepared in the Harwell pile by neutron bombardment of tellurium, was extracted as a solution of elemental iodine in carbon tetrachloride. No carrier iodine was added, but iodine impurities in the tellurium resulted in there being about 5 micrograms stable iodine per millicurie of ^{131}I.

The iodine solution was dried by standing over concentrated sulphuric acid, and sprayed up as a mist of very fine droplets by means of a Collison spray operated by dried and filtered compressed air.

This method of generating ^{131}I vapour was not very efficient, as there was a considerable loss of ^{131}I by adsorption in the spray, but none better could be found. Since all the measurements consisted of comparisons of the activity deposited on some surface with the activity present in the airstream, the exact amount of ^{131}I vapour generated was not required to be known.

2.2. *Estimation of* ^{131}I *in Airstream and on Surfaces*

The quantity to be measured was the time integral of the activity per cc. of air, or dosage as it will be called, and it was estimated by drawing the vapour at a known rate through bubblers containing 20 ml. of 5% NaOH, to which a few milligrams of KI had been added as carrier. Two bubblers in series were used at each sampling point, and the ratio of activity found in the bubbler first in series to that second in series generally lay between 20 : 1 and 50 : 1.

The deposited activity was measured either by direct counting of a cut out sample under an end-window counter, with allowance for back-scatter, or by soaking the sample in NaOH solution with KI carrier and counting in a liquid counter.

2.3. *Miniature Wind Tunnel*

The wind tunnel used was of square section, 4 in. by 4 in. The very small size had the disadvantage that the area available for working was small if the region near the walls of retarded air flow was to be avoided.

The vapour from a Collison spray, and a much larger volume of air, was drawn into the mouth of the tunnel and passed firstly through an orifice of 2 in. diameter to promote mixing, and secondly through a honeycomb of $\frac{1}{2}$ in. mesh to remove any swirl. A relatively long settling length enabled a uniform distribution of wind velocity and activity concentration to be attained before the working section, in which was placed the trial surface, was reached. The inlet tubes of the sampling bubblers projected through the floor of the working section, four sampling positions usually being used.

Pairs of sampling positions 5 cm apart in the working section usually gave results agreeing to within 10%. There was a slight fall off in

dosage as the sampling position was moved down the tunnel due to adsorption of the ^{131}I vapour on the walls of the tunnel, but this amounted to no more than about 0·3% per cm in the working section.

The wind velocity was measured by a vane anemometer at the front end of the tunnel, calibration being effected by means of a pitot static tube connected to a Chattock–Fry gauge.

§ 3. Results of Wind Tunnel Experiments

3.1. *Definition of Velocity of Deposition*

The velocity of deposition, v_g, of a vapour to a surface is defined by

$$v_g = \frac{\text{Rate of deposition per cm}^2 \text{ per sec}}{\text{Volumetric concentration per cm}^3} \quad . \quad . \quad . \quad . \quad . \quad . \quad . \quad . \quad (1)$$

$$= \frac{\text{Amount of activity deposited per cm}^2}{\text{Time integral of volumetric concentration, or dosage per cm}^3.} \quad . \quad . \quad . \quad . \quad . \quad (2)$$

3.2. *Deposition on Flat Filter Paper Surfaces*

In table 1 are shown the values of v_g obtained with a flat plate covered with filter paper. The experiments are marked H or V according as the plate was placed horizontally or vertically in the tunnel.

The deposition on the upper and lower surfaces of the plate when it was placed horizontally was found to be equal to the accuracy obtained in the experiment. Activity deposited on the filter paper was quite firmly fixed, the half-life of samples exposed to the air being only slightly less than the normal ^{131}I half-life of 8·0 days.

The reproducibility between different experiments at the same wind speed was fair, the average difference between corresponding entries being 13%, and there was no apparent dependence of the velocity of deposition on the dosage of activity passed.

In all cases there was a fall-off in the velocity of deposition down-wind from the leading edge of the plate. At a given distance from the leading edge, the velocity of deposition increased with increasing wind velocity, approximately as the square root of the wind velocity.

3.3. *Effect of Laminar Boundary Layer*

The falling off in velocity of deposition down-wind from the leading edge of a flat surface is due to the building up of a laminar layer of flow over the surface. In the turbulent stream of air in the open tunnel, eddy diffusion causes the concentration of vapour to be effectively the same everywhere. When an absorbing surface is present the air close to it is denuded of activity, and the rate at which activity is brought to the surface depends on the characteristics of the air flow over it. Where the laminar layer is big, there is a considerable distance, of the order of a millimetre in these experiments, over which the transporting agency is molecular, not eddy diffusion.

Table 1. Velocity of Deposition (v_g) of ^{131}I Vapour to Flat Filter Paper Surface (cm/s)

Wind velocity, u (cm sec)		38		77		115		158		230	
Dosage, c ($\mu\mu$c-sec/cm^3)		$2{\cdot}26\times10^4$	$1{\cdot}30\times10^4$	$1{\cdot}80\times10^4$	$1{\cdot}04\times10^4$	$4{\cdot}64\times10^3$	$1{\cdot}42\times10^4$	$4{\cdot}85\times10^3$	$1{\cdot}15\times10^3$	$3{\cdot}54\times10^3$	$9{\cdot}46\times10^2$
Plate vertical or horizontal		H	V	H	H	H	H	H	V	V	H
Distance from leading edge, x (cm)	1	0·58	0·66	0·70	0·56	1·03	0·80	1·15	1·00	1·48	1·62
	1·5	0·47	0·49	0·63	0·51	0·87	0·60	0·97	0·86	1·25	1·33
	2	0·42	0·43	0·50	0·44	0·77	0·62	0·88	0·74	1·17	1·17
	2·5	0·35	0·37	0·50	0·42	0·69	0·58	0·80	0·75	1·10	1·06
	3·5	0·30	0·32	0·42	0·38	0·61	0·51	0·77	0·67	1·03	0·95
	4·5	0·27	0·29	0·38	0·36	0·59	0·46	0·70	0·66	0·98	0·92
	5·5	0·27	0·25	0·36	0·33	0·55	0·47	0·64	0·65	0·89	0·82
	6·5	0·27	0·24	0·33	0·34	0·54	0·41	0·63	0·64	0·85	0·82
	7·5	0·25	0·21	0·32	0·32	0·51	0·41	0·58	0·59	0·84	0·72
	8·5	0·24	0·21	0·31	0·30	0·51	0·39	0·55	0·58	0·82	0·74
	9·5	0·23	0·21	0·29	0·27	0·49	0·34	0·52	0·58	0·83	0·75

In the radioautograph of Plate 48 the effect is shown of breaking up of a well developed laminar layer over a flat surface by an obstacle, a screw inserted perpendicular to the surface. In the wake of the screw, a heavier deposition of activity has taken place, shown by the dark trail on the radioautograph, due to the turbulence created by the screw.

3.4. *Deposition and Boundary Layer Theory*

The results of table 1 can be expressed in terms of a dimensionless number N_m analogous to the Nusselt number of heat transfer.

$$N_m = \frac{Ix}{cD}, \qquad \ldots\ldots\ldots \quad (3)$$

where I is the activity deposited per cm^2 at distance x from the leading edge of the plate, c the dosage of activity in the free air, and D the molecular diffusivity of iodine vapour in air. D will be taken as 0·080 cm^2/s at 20°C, following the results of Topley and Whytlaw-Gray (1927).

Fig. 1

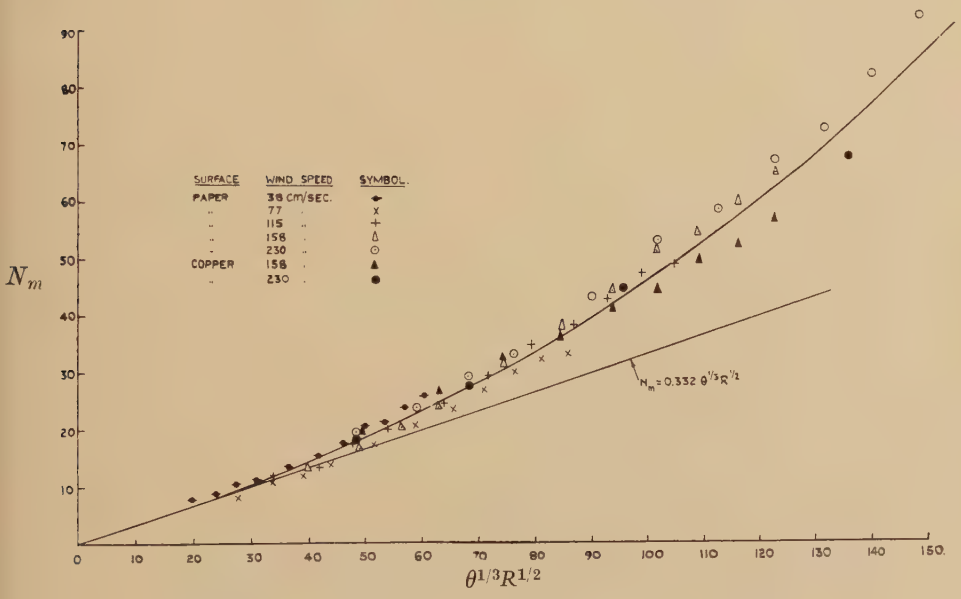

Deposition of ^{131}I vapour from airstream to flat plates.

In fig. 1 the results are shown of plotting the values of N_m derived from the results of table 1 against $\theta^{1/3}\ R^{1/2}$, where R is the local Reynolds number* and θ is the ratio of the kinematic viscosity of air to the diffusivity of iodine vapour. θ has the value 1·88 at 20°C.

---

* $R = \frac{ux}{\nu}$ is the Reynolds number characterizing the flow over the plate at the point in question, and not the Reynolds number of flow in the tunnel as a whole.

The points derived from experiments at different wind speeds lie approximately on the same curve, indicating that the deposition is controlled by aero-dynamical factors.

Also in fig. 1 are shown the values of N_m derived from experiments in which thin copper plate was used as the absorbing surface in place of filter paper. These points lie on the same curve as the filter paper points, except possibly at the upper end of the curve.

Fig. 2

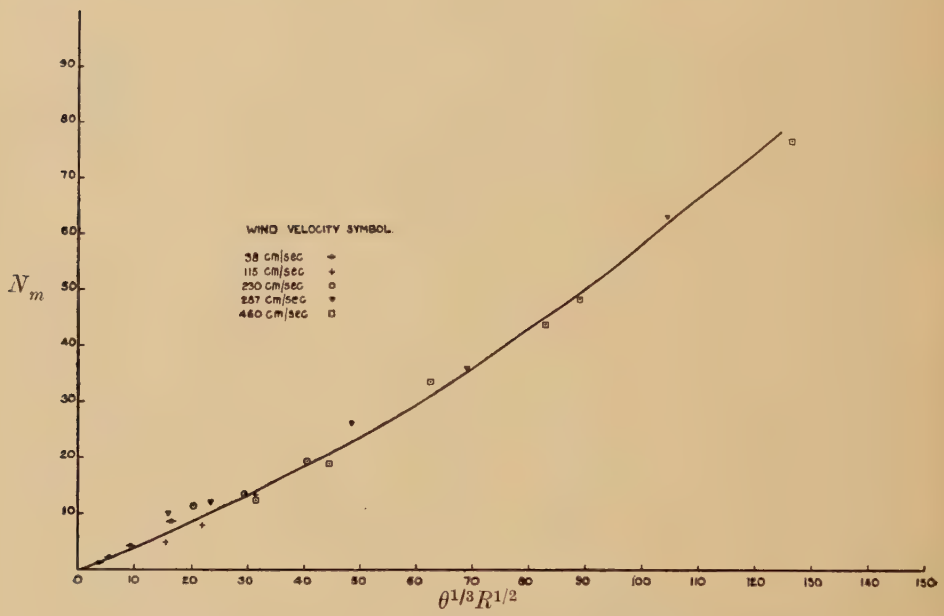

Deposition of ^{131}I vapour from airstream to copper cylinders.

The straight line in fig. 1 is the line

$$N_m = 0{\cdot}332\,\theta^{1/3}\,R^{1/2}. \qquad (4)$$

This is the theoretical (Pohlhausen) value of N_m to be expected on laminar boundary layer theory on the assumptions :

(*a*) that the vapour pressure of ^{131}I at the surface is zero,

(*b*) that the molecular diffusion is the transporting agency across the laminar layer.

The agreement between theoretical and experimental values is good for small values of $R^{1/2}$, but as $R^{1/2}$ increases the experimental values of N_m increase more rapidly than $R^{1/2}$. At the upper end of the velocity range the limiting value of R is approached at which the laminar boundary layer will break up and be replaced by a turbulent boundary layer.

3.5. *Deposition on Copper Cylinders*

Another series of wind tunnel runs were made with copper cylinders, varying in diameter from 1 in. to 0·028 in., and wind velocities from 38 to 460 cm per sec.

The dimensionless number N_m is now given by

$$N_m = \frac{\bar{I}d}{cD}, \qquad \ldots\ldots\ldots \quad (5)$$

where $\bar{I}$ is the deposited activity per cm^2 averaged over the cylinder and d is the diameter of the cylinder.

In fig. 2 N_m is shown plotted against $\theta^{1/3}R^{1/2}$. In evaluating R, the effect of the obstruction caused by the larger cylinders in increasing the local wind velocity in the tunnel had to be allowed for.

3.6. *Comparison of Mass Transfer Numbers and Heat Transfer Numbers, for Different Surfaces*

In fig. 3 the graphs of N_m against $\theta^{1/3}R^{1/2}$ for ^{131}I deposition on flat plates and cylinders are compared with the analogous curves :

(*a*) heat transfer by forced convection given by Hilpert, quoted by Goldstein (1937),

(*b*) heat transfer and evaporation of water from spherical drops, given by Ranz and Marshall (1952).

Fig. 3

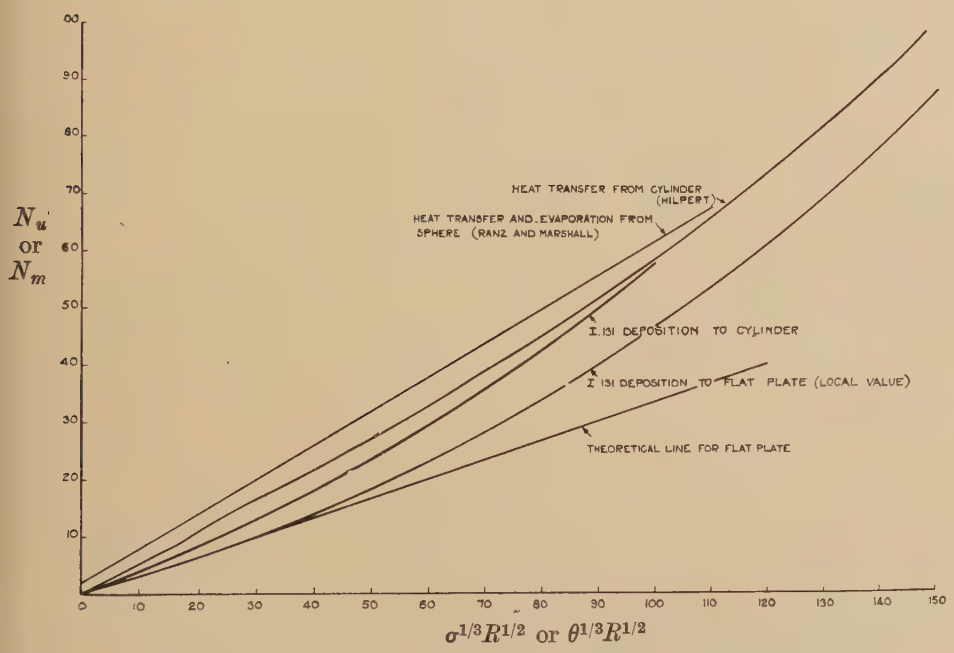

Diffusion transport of matter and heat (laminar boundary layer).

In the heat transfer case the parameters N_m and θ are replaced by the corresponding heat transfer entities namely N_u, the Nusselt number and σ the Prandtl number, which has the value 0·73 at 20°C.

The curves are all quite close together, those for cylinders being between the straight line representing the sphere results and the curve for the flat plate.

The divergence of the experimental line for deposition on a flat plate from the theoretical line at moderate Reynolds numbers is seen as a tendency to approximate more nearly to the experimental curve for cylinders.

§ 4. Deposition on Surfaces of Other Materials

A number of experiments were made to compare the deposition on other surfaces with that on paper and copper.

When flat plates 3 in. × 1 in. were exposed to the same flow of ' carrier-free ' ^{131}I vapour the deposition relative to that on a copper plate was as given in table 2. The level of activity on the copper was 1500 d.p.m./cm^2.

Table 2. ^{131}I Deposition on Flat Plates of Various Materials Relative to Deposition on Copper Plate

Surface	Paper	Steel	Aluminium	Glass	Perspex	Copper with thin film paraffin wax
Relative deposition	0·9	1	0·5	0·3	0·6	0·04

The effect of slight differences in surface conformation, and position in the air stream, were such that these ratios have a possible error of about 10%, and in particular, in the experiments with large plates, the copper : filter paper ratio was almost exactly unity, as shown in fig. 1.

When additional inactive iodine carrier was added to the source at the rate of 20 micrograms per millicurie, and the surfaces again compared, it was found that the ratios of the deposition on the other surfaces to that on copper was reduced. Critical experiments to determine the saturation point in terms of number of iodine molecules per cm^2 have not been completed.

§ 5. Conclusion

Copper and filter paper surfaces are found to act as ' perfect sinks ' for the deposition of tracer amounts of carrier-free ^{131}I vapour. In these circumstances the deposition is controlled by aerodynamical factors, and is analogous to heat transfer by forced convection. The radioautograph technique enables fine detail of the deposition to be seen, and there is a possible practical application to the study of heat transfer problems.

Acknowledgements

I am indebted to Mr. R. C. Chadwick for help with the experiments, and to Mr. C. A. Spinage who made the wind tunnel. This paper is published by permission of the Director, A.E.R.E.

The idea that fission products deposition could be considered as a problem analogous to heat transfer was first suggested by Cockburn (1948).

References

Cockburn, R., 1948 (unpublished).
Goldstein, S., 1937, Editor *Modern Developments in Fluid Dynamics* (Oxford : University Press).
Pasquill, F., 1943, *Proc. Roy. Soc.* A, **182,** 182.
Ranz, W. E., and Marshall, W. R., 1952, *Chem. Eng. Prog.*, **48,** 141.
Topley, B., and Whytlaw-Gray, R., 1927, *Phil. Mag.*, **4,** 873.

CXXII. *Metallic Carbides and Nitrides of the Type MX*

By William Hume-Rothery, F.R.S.
Inorganic Chemistry Laboratory, Oxford*

[Received June 6, 1953]

Abstract

The structures of the metallic carbides and nitrides of the type MX with the sodium chloride structure are discussed. The view that this structure is formed in order to provide the non-metallic atom with an octahedral interstice is shown to be improbable or only part of the truth and it is considered that the face-centred cubic arrangement with the metal atoms is favoured mainly because it provides the metallic atoms with mutually perpendicular bonds to six neighbours. The melting points are discussed, and the need for further work on the electrical properties of these compounds is emphasized.

The metallic carbides and nitrides with the Na–Cl type of structure are of great interest in view of their hardness and high melting points. It has long been recognized that in these compounds there is some kind of homopolar bonding between the metallic and non-metallic atoms. These compounds were discussed by Brager (1941), who unfortunately did not take into account the effect of co-ordination number on the atomic radii. A more recent discussion by Rundle (1948) is of great interest, but appears to us to be only partly correct, and in the present note an attempt is made to remove some of the inconsistencies.

The MX carbides and nitrides of high melting point have the sodium chloride structure, with the metal atoms arranged on a face-centred cubic lattice. The metallic elements concerned nearly all crystallize in the close-packed hexagonal, or body-centred cubic structures, and hence, as pointed out by Rundle, it is not justifiable to regard the MX carbides or nitrides as solid solutions of carbon or nitrogen in the crystals of the metallic elements themselves. The compounds may quite properly be regarded as interstitial compounds, with the small carbon and nitrogen atoms in holes between the larger metallic atoms, but some additional factor must be present to account for the taking up of a face-centred cubic structure by the metallic atoms.

Rundle points out that, whereas in some cases (e.g. LaN) the metal–metal distances in the MX compound are almost the same as those in the metallic element, there are other cases where the former distance is the

* Communicated by the Author.

greater.* Rundle appears to regard this as in contradiction to the previously accepted views of these substances as interstitial compounds controlled mainly by the radius ratios, but it seems doubtful whether this criticism is valid. If the NaCl type of structure is regarded as composed of large and small spheres, the small spheres occupy the 'octahedral holes' between the large spheres, and a radius ratio of 0·41 corresponds to an exact fit. In the previous views of these compounds it was considered that the NaCl type of structure was formed when the radius ratio lay between about 0·4 and 0·6, but it was not suggested† that the M–M distances were independent of the radius ratio. In the following table

Table 1

Metal	Atomic diameter for co-ordination No. 12	Observed M–M distances in compound		Interstitial diameter for exact fit in octahedral holes of hypothetical undistorted f. c. cubic metal
Sc	3·20	ScN	3·14	1·31
La	3·75	LaN	3·73	1·54
Ce	3·64	CeN	3·54	1·50
Pr	3·64	PrN	3·65	1·50
Nd	3·64	NdN	3·64	1·50
Ti	2·93	TiC	3·05	1·20
		TiN	2·99	
Zr	3·19	ZrC	3·32	1·31
		ZrN	3·27	
Hf	3·16	HfC	(3·15)	1·29
Th	3·59	ThC	3·75	1·47
		ThN	3·68	1·47
V	2·71	VC	3·03	1·11
		VN	2·92	
Nb	2·94	NbC	3·16	1·21
		NbN	3·12	
Ta	2·94	TaC	3·14	1·21
U	? 2·8–3·3	UC	3·50	1·15–1·35
		UN	3·45	

we show the atomic diameter for co-ordination number 12 of the metals concerned, together with the observed M–M distances in the carbide or nitride, and the atomic diameter of the sphere which would exactly fit the octahedral holes in the hypothetical undistorted face-centred cubic metals. These interstitial atomic diameters may be compared with the atomic diameters of C 1·54 A and N 1·47 A from the normal co-valent bond length of the C–C and N–N linkages, which require uncertain corrections for co-ordination number and bond-number. As pointed out by Zener

* Rundle's collected table contains no cases of a contraction greater than 0·1 A, which is about the accuracy of the data.

† We do not, of course, imply that nobody suggested this, but it was certainly not the generally accepted view.

(1950), it is not justifiable to apply Pauling's equation uncritically for corrections of this kind, because, quite apart from any theory of resonating co-valent bonds, a shortening of the apparent atomic diameter with decreasing co-ordination number is to be expected on grounds of energy alone. It is clear, however, that the cases of marked expansion in table 1 are those in which the ideal interstitial diameter is considerably smaller than the atomic diameter of carbon or nitrogen, and qualitatively the data are in agreement with the older views, except for UC and ThC where the expansion is abnormally great. The fact that uranium is an actinon and involves the complicated (7s, 6d, 5f) equilibrium may perhaps explain its abnormal behaviour.

Rundle (*loc. cit.*) also pointed out the hardness and brittleness of the MX compounds, and suggested that this implied directed bonds, but this conclusion does not appear justified, except in so far as bonds may be directed in normal transition metals. Thus ruthenium (m.pt. 2550°c) is sufficiently brittle to be ground to powder in a percussion mortar at room temperature, and iron is known to become brittle at low temperatures. It is thus only to be expected that MX compounds with melting points of about 3000°c will be brittle at room temperatures.

Table 2

Substance	Supra conducting transition temperature		Sp. resistance at room temperature $\times 10^4$		Notes
	Cmpd.	Metal	Cmpd.	Metal	
ScN	—	—	3	—	5% impurity mostly oxide.
TiC	1·1?	1·1	1·8–2·5	0·8	0·28% impurity.
TiN	2·6, 1·2	1·1	1·3	0·8	2% impurity. Oxide, alumina, carbon. The 1·2° suggests free Ti.
VC	—	—	1·5	1·6, 0·3	Data for metal variable.
VN	1·3	—	2	1·6, 0·3	VN. 0·1% Yt. 0·02% Ni. 0·5% insol. alumina.
ZrN	3·2	—	1·6	0·4	ZrN 7–10% impurities.
NbC	10·1	8·2	1·75 ?	0·1–0·2	NbC. V impure.
NbN	—	—	2	0·1–0·2	NbN no details.
TaC	9·2	4·4	1–2	0·1	TaC fairly pure, traces of Nb, Zr, Fe.

ScN and VC were shown not to be supraconductors at the lowest temperatures reached. NbN was not examined by Meissner and Franz, and the notes above refer to the paper by Friedrich and Sittig.

The MX carbides and nitrides are commonly said to exhibit normal metallic conductivity of the same order as that of the parent metals. This is probably true, but has not yet been proved conclusively for pure compounds of exact equiatomic composition. Thus, titanium exhibits supraconductivity with a transition temperature of 1·1°K, whilst in the work of Meissner and Franz (1930) TiC was shown to be non-supraconducting, but to exhibit an inflection in the resistance-temperature curve at 1·1°K, which suggested strongly that free titanium was present. The data of Meissner and Franz are summarized in table 2, from which it will be seen that the position as regards purity and exact composition is most unsatisfactory. The notes in table 2 refer to the work of Meissner and Franz (*loc. cit.*) on supraconductivity. As far as can be seen, the values given by these authors for the specific resistances at room temperature are not from their own work. Some appear to be taken from the work of Friedrich and Sittig (1925) and there is seldom evidence that the exact composition MX was obtained. In spite of the higher melting points, the specific resistances of the compounds are greater than those of the constituent metals by factors which may be as high as 10. In so far as the data are valid, one interesting point is the similarity between the specific resistances at room temperatures of all the carbides and nitrides between TiC and TaC in table 2. For all these the specific resistances lie between 1×10^{-4} and 2×10^{-4}.

According to Rundle, the carbon atoms give rise to mutually perpendicular bonds derived from one (sp) and two (p) orbitals, whilst the nitrogen atoms may exhibit the same behaviour, or more probably use three mutually perpendicular p orbitals. Rundle then regards the metal atoms as changing to the face-centred cubic structure, in order to provide ' octahedral interstices ' in which the carbon or nitrogen atoms will have six neighbours. This, however, appears incorrect, because the close-packed hexagonal structure itself contains ' octahedral interstices ' to the number of one per atom, and so far as the environment of the carbon or nitrogen atoms is concerned, this could be obtained equally well in a close-packed hexagonal structure. The difference between the two structures lies in the environment of the metal atoms when the octahedral holes are filled by atoms of carbon or nitrogen. In the NaCl type of structure for the MX compounds, each metal atom has six interstitial neighbours arranged on three mutually perpendicular axes, whereas in an MX interstitial compound built up by filling the octahedral holes of a hexagonal structure of close packed spheres, only some of the MX bonds proceeding from an M atom are mutually perpendicular, and others are at an angle of about 70°. If the axial ratio of the close-packed hexagonal structure is slightly different from that for close-packed spheres [$\sqrt{(8/3)}=1\cdot633$], the bonds to an atom in an octahedral interstice will not be exactly at right angles, but it seems improbable that this would invalidate the above argument. In any case, if we regard the environment of the carbon or nitrogen atom as the controlling factor, we shall be left with the problem

of why the metallic atoms prefer the arrangement of the cubical close packing rather than that of hexagonal close packing of spheres, particularly since the latter could be obtained by such a slight alteration of the lattices of the actual close-packed hexagonal metals. We may thus conclude that, although the provision of octahedral holes for the carbon or nitrogen atoms may be one factor, the face-centred cubic arrangement of the metal atoms is favoured mainly because it provides the *metallic* atoms with mutually perpendicular bonds to six neighbours. This clearly suggests that d^2sp^3 bonding from the metallic atoms is the main factor underlying the formation of these MX carbides and nitrides.

We may now suggest the following qualitative picture of the MX carbides and nitrides with the NaCl type of structure. The interatomic distances make it almost certain that these involve covalent rather than ionic bonding, because the C^{++++} ion would be too small for an interstitial fit, whilst a C^{----} ion would be too large, and also too unstable. In the carbides we may regard each carbon atom as tending to acquire a share in an octet of electrons. Since the carbon atom itself contains four electrons, it must obtain on the average 2/3 of an electron from each of its metallic neighbours which give rise to resonating co-valent bonds. This is essentially the same view as that of Rundle, and in TiC, ZrC, and HfC, where the metal atoms are tetravalent, all the electrons of the metal atoms are needed to build up the octet, and the conductivity arises from the fact that only some of the hybrid (spd) orbitals are filled. On passing to VC, NbC and TaC, Rundle's view is that the additional electron goes to form M–M bonds, but the melting points in table 3 do not support this view. On passing from TiC–VC, there is a fall in melting point, and on passing from ZrC–NbC, and from HfC–TaC the melting point is unchanged (see below).

In the nitrides, each nitrogen atom has five electrons and so requires half an electron from each neighbour to complete its octet. Unless charges are to be built up, the nitrogen atom will not contribute more than it gains, and consequently the bonding in the nitrides will be weaker than in the carbides, because the former involve three and the latter four electrons per atom. This is strikingly borne out by the data in table 3, which show that in every case there is a fall in melting point on passing from the carbide to the nitride of a given metal. At the same time we can understand why the M–M distance in the nitride is less than that in the carbide, because the atomic diameter of nitrogen is less than that of carbon. We can also understand why there are compounds ScN and LaN with the NaCl structure, but not ScC or LaC. Rundle's view is that in passing along a sequence such as TiN–VN, the additional electrons are used to form M–M bonds, until the latter are so strong that the metallic atoms are pulled into some other structure, but the melting point data for the nitrides do not support this view. The marked fall in melting point on passing from TiN → VN, and from ZrN → NbN suggests that the additional electrons weaken rather than strengthen the bonding.

We have next to consider why the MX nitrides and carbides are not formed by the elements of Group VI, and here it is interesting to note that WC and MoC have not structures in which the metal atoms considered alone are in close-packed assemblies. Instead we find hexagonal structures with the atoms arranged so that each metal atom is surrounded by six carbon atoms forming a trigonal prism, and each carbon atom is surrounded by metal atoms in the same way. The actual dimensions of the lattices are :

MoC :	$a=2{\cdot}90$	WC :	$a=2{\cdot}91$
	$c=2{\cdot}77$		$c=2{\cdot}83$
	$c/a=0{\cdot}955$		$c/a=0{\cdot}975$

The vertical side of the trigonal prism is thus nearly a square.

Table 3

Substance	Melting point °C	Source
TiC	3150	Goldschmidt
	3137	Emeleus
TiN	2930	F. and S.*
	2947	Sidgwick
	2947	Emeleus
ZrC	3500	Goldschmidt
	3532	Emeleus
ZrN	2982	Emeleus
	2982	Sidgwick
	2930	F. and S.
HfC	3900	Goldschmidt
		Emeleus
VC	2750	Goldschmidt
	2750	Emeleus
VN	2300	Sidgwick
	2050	F. and S.
NbC	3500	Goldschmidt
NbN	2300	Sidgwick
	2050	F. and S.
TaC	3900	Goldschmidt
	3877	Emeleus
TaN	3087	Sidgwick
	3087	Emeleus
	2800	F. and S.

* F. and S.=Friedrich and Sittig (1925).

If the transition elements are considered as a whole, we know that on passing along any one Long Row of the Periodic Table, the (n—1)d states, which are above the ns states in Group IA pass to relatively lower energies until at Group IIB the (n—1)d states are below the ns states. As we pass along the Period, we may therefore expect a tendency for the d part of the hybrid bonds to increase to a maximum, and then to diminish. We have suggested that in Groups IV and V, the MX carbides and nitrides result from octahedral d^2sp^3 bonds, and it is of interest to note that the trigonal prism arrangement of six neighbours corresponds to d^4sp or d^5p bonding (see Eyring *et al.* 1944), and we may suggest that this type is now involved. Each carbon atom has again six neighbours, and must absorb 2/3 electrons per bond in order to complete its octet. If this view is acceptable we can perhaps understand why WC has a lower melting point than metallic tungsten. The latter crystallizes in the body-centred cubic structure in which each atom has six valency electrons to bind it to eight close neighbours, whilst, if our picture is correct, the cohesion in WC results from each tungsten atom using four electrons to bind itself to six carbon atoms. The fact that there is no analogous compound CrC would agree with the scheme of valencies proposed by Hume-Rothery, Irving and Williams (1951), who pointed out that in the chemistry of these metals, the higher valencies were favoured in the later Periods.

References

Brager, A., 1941, *Acta Physicochim., U.R.S.S.*, **14,** 1.

Emeleus, H. J., 1940, *Modern Aspects of Inorganic Chemistry* (Routledge and Paul).

Eyring, H., Walter, J., and Kimball, G. E., 1944, *Quantum Chemistry* (New York: John Wiley; London: Chapman & Hall).

Friedrich, E., and Sittig, L., 1925, *Zeit. anorg. Chem.*, **143,** 293.

Goldschmidt, H. J., 1948, *J. Iron and Steel Inst.*, **160,** 345.

Hume-Rothery, W., Irving, H. M., and Williams, R. J. P., 1951, *Proc. Roy. Soc.* A, **208,** 437.

Meissner, W., and Franz, H., 1930, *Zeit. Physik*, **65,** 30.

Rundle, R. E., 1948, *Acta Crystallog.*, **1,** 180.

Sidgwick, N. V., 1950, *Chemical Elements and their Compounds* (Oxford: Clarendon Press).

Zener, C., 1950, *Acta Crystallog.*, **3,** 352.

CXXIII. *The Dielectric Properties of Barium Titanate Single Crystals in the Region of their Upper Transition Temperature*

By L. E. Cross
Physics Department, The University, Leeds*

[Received July 6, 1953]

Abstract

Measurements have been made of the ferroelectric hysteresis and dielectric constant of small single crystals of barium titanate from 20°c to 150°c.

In untwinned crystals, free from external constraint the results clearly indicate that the ferroelectric transition occurring in the region of 120°c is a thermodynamically first order transition. Over a small range of temperature above the zero field transition electric hysteresis is reintroduced by the application of a sufficient electric field. The forms of the hysteresis figures in this temperature range are qualitatively explained in terms of Devonshire's treatment of the ferroelectric effects.

In twinned crystals, optical and electrical measurements show that it is not possible to fix accurately a transition temperature for the whole specimen, as different regions transform at different temperature. It is suggested that the behaviour of these specimens may be due to imperfections in the crystal lattice, which give rise to local stresses in the region of the transition.

§ 1. Introduction

Until recently, the ferroelectric transition which occurs in barium titanate in the region of 120°c has been considered to be a thermodynamically second order effect (Forsbergh 1949, Megaw 1947), though it was recognized that the changes in the dimensions of the unit cell which occur immediately below this temperature, are more rapid than would be expected for such a λ type transition.

In a phenomenological treatment of the ferroelectric effects in barium titanate, it was suggested by Devonshire (1949) that the available data was more consistent with a first order change. Recently, several further experiments have been carried out which tend to confirm this suggestion (Känzig 1951, S. Roberts 1952) but no evidence appears yet to have been produced of any direct measurement of the discontinuous changes which occur in the electric polarization in a first order transition.

Over the past three years, we have made extensive measurements of optical and dielectric effects in both twinned and untwinned crystals of barium titanate (Cross 1952). As some of these results give direct

* Communicated by the Author.

evidence of the polarization changes in the region of the transition, which are not in agreement with those of previous observers, it seems desirable to place them on record.

§ 2. Experimental Details

Previous optical measurements (Kay and Vousden 1949, Forsbergh 1949, Cross *et al.* 1949), have shown that the internal twinning in the ferroelectric tetragonal phase of barium titanate is easily changed by mechanical, thermal or electrical treatment. To make any correlation between the electrical properties and the internal structure it is thus desirable to maintain a constant check on this feature. In these measurements this was accomplished by making simultaneous optical observations through semi-transparent electrodes. The individual twin components are uniaxial, and in the simpler specimens it is easy to determine the distribution and orientation of all the components by an examination in polarized light.

Measurement of the electric hysteresis was carried out by a modified ' Sawyer and Tower ' method (Von Hippel *et al.* 1946), and the dielectric constant values were deduced from the capacity of the specimen measured on a modified Maxwell bridge. For small values of the exciting field, the specimen behaves as a linear condenser, and the bridge may be perfectly balanced. If the measuring field is increased, no complete balance may be obtained, as the curvature of the polarization field curve introduces higher harmonics in the specimen polarization. An approximate balance may, however, be obtained for the component of the polarization in phase with the fundamental bridge frequency.

The value of the dielectric constant for weak fields we have called ϵ_R, and the values deduced for higher field strengths ϵ_I.

The crystals used were small flat plates of average dimensions 1 mm $\times$ 1 mm $\times$ 0·05 mm, only the more perfect rectangular shapes being selected. Semi-transparent gold electrodes were deposited on the larger faces by evaporation at reduced pressure. Contact was made onto the plated faces by lightly pressing platinum probes, which in no case exerted sufficient pressure to effect any optically detectable change in the specimen.

For work at elevated temperature, the specimen holder was placed in a well lagged viewing chamber, on the stage of a polarizing microscope, and heated by a stream of hot air. The temperature was recorded on a copper constantan thermocouple in contact with the specimen, and temperatures up to 150°C could be maintained with a regulation of better than $\pm$0·5°C.

§ 3. Observations

To allow direct intercomparison of the performances of different specimens, the electric hysteresis figures have been re-plotted from the original oscillograms with the scale suitably adjusted. Where the spontaneous polarization is given, this has been deduced by extrapolating

to zero field the linear regions of the hysteresis curve of a saturated specimen.

3.1. *Untwinned Crystals*

All the specimens used in these measurements had their tetragonal *c* axis perpendicular to the plane of the crystal plate.

Fig. 1

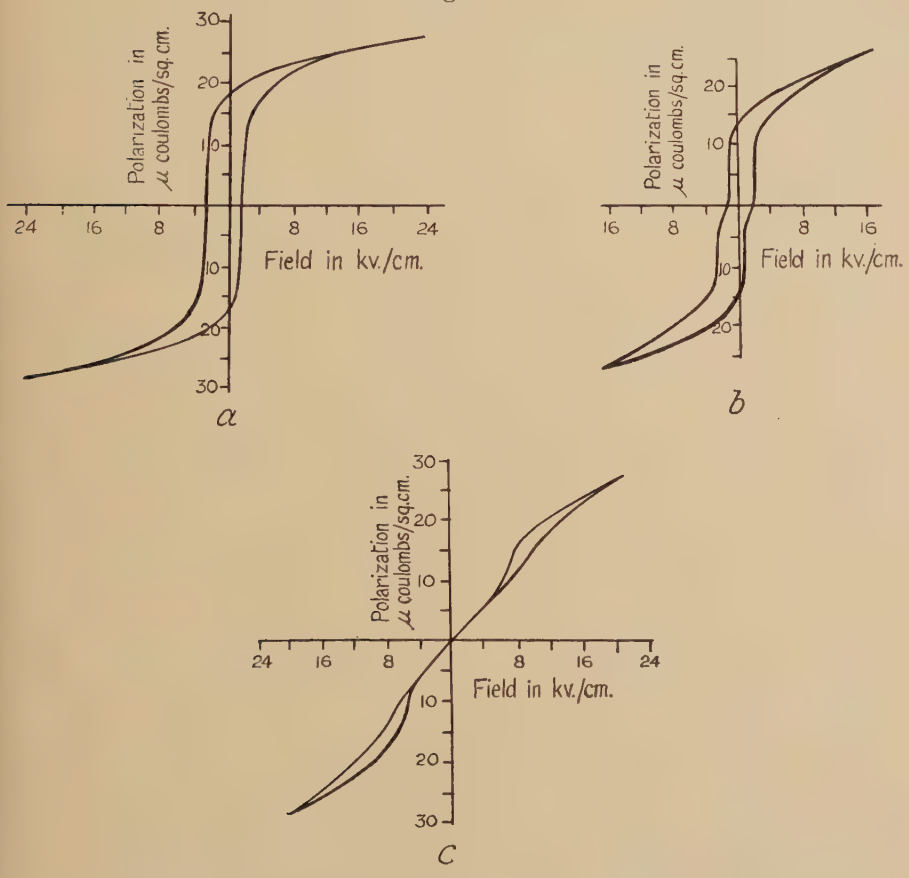

Electric hysteresis in a typical untwinned crystal at increasing temperatures (*a*) 24°C, (*b*) 120·5°C, (*c*) 129°C.

A typical hysteresis figure, taken at 24°C is shown in fig. 1 (*a*). On elevating the temperature, only minor changes occurred in the hysteresis figure up to the transition temperature. Figure 2 shows the spontaneous polarization obtained by extrapolating the hysteresis curves in this region.

At temperatures from 1°C to 5°C below the transition temperature, bright birefringent bands usually appeared, due to transient internal twinning. From the hysteresis figures, however, it was evident that this had a negligible effect on the polarization.

In the absence of an electric field, the crystal of fig. 1 (*a*) transformed suddenly at 120°C, losing all its birefringent areas at this temperature. Immediately below the transition there was a normal hysteresis curve. Just above 120°C, a peculiar kinking occurred at the coercive field, fig. 1 (*b*), and this became more marked as the temperature was raised. At 123°C, a loss free region began to develop in the centre of the curve, and at 129°C a well marked almost linear region was evident (fig. 1 (*c*)). This loss free region continued to extend as the temperature was raised, until at 135°C, with a field approaching the breakdown strength of the crystal, only the tips of the curve showed hysteresis.

Fig. 2

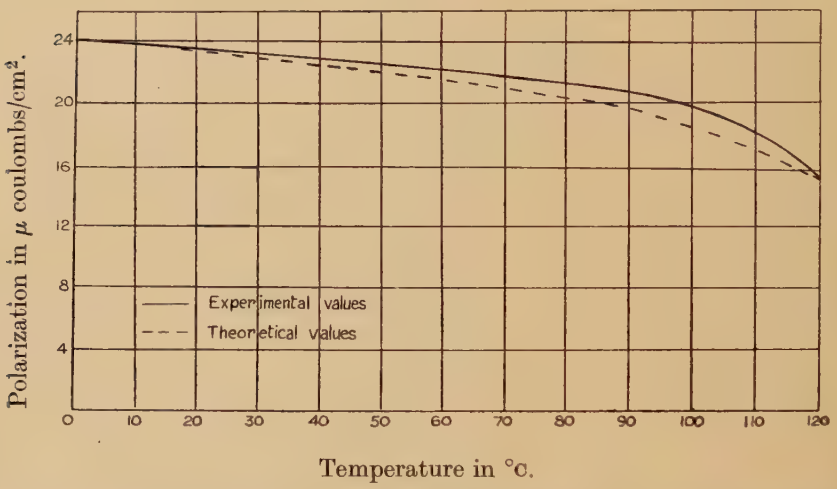

Spontaneous polarization P_s as a function of temperature in untwinned crystals.

An optical examination at any temperature in the above range showed an interesting series of changes as the electric field was increased. At zero field the crystal appeared completely black, and was obviously above its transition temperature. On increasing the field, no change was evident over the loss free region of the hysteresis curve, but immediately the field attained a sufficient value to excite hysteresis, bright birefringent bands flashed out, similar to those observed in the field free crystal just below the transition, and these were again cleared as the field was further increased.

The variation of reversible dielectric constant ϵ_R with temperature, measured with an alternating field of 10 volts/cm and without any steady biasing field, is shown in fig. 3. The curve of in-phase dielectric constant ϵ_I against temperature, for a measuring field of 1300 volts per cm is shown in fig. 4. The manner in which ϵ_R varies with temperature when a steady biasing field is also applied has been determined, and shows an elevation of the transition temperature by electric fields of 0·9°C/kv/cm, the graphs are not, however, reproduced here as similar results have already been published (Känzig *loc. cit.*).

3.2. *Twinned Crystals*

It is difficult to summarize completely the very varied performance of the twinned crystals, but the following features were generally evident.

(*a*) Even for a simply twinned crystal containing only a single twin boundary, the coercive field was very much greater than obtained from an untwinned specimen under similar conditions.

Fig. 3

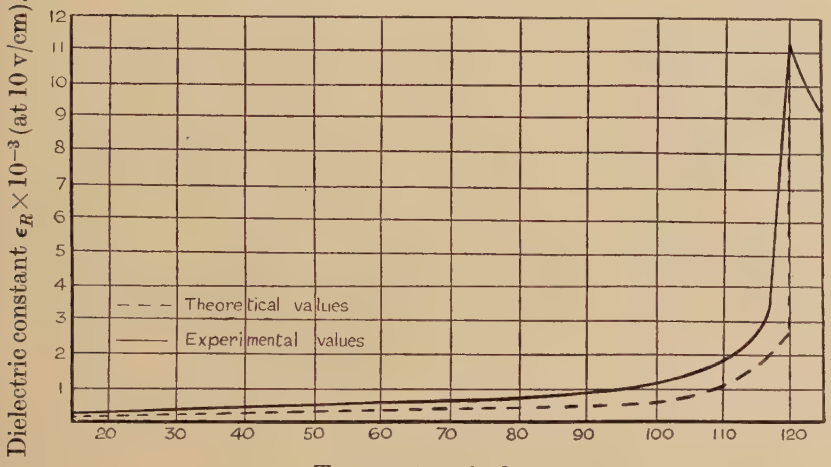

Variation of dielectric constant ϵ_R with temperature.

Fig. 4

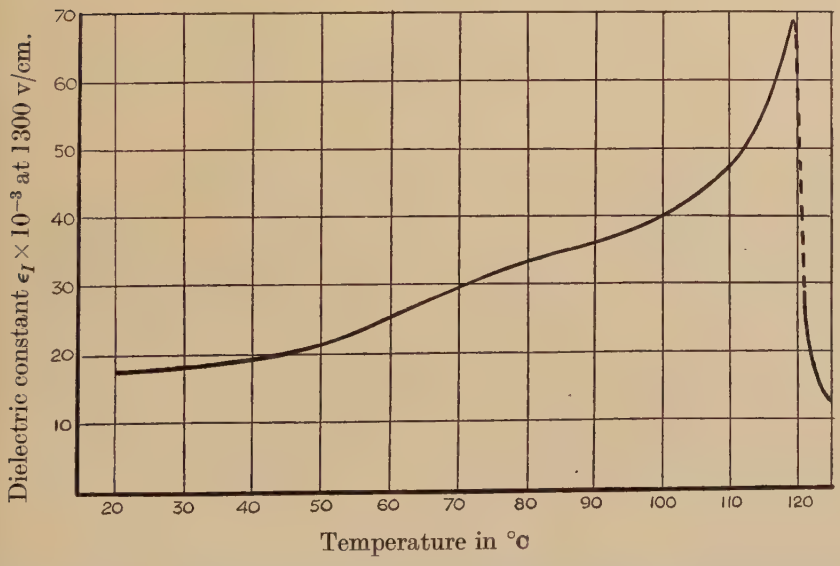

The variation with temperature of the dielectric constant ϵ_I measured at 1300 volts/cm.

(*b*) The crystals were difficult to saturate electrically, but even where the optical properties showed that the tetrad axis was completely oriented in the field direction, the extrapolated spontaneous polarization was considerably smaller than for an untwinned crystal.

(*c*) Optical observations showed that the transition in the region of 120°C was not discontinuous, but often the specimen contained a patchwork of transformed and untransformed regions for a range of temperature.

Fig. 5

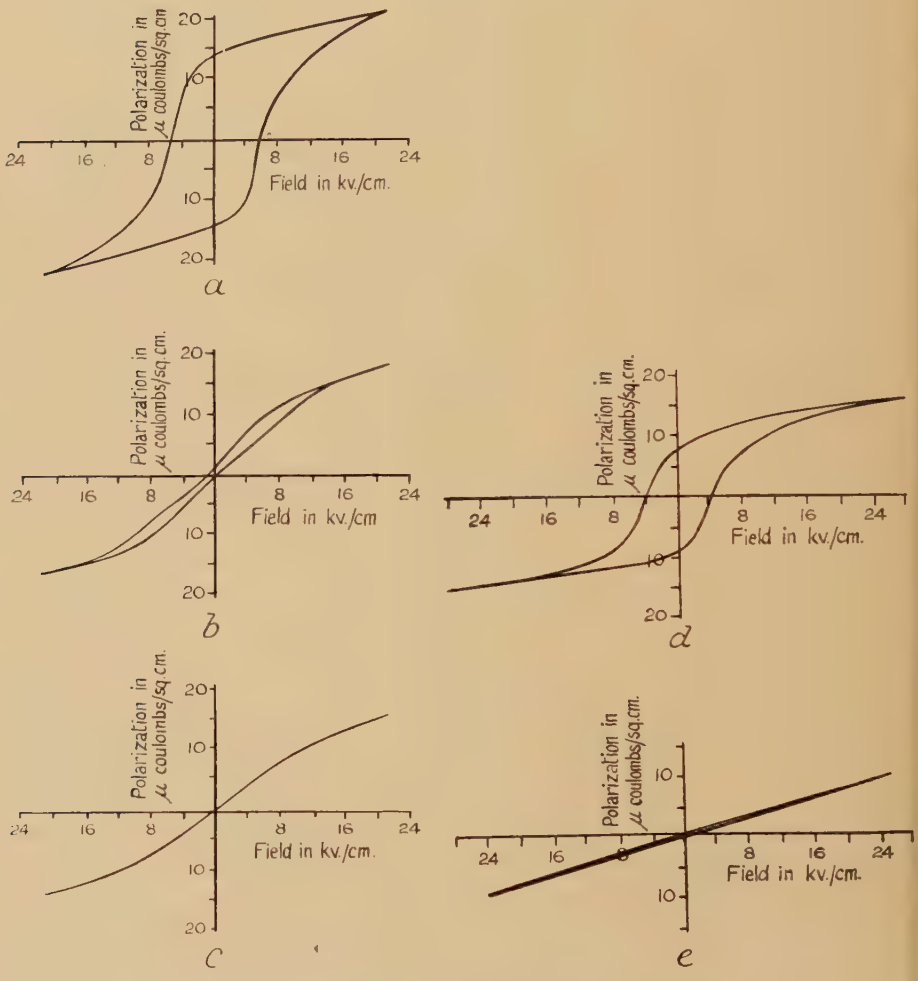

Hysteresis effects in twinned crystals.
In a simply twinned crystal (*a*) 20°C, (*b*) 109°C, (*c*) 112°C.
In a crystal with more complex twin structure (*d*) 15°C, (*e*) 115°C.

In some crystals, the change could be made to occur behind a moving boundary, and by maintaining a constant temperature, this boundary

could be halted and the two phases retained indefinitely in the same specimen.

Some typical hysteresis curves for various types of twinned crystal are shown in fig. 5.

§ 4. Comparison between Experimental and Theoretical Values

It has already been indicated that the phenomenological treatment first applied to barium titanate by Devonshire (1949), assumes a first order transition in the region of 120°C. This type of change is a direct consequence of the expression chosen for the free energy of the unstressed crystal. In the original paper expressions are derived for the variation with temperature of spontaneous electric polarization, and of weak field dielectric constant in terms of four constants, T_1 the transition temperature, T_0 the extrapolated Curie temperature, P_1 the spontaneous polarization at T_1, and $\chi_0{}^1$ the reciprocal electric susceptibility at T_1.

The effects of an external electric field may be considered by adding a further term to the expression for the free energy (Devonshire's eqn. (6.1)). For a field E applied in the z direction the additional term will be $-E.P_z$. In the region of the transition temperature $Px=Py=0$, and the necessary condition for a stationary value of the free energy may be shown to be

$$\beta=a\,(t-4a^2+3a^4), \qquad . \; . \; . \quad (1)$$

where $\beta=E/P_1\chi_0{}^1$, $a=P_z/P_1$, $t=(T-T_0)/(T_1-T_0)$.

From (1) the electric hysteresis figure at zero frequency may be computed for any value of temperature.

Taking the values

$$P_1=15{\cdot}4\,\mu \text{ coulombs/cm}^2,$$
$$T_1=120°\text{C},$$

from our measurements on untwinned crystals, and

$$T_0=110°\text{C},$$
$$\chi_0{}^1=1{\cdot}0\times10^{-3},$$

from the measurements of S. Roberts (1949), the theoretical values of polarization and dielectric constant have been plotted on fig. 2 and fig. 3, and the relation between polarization and electric field for three temperatures above the transition temperature in fig. 6.

It is evident from a consideration of the energy, that in regions such as AB in fig. 6 (*b*) the free energy is a maximum. If it is assumed that the system must have sufficient energy to surmount this barrier there will be irreversible polarization changes at A and B and the dotted hysteresis curve will be traced out. In practice it is probable that inhomogeneity in the specimen will facilitate a reversal of the polarization of lower energy.

§ 5. Discussion of Results

Devonshire's treatment clearly gives a satisfactory correlation of the polarization measurements taken on the untwinned crystals. With the

simplifications which are necessary in such a treatment exact agreement with the experimental values is not to be expected, but the general form is well reproduced. In particular, the first order change in the polarization is confirmed, and the hysteresis above the transition temperature explained.

The reintroduction of the ferroelectric state by a sufficient electric field above the transition temperature shown by the hysteresis effects is also evident in the optical and dielectric measurements. The sudden

Fig. 6

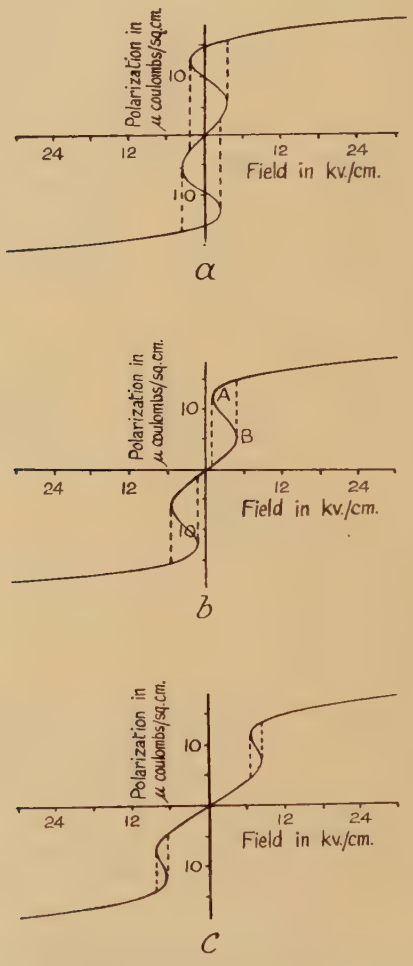

Hysteresis figures above the upper transition temperature from Devonshire's treatment (*a*) 121°C, (*b*) 124°C, (*c*) 129°C.

increase in polarization in the ferroelectric region produces an electrostrictive distortion, transient internal twinning occurs, and the change is evident optically by bright birefringent regions which appear in the crystal.

In dielectric measurements, the effect is most easily observed in measurements of the temperature variation of ϵ at constant field, the sharp peak in ϵ_R which occurs at 120°C being moved to higher temperature. Using this method Känzig (*loc. cit.*) finds an elevation of 1·2°C/kv/cm, and similar measurements on our crystals give a value of 0·9°C/kv/cm.

Further confirmation of the discontinuous transition in the polarization is provided by the measurements of ϵ_I. The very high values of ϵ_I just below the transition are clearly associated with the reorientation of spontaneously polarized ' domains ', and the discontinuous change in ϵ_I is therefore further evidence of a discontinuity in the polarization.

The continuous change observed in ϵ_R in the region of the transition temperature (fig. 3) is not in agreement with the postulated polarization change, but it must be remembered that even in the best single crystals there is transient internal twinning in the region of the transition. This inhomogeneity in the crystal must influence the dielectric properties, and is probably sufficient to account for the observed effects.

The only previous measurements of polarization in untwinned crystals (Merz 1949) show a generally lower value of polarization than our results, with a rapid but continuous change in the region of 120°C. There is, however, some evidence in the shape of the temperature variation of polarization to suggest that saturation is incomplete, and in certain specimens hysteresis curves similar to our fig. 1 (*c*) were obtained. Unfortunately simultaneous optical measurements were not carried out, and subsequent piezoelectric measurements (Caspari and Merz 1950) on similar specimens indicate the presence of some internal twinning.

No complete explanation of the different properties of the twinned crystals will be attempted here. Piezoelectric and dielectric measurements suggest that the individual twin components are electrically neutral, and it is therefore unlikely that the twinning is a ' domain ' formation necessary to eliminate free poles. Forsbergh (*loc. cit.*) has suggested that the twinning is due to lattice imperfection, and has demonstrated that in certain impure crystals, the spontaneous distortion in the ferroelectric region is utilized by suitable twinning to relieve strain caused by a local concentration of impurities in the specimen.

This suggested association of the twin structure with defects in the crystal lattice provides a qualitative explanation for our results. It may be shown from Devonshire's treatment that constraint applied to the specimen is likely, both to reduce the transition temperature, and by modifying the coefficient of the terms in P^4 in the free energy, to reduce the discontinuous change in polarization at this temperature. Thus to explain the observed effects, it is suggested that the lattice defects give rise to local constraints, which produce inhomogeneity in the dielectric performance in the region of the transition.

Clearly, although this suggestion gives some explanation for the differences observed in the dielectric performance, quantitative calculations of the magnitudes involved could only be made after much more detailed information of the behaviour of the twin boundaries has been obtained.

It is hoped to obtain further information of the properties of twinned crystals, by examining the electric hysteresis at much lower frequency, where optical tracking of the twin boundary motion should be possible. Also a further examination of the hysteresis above the transition is being carried out, using measuring fields of higher frequency, to obtain information of the relaxation process between ferroelectric and unpolarized states.

Acknowledgment

I wish to express my sincere thanks to Dr. P. Vousden for his valuable help in the preparation of this paper.

References

Caspari, M. E., and Merz, W., 1950, *Phys. Rev.*, **80,** 1082.
Cross, L. E., 1952, *Thesis*, Leeds.
Cross, L. E., Dennison, A. T., Nicolson, M. M., and Whiddington, R. W., 1949, *Nature, Lond.*, **163,** 635.
Devonshire, A. F., 1949, *Phil. Mag.*, **40,** 1040.
Forsbergh, P. W., Jr., 1949, *Phys. Rev.*, **76,** 1187.
Hippel, A. von, Brockenridge, R., Chelsey, P., and Tisza, L., 1946, *Ind. and Eng. Chem.*, **38,** 1097.
Känzig, W., 1951, *Helv. Phys. Acta*, **24,** 343.
Kay, H. F., and Vousden, P., 1949, *Phil. Mag.*, **40,** 1019.
Megaw, H. D., 1947, *Proc. Roy. Soc.* A, **189,** 261.
Merz, W., 1949, *Phys. Rev.*, **76,** 1221.
Roberts, S., 1947, *Phys. Rev.*, **71,** 890 ; 1952, *Ibid.*, **85,** 925.

CXXIV. *A Note on the Quantum Dynamical Principle*

By Julian Schwinger
Harvard University, Cambridge, U.S.A.*

[Received May 18, 1953]

Abstract

It is shown that commutation relations are derived consistently from the quantum dynamical principle, for systems obeying first order equations of motion.

§ 1. Introduction

The author (Schwinger 1951) has developed a formulation of quantum dynamics which enables one to deduce all properties of a quantum mechanical system from a single dynamical principle. It has been asserted, in a paper published in this journal (Burton and Touschek 1953), that the scheme fails for systems obeying first order equations of motion. That statement is not correct.

In order to clarify the origin of this misunderstanding, we shall present a brief discussion of such systems with a finite number of degrees of freedom. It should be realized that the employment of first order equations of motion is not a restriction but rather a standardization of systems that obey the conventional determinism principle—that knowledge of the values of a complete set of compatible physical quantities at a given time constitutes a state of maximum information which permits the determination of such states at any other time. The differential equations of motion for systems of this type must be of finite order, and can therefore always be presented as first order equations by suitable adjunction of variables.

§ 2. The Dynamical Principle

It is the object of quantum dynamics to construct transformation functions of the type

$$(\zeta_1' \, t_1 | \zeta_2'' \, t_2) = (\Psi(\zeta_1' \, t_1)^\dagger \, \Psi(\zeta_2'' \, t_2)) \quad . \quad . \quad . \quad . \quad . \quad (1)$$

where ζ_1 and ζ_2 are complete sets of commuting Hermitian operators. The fundamental dynamical principle is a differential characterization of such transformation functions. Any infinitesimal change can be represented by

$$\delta(\zeta_1' \, t_1 | \zeta_2'' \, t_2) = (i/\hbar)(\zeta_1' \, t_1 | \delta W_{12} | \zeta_2'' \, t_2),$$

which is the definition of the infinitesimal operator δW_{12}. The composition and reality properties of transformation functions imply that

$$\delta W_{13} = \delta W_{12} + \delta W_{23},$$
$$\delta W_{12}^\dagger = \delta W_{12}.$$

* Communicated by the Author.

The basic postulate of the dynamical principle is that there exists a class of alterations for which the associated operators δW_{12} are obtained by appropriate variation of a single operator, the action operator W_{12},

$$\delta W_{12}=\delta(W_{12}).$$

According to the additivity property of the action operator, it must possess the form

$$W_{12}=\int_{t_2}^{t_1} dt\, L[t],$$

where $L[t]$ is a Hermitian function of fundamental dynamical variables $x_a(t)$, in the infinitesimal neighbourhood of the time t. There is no loss of generality in requiring that the x_a be Hermitian.

For a given dynamical system, that is, for a given form of the Lagrangian operator L, we can alter the dynamical variables x_a, and the times t_1 and t_2. This must correspond to the freedom in description of a given dynamical system, the possibility of introducing infinitesimal changes in the states occurring in the transformation function (1)—infinitesimal alterations of the complete sets of operators, or of the times to which they refer. These variations are localized at the times t_1 and t_2, and are described by infinitesimal unitary transformations of the eigenvectors

$$\delta\,\Psi(\zeta_2''\,t_2)=-(i/\hbar)\,G_2\,\Psi(\zeta_2''\,t_2),$$

$$\delta\,\Psi(\zeta_1'\,t_1)^\dagger=(i/\hbar)\,\Psi(\zeta_1'\,t_1)^\dagger\,G_1,$$

where G_1 and G_2 are infinitesimal Hermitian operator functions of the dynamical variables at t_1 and t_2, respectively. Thus, for a given system,

$$\delta W_{12}=G_1-G_2, \quad . \quad . \quad . \quad . \quad . \quad . \quad . \quad . \quad (2)$$

which is the quantum form of Hamilton's principle. It asserts that W_{12} is stationary with respect to variations of the dynamical variables in the interval between t_1 and t_2, since G_1 and G_2 only contain variables referring to t_1 and t_2. This action principle implies equations of motion for the dynamical variables and yields expressions for the generators of infinitesimal unitary transformations, G_1 and G_2.

Note that two Lagrangians differing by a time derivative describe the same system. Thus

$$\bar{L}=L-(d/dt)W, \qquad W=W(x,t),$$

yields

$$\bar{W}_{12}=W_{12}-(W_1-W_2).$$

Accordingly, the action principle for $\bar{W}_{12}$ is satisfied if it is obeyed by W_{12}. That is, W_{12} and $\bar{W}_{12}$ imply the same equations of motion, but

$$\delta\bar{W}_{12}=\bar{G}_1-\bar{G}_2,$$

where

$$\delta W_1=G_1-\bar{G}_1, \qquad \delta W_2=G_2-\bar{G}_2,$$

defines new generators of infinitesimal transformations at t_1 and t_2. The latter equations are a special case of (2), in which all operators refer to the same time.

In order that the Lagrangian yield first order, explicit equations of motion, it must possess the general form

$$L=\frac{1}{2}\sum_{a,\,b}\left(x_a\,A_{ab}\frac{dx_b}{dt}-\frac{dx_a}{dt}A_{ab}\,x_b\right)-H\,(x_a,\,t)$$
$$=\frac{1}{2}\left(xA\frac{dx}{dt}-\frac{dx}{dt}Ax\right)-H\,(x,\,t),$$

in which the time derivative term has been symmetrized with respect to the operation of integration by parts, corresponding to the freedom of adding a time derivative to the Lagrangian. If L is to be a Hermitian operator, this property must apply to H, the Hamiltonian operator, and the numerical matrix A must be skew-Hermitian.

The action operator is

$$W_{12}=\int_{t_2}^{t_1}[\tfrac{1}{2}(xA\,dx-dx\,Ax)-Hdt]$$

in which form the limits of integration are objects of variation. We can introduce an auxiliary variable τ, which is such that the variations δt_1 and δt_2 are represented by a change in the functional dependence of t upon τ. This enables us to vary the x_a and t, with fixed limits τ_1 and τ_2. The auxiliary variable τ need not be written explicitly, since it is not subject to variation. Hence

$$\delta W_{12}=\int[\delta xA\,dx-dx\,A\delta x-\delta H\,dt+dH\,\delta t]$$
$$+\int d[\tfrac{1}{2}(xA\,\delta x-\delta x\,Ax)-H\delta t].$$

The action principle now asserts that

$$\delta xA\,dx-dxA\,\delta x=\delta H\,dt-dH\,\delta t,$$

or

$$\delta H=\frac{dH}{dt}\,\delta t+\delta xA\,\frac{dx}{dt}-\frac{dx}{dt}A\delta x, \qquad \ldots\ldots \quad (3)$$

and supplies the information that

$$G=\tfrac{1}{2}\,(xA\,\delta x-\delta x\,Ax)-H\delta t,$$

at times t_1 and t_2.

The Hamiltonian operator is an arbitrary function of the x_a. If its variation is to possess the form (3), with δx_a appearing only on the left and on the right, these variations must possess elementary operator properties, characterizing the class of variations to which the dynamical principle refers. Thus, we should be able to displace δx_a entirely to the left, or to the right, in the structure of δH,

$$\delta H-(\partial H/\partial t)\delta t=\delta x(\partial_l H/\partial x)=(\partial_r H/\partial x)\,\delta x,$$

which defines the left and right derivatives of H. In view of the complete symmetry between left and right in the multiplication process, we infer that the terms in (3) with δx on the left, and on the right, are in fact equal.

We thus obtain

$$dH/dt=\partial H/\partial t, \qquad (4)$$

and

$$2A(dx/dt)=\partial_l H/\partial x,$$
$$-(dx/dt)2A=-2A^T(dx/dt)=\partial_r H/\partial x,$$

where the latter must be equivalent forms of the equations of motion. Similarly,

$$G=-\delta x A x-H\delta t$$

and

$$G=xA\delta x-H\delta t=(A^T x)\delta x-H\delta t$$

must be equivalent forms of the infinitesimal generator G.

If the matrix A completely decomposes into two submatrices, with a corresponding decomposition of the dynamical variables into two sets, we speak of the two sets of variables as being kinematically independent, since the derivative term of the Lagrangian is additively constructed from the two sets, as is the infinitesimal generator G, apart from the term $-H\delta t$. (Should the Hamiltonian also decompose in this manner, the two sets are dynamically independent.) Now the matrix A can always be written as the sum of an anti-symmetrical, real matrix a, and of a symmetrical, imaginary matrix s. In view of the manner in which A and the transpose of A enter in equivalent versions of the equations of motion, and of G we anticipate that a consistent theory can be constructed only if the expression of A as

$$A=a+s$$

is a complete decomposition. Accordingly, there exist two kinematically independent sets of dynamical variables; variables of the first kind, x_i, associated with a, and variables of the second kind, ξ_α, associated with s. The Lagrangian now becomes

$$L=\frac{1}{2}\left\{x,\ a\frac{dx}{dt}\right\}+\frac{1}{2}\left[\xi,\ s\frac{d\xi}{dt}\right]-H(x,\ \xi,\ t).$$

The equations of motion appear in two sets,

$$2a(dx/dt)=\partial_l H/\partial x=\partial_r H/\partial x, \qquad (5)$$

and

$$2s(d\xi/dt)=\partial_l H/\partial\xi=-\partial_r H/\partial\xi, \qquad (6)$$

while the infinitesimal generator reads

$$G=-\delta x(ax)-\delta\xi(s\xi)-H\delta t$$
$$=-(ax)\delta x+(s\xi)\delta\xi-H\delta t.$$

Concerning the variables of the first kind, we see from the identity of the left and right derivatives of H that the δx_i must commute with all operators. This is consistent with the equivalent expressions for G. Hence

$$[\delta x_i,\ x_j]=[\delta x_i,\ \xi_\alpha]=0,$$

which is to say that the δx_i are infinitesimal multiples of the unit operator.

On comparing the two forms of G, we infer that the $\delta\xi_\alpha$ anti-commute with the variables of the second kind,

$$\{\delta\xi_\alpha, \xi_\beta\}=0.$$

The opposite signs of the left and right derivatives of H with respect to variables of the second kind implies that H must be an even function of the ξ_α, but it remains an arbitrary function of the x_i provided that

$$[\delta\xi_\alpha, x_i]=0.$$

We have, in these operator properties of δx_i and $\delta\xi_\alpha$, the precise specification of the class of variations to which the fundamental dynamical principle refers.

We shall assume, for simplicity, that the equations of motion can be solved explicitly for the dx_i/dt and $d\xi_\alpha/dt$ which requires that the matrices a and s be non-singular. In order that this property holds for the anti-symmetrical matrix a, the number of variables of the first kind must be even $(2n_1)$. We shall later present an argument indicating that the number of variables of the second kind must also be even $(2n_2)$. The separation of the $2n$ variables of either type into two sets of n variables leads to the canonical version of the formalism.

§ 3. Variables of the First Kind

We employ the fact that, by means of real linear transformations of the variables, the anti-symmetrical real matrix $2a$ can be brought into a diagonal form in which the n_1 diagonal elements are the two-dimensional matrices

$$\begin{pmatrix} 0 & -1 \\ 1 & 0 \end{pmatrix}.$$

If the dynamical variables associated with the kth two-dimensional matrix are called q_k and p_k, the relevant time derivative term in the Lagrangian becomes

$$\frac{1}{2}\sum_{k=1}^{n_1}\left(\frac{1}{2}\left\{p_k, \frac{dq_k}{dt}\right\}-\frac{1}{2}\left\{\frac{dp_k}{dt}, q_k\right\}\right),$$

the equations of motion read

$$dq_k/dt=\partial H/\partial p_k, \quad -dp_k/dt=\partial H/\partial q_k, \qquad \ldots\ldots \quad (7)$$

while the contribution to G arising from variations of the variables of the first kind is

$$G_{q,\,p}=\tfrac{1}{2}\sum_{k=1}^{n_1}(p_k\,\delta q_k-\delta p_k\,q_k). \qquad \ldots\ldots \quad (8)$$

Less symmetrical but more convenient forms are obtained by adding a suitable time derivative to the Lagrangian with a corresponding alteration of the generator G. Thus, with

$$W=-\tfrac{1}{2}\sum_k \tfrac{1}{2}\{p_k, q_k\},$$

the derivative term in L becomes

$$\sum_k \frac{1}{2}\left\{p_k, \frac{dq_k}{dt}\right\},$$

and the contribution to the infinitesimal generator is

$$G_q = \sum_k p_k \, \delta q_k.$$

If we reverse the sign of W, these quantities are

$$-\sum_k \frac{1}{2}\left\{\frac{dp_k}{dt}, q_k\right\}$$

and

$$G_p = -\sum_k \delta p_k \, q_k = -\sum_k q_k \, \delta p_k.$$

The advantage of these forms is the unambiguous interpretation attached to the infinitesimal generators G_q and G_p. Evidently G_q describes that infinitesimal unitary transformation in which the operators q_k are changed by δq_k ($\bar{q}_k = q_k - \delta q_k$), with no alteration of the operators p_k, and similarly for G_p. The expression of this for an arbitrary function F of the canonical variables, q_k and p_k, is

$$(1/i\hbar)[F, G_q] = \sum_k (\partial F/\partial q_k) \, \delta q_k,$$

and

$$(1/i\hbar)[F, G_p] = \sum_k (\partial F/\partial p_k) \, \delta p_k,$$

or, remembering that the δq_k and δp_k commute with all operators,

$$(1/i\hbar)[F, p_k] = \partial F/\partial q_k,$$
$$(1/i\hbar)[q_k, F] = \partial F/\partial p_k,$$

from which we obtain the commutation properties of the canonical variables

$$[q_k, q_l] = [p_k, p_l] = 0,$$
$$[q_k, p_l] = i\hbar \, \delta_{kl}.$$

The evident interpretation of

$$G_t = -H\delta t$$

as the generator of the infinitesimal unitary transformation from variables at time t to variables at time $t+\delta t$ supplies the important verification of the consistency of the information concerning equations of motion and generators of infinitesimal unitary transformations. We have

$$(1/i\hbar)[F, G_t] = -(dF/dt - \partial F/\partial t)\delta t,$$

or

$$dF/dt = \partial F/\partial t + (1/i\hbar)[F, H].$$

By successively placing $F = H$, q_k, p_k, we deduce (4) and the canonical equations of motion (7) from the properties of infinitesimal transformations.

We now remark that the generator (8) is

$$G_{q,\,p} = \tfrac{1}{2} G_q + \tfrac{1}{2} G_p,$$

which clearly produces the transformation in which the q_k and p_k are

changed by $\frac{1}{2}\delta q_k$ and $\frac{1}{2}\delta p_k$, respectively. Since this statement refers symmetrically to the two sets of canonical variables, the same interpretation applies to the generator which employs no special form of the matrix a,

$$G_x = -\delta x\, ax,$$

namely, that it describes changes of x by $\frac{1}{2}\delta x$. The equivalent commutation statement is

$$(1/i\hbar)[2ax, F] = \partial F/\partial x,$$

which yields equations of motion in the form (5), and exhibits the commutation properties of the variables of the first kind in the single equation

$$[x_k, x_l] = i\hbar\, \tfrac{1}{2}\,(a^{-1})_{kl}. \qquad \ldots\ldots\ldots \quad (9)$$

The oversight that occurs in the paper of Burton and Touschek (1953) is the treatment of the $2n_1$ variables x as canonical coordinates, and the linear combinations of these same variables, $-ax$, as canonical momenta. This results in a commutator which lacks the factor 1/2 of (9).

§ 4. Variables of the Second Kind

It is convenient to anticipate that the real, symmetrical matrix $(1/i\hbar)s$ must be positive-definite. Hence there exists a real, linear transformation of the variables which reduces this matrix to the unit matrix. The generator of changes in the variables of the second kind then reads

$$G_\xi = i\hbar \sum_\alpha \xi_\alpha \delta\xi_\alpha, \qquad \ldots\ldots\ldots \quad (10)$$

which shows that the various ξ_α are kinematically independent. The operator expression of this statement is

$$[\xi_\alpha, \xi_\beta\, \delta\, \xi_\beta] = 0, \quad \alpha \neq \beta,$$

which implies that

$$\{\xi_\alpha, \xi_\beta\} = 0, \quad \alpha \neq \beta,$$

in virtue of the anti-commutitivity of $\delta\xi_\beta$ with ξ_α.

Now, if the number of variables of the second kind were odd, the product of all these operators would commute with every ξ_α, and would therefore be a multiple of the unit operator, contradicting the independence of the various ξ_α. An alternative version of the argument stems from the requirement that the set of operators ξ_α be algebraically complete, in the sense that an operator possessing the properties of $\delta\xi_\alpha$ can be constructed from them. For an even number of variables, the product of all the ξ_α anti-commutes with each ξ_α, but no such operator exists for an odd number of variables. We conclude that there must be an even number of dynamical variables of the second kind.

To introduce the canonical formulation for variables of the second kind, we observe that, in virtue of the anti-commutitivity property of the $\delta\xi_\alpha$,

a pair of terms in (10) can be combined in the following way :

$$i\hbar\,(\xi_1\,\delta\xi_1+\xi_2\,\delta\xi_2)=i\hbar\tfrac{1}{2}\,[(\xi_1-i\xi_2)\,\delta(\xi_1+i\xi_2)-\delta(\xi_1-i\xi_2)(\xi_1+i\xi_2)]$$
$$=\tfrac{1}{2}[p\delta q-\delta p q].$$

Here p and q are non-Hermitian operators, which are related by

$$p=i\hbar q^{\dagger},$$

if we choose q as $\xi_1+i\xi_2$. On pairing the $2n_2$ terms of (10) in this manner, we obtain the canonical form of the contribution to G associated with variables of the second kind,

$$G_{q,\,p}=\tfrac{1}{2}\sum_{\alpha=1}^{n_2}(p_\alpha\,\delta q_\alpha-\delta p_\alpha\,q_\alpha). \quad . \quad . \quad . \quad . \quad . \quad . \quad (11)$$

The derivative term in the Lagrangian and the equations of motion, expressed in canonical variables, are

$$\frac{1}{2}\sum_\alpha\left(\frac{1}{2}\left[p_\alpha,\frac{dq_\alpha}{dt}\right]-\frac{1}{2}\left[\frac{dp_\alpha}{dt},q_\alpha\right]\right),$$

and

$$dq_\alpha/dt=\partial_l H/\partial p_\alpha,\ -dp_\alpha/dt=\partial_r H/\partial q_\alpha.$$

On adding suitable time derivatives to the Lagrangian, we obtain modified forms of the time derivative term and the associated generator, namely

$$\sum_\alpha \tfrac{1}{2}[p_\alpha, dq_\alpha/dt],$$
$$G_q=\sum_\alpha p_\alpha\,\delta q_\alpha,$$

and

$$-\sum_\alpha \tfrac{1}{2}[dp_\alpha/dt,\ q_\alpha],$$
$$G_p=-\sum_\alpha \delta p_\alpha\,q_\alpha=\sum_\alpha q_\alpha\,\delta p_\alpha.$$

According to the evident interpretation of the infinitesimal generators G_q and G_p, we have

$$(1/i\hbar)[F, G_q]=\sum_\alpha(\partial_r F/\partial q_\alpha)\,\delta q_\alpha$$

and

$$(1/i\hbar)[F, G_p]=\sum_\alpha \delta p_\alpha(\partial_l F/\partial p_\alpha).$$

If F contains an odd number of variables, of the second kind, these relations imply that

$$(1/i\hbar)\{F, p_\alpha\}=\partial_r F/\partial q_\alpha=\partial_l F/\partial q_\alpha,$$
$$(1/i\hbar)\{q_\alpha, F\}=\partial_l F/\partial p_\alpha=\partial_r F/\partial p_\alpha,$$

while, for operators constructed from an even number of second kind variables,

$$(1/i\hbar)[F, p_\alpha]=\partial_r F/\partial q_\alpha=-\partial_l F/\partial q_\alpha,$$
$$(1/i\hbar)[q_\alpha, F]=\partial_l F/\partial p_\alpha=-\partial_r F/\partial p_\alpha.$$

From the first set, we obtain the commutation properties of canonical variables of the second kind,

$$\{q_\alpha, q_\beta\}=\{p_\alpha, p_\beta\}=0,$$
$$\{q_\alpha, p_\beta\}=i\hbar\,\delta_{\alpha\beta}.$$

As applications of the second set of relations, we deduce that variables of the first kind commute with variables of the second kind, and verify that the equations of motion for second kind variables follow from the properties of infinitesimal transformations, thus ensuring the consistency of the theory for both types of dynamical variables.

Since the generator (11) produces the transformation in which the q_α and p_α are changed by $\frac{1}{2}\delta q_\alpha$ and $\frac{1}{2}\delta p_\alpha$, respectively, the same interpretation applies to the generator which employs no special form for s,

$$G_\xi = -\delta\xi\, s\xi,$$

namely, that it describes changes of ξ by $\frac{1}{2}\delta\xi$. Hence, for operators F which are, respectively, even and odd functions of the variables ξ, we have

$$(1/i\hbar)[2s\xi, F] = \partial_l F/\partial\xi = -\partial_r F/\partial\xi,$$

and

$$(1/i\hbar)\{2s\xi, F\} = \partial_l F/\partial\xi = \partial_r F/\partial\xi.$$

The first relation, applied to the Hamiltonian, yields the equations of motion in the form (6), while the commutation properties of the Hermitian variables of the second kind, ξ_α, emerge from the second equation,

$$\{\xi_\alpha, \xi_\beta\} = i\hbar\tfrac{1}{2}(s^{-1})_{\alpha\beta}. \quad . \quad . \quad . \quad . \quad . \quad . \quad . \quad . \quad (12)$$

Incidentally, the structure of the left side, in this result, provides the basis for the statement that $(1/i\hbar)s$ must be positive-definite. In their discussion of this type of system, Burton and Touschek regarded the $2n_2$ variables ξ as canonical coordinates, and the linear combinations of these same variables, $s\xi$, as canonical momenta, which produced an anti-commutator that lacked the factor $\frac{1}{2}$ of (12).

We shall carry the discussion no further here, since our objective was to show that the dynamical principle yields consistent commutation properties for systems obeying first order equations of motion. The reader is referred to the second paper of a series by the author (1953), "The Theory of Quantized Fields", in which fields obeying first order equations are considered.

References

Burton, W. K., and Touschek, B. F., 1953, *Phil. Mag.*, **44**, 161.
Schwinger, J., 1951, *Phys. Rev.*, **82**, 914; 1953, *Ibid.*, **91**, 713.

CXXV. *Schwinger's Dynamical Principle*

By W. K. Burton and B. F. Touschek
Department of Natural Philosophy, University of Glasgow
Istituto di Fisica, Universita degli Studi, Rome*

[Received July 1, 1953]

Abstract

A comparison is made of the methods applied by Schwinger and by the authors to the derivation of commutation relations for systems whose equations of motion are of the first order in the time derivatives.

In the foregoing note Schwinger (1953) criticizes our paper (Burton and Touschek 1953) on the commutation relations in Lagrangian quantum mechanics. A misunderstanding as to the scope and the contents of this paper seems to have arisen.

We did not wish to suggest that Schwinger's dynamical principle as such was wrong ; in fact we used it in our treatment of first order systems. Our intention was to point out an inconsistency arising from an uncritical application of this principle in the form in which it was published by Schwinger (1951), and to show how this difficulty could be avoided. Our method consisted in the consideration of variations of the variables induced by variations of the sources, a method originally introduced by Peierls (1952). In this way we obtained by applying Schwinger's principle, and without recourse to the canonical formalism, the correct commutation relations for the systems under consideration. In field theory, this method gives the covariant commutation relations.

In his note Schwinger gives a discussion of a generalized form of the two examples investigated in our paper, showing that by using canonical variables the correct commutation relations can be recovered from his formalism. However, the necessity for introducing these variables was not suggested in the original (1951) form of the theory. In the case of variables of the second kind for which no correspondence with classical mechanics exists, the introduction of canonical variables is by no means trivial. In fact, previous to the publication of our paper we discussed at a conference at Glasgow in July, 1952, the introduction of the variables $q=q_1+iq_2$ and $q^+=q_1-iq_2$ (Schwinger's canonical variables of the second kind) in place of the Hermitian variables q_1 and q_2, but we discarded this procedure later in favour of the Peierls method, which we felt to be more cogent and powerful.

---

* Communicated by the Authors.

The combination of the Schwinger principle and the Peierls method seems to us to have the advantage that it is not necessarily restricted to Lagrangians which allow a canonical formulation, so that our method seems more in keeping with the spirit of Schwinger's dynamical principle than the recourse to canonical variables.

References

Burton, W. K., and Touschek, B. F., 1953, *Phil. Mag.*, **44,** 161.
Peierls, R., 1952, *Proc. Roy. Soc.* A, **214,** 143.
Schwinger, J., 1951, *Phys. Rev.*, **82,** 914 ; 1953, *Phil. Mag.*, **44,** 1171.

Comment on the above Note

There is no objection to deriving commutation relations from the consideration of source variations. Indeed, the use of external sources has always been an integral part of the technique associated with the dynamical principle (see (1951) and (1953) which, incidentally, was submitted before the paper of Burton and Touschek became available). But one cannot ignore the commutation properties implied by the variations of the dynamical variables. The theory must be consistent, and this requirement applies to the consequences of all the variations to which the fundamental dynamical principle refers.

References

Schwinger, J., 1951, *Proc. Natl. Acad. Sci. U.S.*, **37,** 452 ; 1953, *Phys. Rev.*

Julian Schwinger.

CXXVI. CORRESPONDENCE

Measurement of the Elasticity of Solid Argon by Ultrasonic Methods

By J. R. Barker, E. R. Dobbs and G. O. Jones
Department of Physics, Queen Mary College, University of London

[Received July 16, 1953]

The importance of a knowledge of the elastic constants of the solidified inert gases for the development of the theory of interatomic forces has been recognized by many authors, but no measurements have previously been reported because of the difficulty of producing and handling crystals at low temperatures. We have carried out measurements of the velocity of longitudinal ultrasonic waves in solid argon leading to preliminary estimates of the compressibility at two temperatures.

The freezing of liquid argon usually produces a loose heap of small crystals (de Smedt and Keesom 1925), but we have found that slow deposition from the vapour at temperatures below the triple point (83·8°K) results in a compact, transparent, polycrystalline solid. For the measurement of the ultrasonic velocity it was possible to deposit the solid directly on to one face of a gold-plated, ' X-cut ', quartz crystal, whose other face was in contact with a copper rod maintained at the desired temperature of the experiment. When the crystal had been covered by a layer of several millimetres of solid argon, a metal piston whose surface was parallel to that of the quartz crystal could be pressed slowly into the argon to produce a flat reflecting surface for the longitudinal ultrasonic waves—the excess solid being caused to vapourize by maintaining the piston at a slightly higher temperature.

The quartz crystal was excited by a 3 Mc/s sine-wave generator, producing standing waves in the solid argon which could be recovered each time the piston was moved (by a micrometer screw) a half wavelength further into the solid. The following preliminary values were obtained for the velocity (v) of longitudinal waves in an infinite solid : 1600 m sec^{-1} at 60°K ; 1300 m sec^{-1} at 78°K. Results previously obtained with the same apparatus for the liquids ether and carbon tetrachloride at room temperature agreed with the published values to within 1%. Because of severe attenuation, however, the indications of resonance in the polycrystalline argon were relatively weak, and the accuracy of these results cannot be so high. Attenuation at the grain boundaries probably accounts also for the complete failure of our first attempts, carried out at 15 Mc/s using a pulse technique, because at this frequency the wavelength is about 0·1 mm—of the same order as the grain size of the solid argon as estimated from x-ray diffraction photographs.

Since we have not yet measured the velocity of shear waves, we can give an estimate of the compressibility (κ) only if we assume a value for Poisson's ratio (σ). Assuming $\sigma=\frac{1}{3}$ and the density (Δ) of solid argon to be 1·63 g cm^{-3} (Simon and von Simson 1924, de Smedt and Keesom 1925, Clusius and Weigand 1940), we estimate from

$$v=\sqrt{\{3(1-\sigma)/[(1+\sigma)\kappa\Delta]\}}$$

that κ is $0{\cdot}36\times10^{-10}$ cm^2 dyne^{-1} at 60°K and $0{\cdot}54\times10^{-10}$ cm^2 dyne^{-1} at 78°K. The chief causes of uncertainty in these values are: (*a*) the necessity at present to assume a value of Poisson's ratio (a change of σ from $\frac{1}{3}$ to 0·45 would decrease κ by 25%); (*b*) the possible existence of up to 0·5% impurity in the argon; (*c*) an uncertainty of perhaps 2% in the assumed value of density; (*d*) the possible existence of a small temperature gradient in the argon; (*e*) an effect of dispersion due to scattering at the grain boundaries.

Herzfeld and Goeppert-Mayer (1934), using an interatomic potential of the form $Ar^{-6}+Be^{-r/\varrho}$, have set up an equation of state for solid argon, which has been re-calculated by Kane (1939) with the use of improved empirical data. We have evaluated the compressibility for our temperatures from Kane's p–V isothermals for two values of ρ. Another estimate may be obtained from the work of Rice (1944, 1951), who calculated the potential energy of the lattice for various values of the lattice parameter by subtracting the Debye thermal and zero-point energies from the experimentally determined total energy (we have added a small correction to κ to take account of the thermal pressure). These theoretical estimates are listed in the following table for comparison with the experimental results :—

T(°K)	$\kappa\times10^{10}$ (cm^2 dyne^{-1})			
	Experimental	After Kane (1939)		After Rice (1951)
		(ρ=0·2091)	(ρ=0·345)	
60	0·36	0·50	0·85	0·15
78	0·54	1·1	1·6	0·21

Although, strictly, the experiments yield values of the adiabatic compressibility, the differences between the isothermal and adiabatic compressibilities are much smaller than the experimental uncertainty and we have not distinguished between them. It will be seen that the experimental values lie in the range covered by these theoretical estimates. Because of inconsistencies in the data used by the authors referred to, and because of the present experimental uncertainty, we do not wish at present to comment in greater detail on the agreement between the experimental and theoretical estimates of compressibility. It is interesting to note, however, that the observed compressibility of argon is higher

than that of its neighbouring alkali metal, potassium, in agreement with the suggestion of Bridgman (1949) that the peaks in the curve of compressibility of the elements against their atomic numbers would be occupied by the solidified inert gases. We hope to carry out further measurements with refined techniques, using both pulse and resonant methods with shear and longitudinal waves.

We wish particularly to thank Professor Kathleen Lonsdale, F.R.S., for her advice and for the help given in carrying out the x-ray measurements in her laboratory. We are grateful to Professor H. R. Robinson, F.R.S., for his friendly encouragement throughout the work, and to Dr. R. O. Davies for helpful discussions. We acknowledge with thanks the assistance of the Central Research Fund of the University of London and of the Department of Scientific and Industrial Research.

References

Bridgman, P. W., 1949, *The Physics of High Pressure* (Bell).
Clusius, K., and Weigand, K., 1940, *Z. Phys. Chem.* (B), **46,** 1.
de Smedt, J., and Keesom, W. H., 1925, *Leiden Commun.* 178b.
Herzfeld, K. F., and Goeppert-Mayer, M., 1934, *Phys. Rev.*, **46,** 995.
Kane, G., 1939, *J. Chem. Phys.*, **7,** 603.
Rice, O. K., 1944, *J. Chem. Phys.*, **12,** 289 ; see also 1951, *Phase Transformations in Solids*, ed. Smoluchowski *et alia* (Wiley), pp. 212–237.
Simon, F., and von Simson, C., 1924, *Z. Phys.*, **25,** 160.

Determination of the Widths of the Levels of p^{31} *from the Reaction* $^{27}Al\ (\alpha, p)\ ^{30}Si$

By R. R. Roy and C. Godeau
Université Libre de Bruxelles, Laboratoire de Physique, Bruxelles*

[Received July 28, 1953]

The reaction $^{27}Al\ (\alpha, p)\ ^{30}Si$ has been investigated by many workers. It is known that the resonance reaction takes place corresponding to the incident energies of α-particles $E_\alpha = 4{\cdot}0$ Mev and 4·4 Mev which produce excitations of 14·3 Mev and 14·8 Mev in the compound nucleus p^{31}—above its ground state. At these excitations the compound nucleus decays with the emission of four groups of protons of Q-values 2·26 Mev, −0·02 Mev, −1·32 Mev and −2·49 Mev. In the present experiment we have investigated the widths of the levels of p^{31} for energies of α-particles $E_\alpha = 4{\cdot}0$ Mev and 4·4 Mev, for the group $Q = -1{\cdot}32$ Mev.

A diffusion chamber was used for the detection of proton tracks. The dimension of the chamber was 24 cm in diameter and 15 cm in height, and, filled with air, it was operated at atmospheric pressure, at a gradient of temperature of 7°c/cm. The vapour source was a mixture of 70%

* Communicated by the Authors.

methyl alcohol and 30% water. The cold plate was in contact with solid CO_2. The aluminium target was bombarded by α-particles from polonium of strength 10 mc.

Photographs, 5 000 in all, were taken by a vertical camera through a glass window fixed on the top hot plate. The background drops could be reduced considerably simply by rubbing the glass window with a woollen cloth ; this produced an electric field across the chamber which removed the previous ions. The operation of rubbing the glass plate was repeated every five minutes during which period 20 photographs could be taken. Photographs obtained under these conditions were very sharp. The accompanying plate (Plate 49) shows the track of a proton in which the phenomenon of ' depletion ' can clearly be seen. The depletion of vapour was caused by the earlier passage of a cosmic-ray particle across the proton track—a passage marked by very diffused ions.

Fig. 1

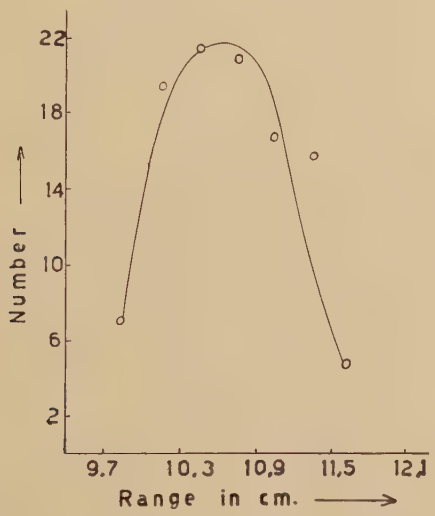

The distribution of dispersion in ranges of the 107 proton tracks for E_α=4·0 MeV, Q=—1·30 MeV.

Considering the dimensions of the chamber, the group for Q=—1·32 MeV for incident energies 4·0 MeV and 4·4 MeV could be most conveniently studied : the number of proton tracks measured was 107 and 85 respectively. The actual Q-values for the energies 4·0 MeV and 4·4 MeV were found to be —1·30 MeV and —1·37 MeV. The proton tracks of a particular group, emitted at a definite angle with respect to the direction of the α-particles, should show a dispersion in their ranges due to the width of the level. Since the protons are of about the same energy, error owing to straggling of protons in the target is small. As the number of protons observed at any particular angle was not large, we have reprojected all the tracks at 0° with respect to the incident direction of α-particles.

Figures 1 and 2 give the distribution of the ranges of protons for E_α=4·0 MeV and 4·4 MeV respectively. The widths deduced from these

curves are $0{\cdot}36\pm0{\cdot}06$ MeV for $Q=-1{\cdot}30$ MeV, $E_\alpha=4{\cdot}0$ MeV and $0{\cdot}30\pm0{\cdot}06$ MeV for $Q=-1{\cdot}37$ MeV, $E_\alpha=4{\cdot}4$ MeV.

The two earlier experiments to determine the widths of the levels for the reaction ^{27}Al (α, p) ^{30}Si, are due to Chadwick and Constable (1932) and Duncanson and Miller (1934). Their results are given along with ours in the following table.

Fig. 2

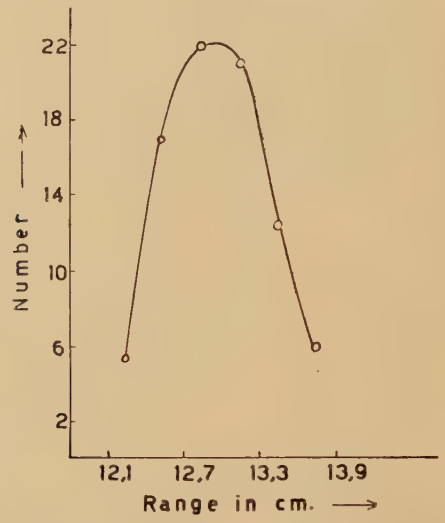

The distribution of dispersion in ranges of the 85 proton tracks for $E_\alpha=4{\cdot}4$ MeV, $Q=-1{\cdot}37$ MeV.

Authors	Resonance levels corresponding to E_α (MeV)	Width of the level
Duncanson and Miller	5·8	$0{\cdot}3\pm0{\cdot}2$ MeV
Chadwick and Constable	5·2	$0{\cdot}12<\Gamma<0{\cdot}32$ MeV
	4·8	0·20 MeV
Roy and Godeau	4·4	$0{\cdot}30\pm0{\cdot}06$ MeV
	4·0	$0{\cdot}36\pm0{\cdot}06$ MeV

The values obtained in the present experiment cannot strictly be compared with theirs as we have confined ourselves to the protons of one group only, that is $Q=-1{\cdot}32$ MeV, whereas their values refer to all the proton groups for the incident energies studied.

References

Chadwick and Constable, 1932, *Proc. Roy. Soc.* A, **135**, 48.
Duncanson and Miller, 1934, *Proc. Roy. Soc.* A, **146**, 396.

Temperature Change in Paramagnetic Resonance Absorption of Solutions of Organic Free Radicals

By D. Bijl and A. C. Rose-Innes
Clarendon Laboratory, Oxford*

[Received August 10, 1953]

We have investigated solutions (about 0·01 molar) of three organic radicals in different solvents (compare table 2) between room temperature and 90°K at about 10 000 Mc/s and in magnetic fields of about 3000 oersted. The substances studied were :

(1) Banfield and Kenyon's radical (β-(phenyl nitric oxide)-β methyl pentane-δ-one oxime N-phenyl ether)

$$ON\,(C_6H_5)\,C\,(CH_3)_2\,CH_2\,C\,(CH_3)\,N\,(C_6H_5)\,O\,;$$

(2) Di-phenyl nitric oxide ϕ_2 NO ;

(3) Di-p-anisyl nitric oxide (p-An)$_2$ NO.

At room temperature in sufficiently dilute solutions we always found three practically equidistant, not completely resolved, absorption lines. The separation, ΔH, of the central line and one of the outer lines is listed in table 1.

Table 1

Substance	g (solid)	g (solution)		ΔH (oersted)	$10^3\,A$ (cm^{-1})	$\Delta\nu$ (Mc/s)
		Low temperature	Room temperature			
ϕ_2 NO	—	2·0066	2·0066	9·5	0·88	39·5±1
B. and K.'s radical	2·0052	2·0050	2·0052	11·0	1·03	46·2±1
(An)$_2$ NO	2·0072	2·0048	2·0037	10·4	0·97	44·6±1

The accuracy of all g-values is about ±0·0005.

Originally we hoped to improve the resolution of the absorption lines by cooling the solution, but at low temperatures the three lines merged into a single line. This effect was studied in detail in solutions of B. and K.'s radical, but occurred as well in solutions of the other radicals. In table 2 are listed the different solvents used and the temperature range in which, on cooling, the transitions occurred. The results were reproducible.

Further details of the transitions are given in fig. 1 (Plate 50), where we reproduce some absorption lines observed as traces on the screen of a C.R.O. In one group of solvents (marked ' A ' in fig. 1 and table 2) the pattern is

* Communicated by Professor F. Simon, F.R.S.

symmetric at the highest and lowest temperatures, but is clearly asymmetric in between. In *n*-heptane the transition occurs below the melting point of the solvent. In the other group of solvents (marked ' B ') the pattern is symmetric at all temperatures, and the transitions occur above the melting point of the solvent. Further analysis is made more difficult by the incomplete resolution of the lines. Assuming, however, that the line shape is the same for all lines at all temperatures, it was possible to reconstruct the experimental traces by composition of three curves of different width and peak intensity. This procedure led us to the following qualitative conclusions.

Table 2

Solvent	Type	Temperature range (°K)	Remarks
Methyl alcohol	' A '		No change in H.F.S. 100° to 155°K
CCl_4	' A '		No change in H.F.S. 120° to 250°K
n-heptane	' A '	155–180	
i-pentane	' B '	150–185	
CS_2	' B '	180	Sudden change
n-pentane	' B '	150–185	
Pet.-ether (b.p.<40°C)	' B '	141–155	

If the temperature is lowered in both cases ' A ' and ' B ', the width of all lines increases and, moreover, the central line becomes more intense relative to the outer lines. In case ' B ' the distance between the lines becomes smaller; the same effect probably occurs in case ' A '.

The pattern observed at the higher temperatures strongly suggests a hyperfine structure caused by the ^{14}N nucleus in the NO-group. This is corroborated by the hyperfine structure observed in solutions of a radical of the same class as the radicals we investigated, the nitroso disulfonate ion $(SO_3)_2NO^{--}$ (Townsend *et al.* 1953). We therefore will interpret the observed lines as a hyperfine structure. This H.F.S. must be virtually isotropic and therefore can be described by the spin Hamiltonian

$$\mathcal{H} = g\beta\,(S \,.\, H) + A\,(S \,.\, I),$$

where β is the Bohr-magneton, H is the magnetic field, g and A are constants, and S and I are the spin operators of the unpaired electron and the nitrogen nucleus respectively ($S=\frac{1}{2}$, $I=1$).

Table 1 contains the observed g-values (both for solution and solid), the separation, ΔH, of the central line and one of the outer lines, the value of

A and the splitting in zero field, $\Delta\nu$. The values of g and ΔH were independent of the solvent; the magnetic field was calibrated with α, α-diphenyl β-picryl hydrazyl ($g=2{\cdot}0036\pm0{\cdot}0002$).

It is very unlikely that the change in relative intensity of the central line and the outer line during cooling of the solution can be explained in terms of a hyperfine structure. It is quite feasible, however, that on cooling one of the components of the system crystallizes out until a possible eutectic point is reached, below which both components would crystallize. This would probably make the observed pattern a superposition of a hyperfine structure of decreasing intensity and a single line of increasing intensity, coinciding (for B. and K.'s radical) with the central line of the hyperfine structure.

The decrease in hyperfine structure is probably a more interesting effect, as it may throw some light on details of the interaction between the unpaired electron and a nuclear magnetic moment in a free radical. Further experiments on this phenomenon are in course of preparation.

We would like to thank Mr. R. Foster, B.A., Dyson Perrins Laboratory, Oxford, and Dr. A. Burawoy, Chemistry Department, College of Technology, Manchester, for providing us with samples. One of us (D.B.) is indebted for the award of a Pressed Steel Company, Ltd. Research Fellowship; the other (A.C.R.-I.) for a maintenance grant of the Department of Scientific and Industrial Research.

Reference

Townsend, J., Weissmann, S. I., and Pake, G. E., 1953, *Phys. Rev.*, **89**, 606.

On the Reaction $^{18}O(p, \alpha)\,^{15}N$

By R. R. Roy, A. Lagasse and Miss M. J. Decock
Université Libre de Bruxelles, Laboratoire de Physique, Bruxelles

[Received July 31, 1953]

The reaction ^{18}O (p, α) ^{15}N was established by Burcham and Smith (1939) and by Freeman (1950); since then, the resonance reaction has been reported by Mileikowsky and Pauli (1950) and Seed (1951). The first resonance, according to Mileikowsky and Pauli, occurs for energy of proton $E_p=680$ kev and according to Seed at 640 kev: the latter value is now generally accepted. At this incident energy the compound nucleus ^{19}F receives an excitation of 8·59 Mev above its ground state, and then decays with the emission of α-particles. The nucleus ^{15}N is similar to the nuclei of ^{7}Li, ^{11}B and ^{19}F in that it can be regarded as composed of α-particles minus one nucleon. The lowest levels reported so far for ^{7}Li, ^{11}B and ^{19}F are at 0·478 Mev, 2·14 Mev and 1·4 Mev respectively; on the other hand,

the first low level observed in ^{15}N is at 5·28 Mev from the reaction ^{14}N (d, p) ^{15}N (Hornyak *et al.* 1950).

We have investigated the possible existence of low lying excited levels in ^{15}N using the reaction ^{18}O (p, α) ^{15}N with energies of protons up to 700 kev.

The 4·7% enriched ^{18}O target was in the form of water which was deposited as ice on a copper disc inside an evacuated glass cylinder of pyrex, while the proton beam, the current of which was measured by an integrator connected with the target assembly, bombarded the target after it had been deflected by the magnetic analyser. The voltage scale of the generator was calibrated in accordance with the standard reaction ^{7}Li (p, α) ^{8}Be. For the detection of the γ-rays which might be emitted from an excited level of ^{15}N in the process of de-excitation, a scintillation counter unit with a NaI-thallium enriched crystal was employed.

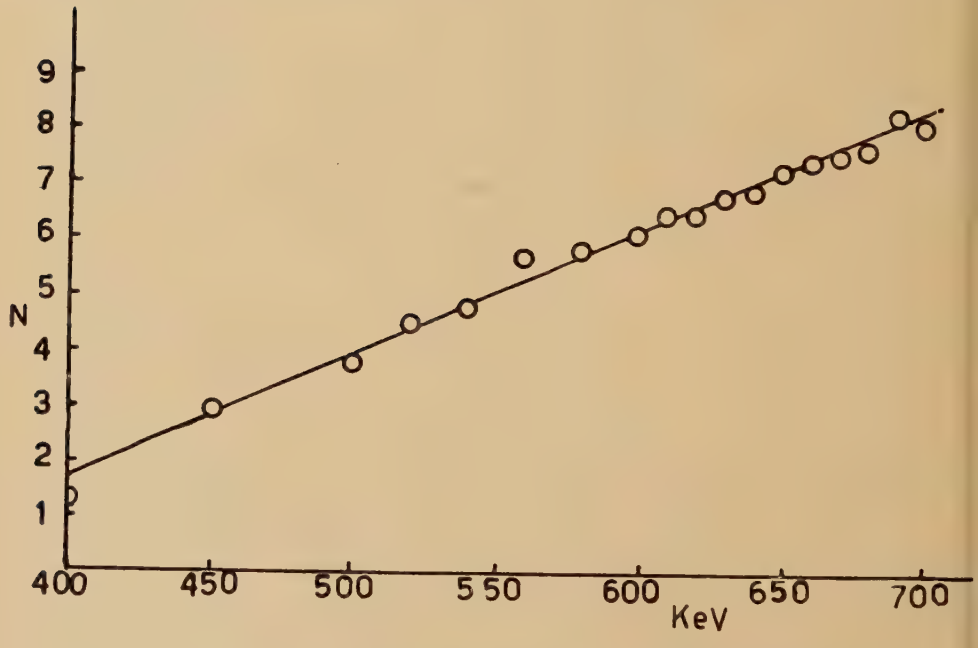

Excitation curve of the reaction ^{18}O (p, α)^{15}N for energies of proton up to 700 kev.

The figure shows the result obtained: the ordinate N represents the number of counts per μ-Coulomb and the abscissa the energy of the proton. Between 600 kev and 700 kev the number of counts, which varies linearly with the incident energy of protons, was noted at intervals of 10 kev. The width of the resonance level, as can be inferred from the curve published by Seed, is about 45 kev, corresponding to the proton energy 640 kev. If there had been an excited level in ^{15}N for the incident energy 640 kev, we should have expected a sudden increase in the number

of counts, starting from about 618 kev. The absence of such an increase leads us to conclude that, in the first place, no excited level is formed in ^{15}N for the reaction ^{18}O (p, α) ^{15}N at the resonance energy of proton 640 kev and, secondly, that the compound nucleus ^{19}F decays with the emission of one group of α-particles, leaving the final nucleus ^{15}N in the ground state. It should be mentioned that, with an ice target from pure distilled water, a curve similar to that in the figure was obtained.

Our results might be interpreted in the following way. Protons falling upon the ice target produced x-radiations ; the higher the energy, the greater the depth of penetration of the protons into the target which gives rise to the linear increase in the number of counts.

References

Burcham, W. E., and Smith, C. L., 1939, *Nature, Lond.*, **143,** 795.
Freeman, J. M., 1950, *Proc. Phys. Soc.* A, **63,** 668.
Hornyak, W. F., Lauritsen, T., Morrison, P., and Fowler, W. A., 1950, *Rev. Mod. Phys.*, **22,** 291.
Mileikowsky, C., and Pauli, R. T., 1950, *Nature, Lond.*, **166,** 602.
Seed, J., 1951, *Phil. Mag.*, **42,** 566.

The Cross Section for ^{181}Ta (γ, n) ^{180}Ta *at* 17·6 MeV

By J. H. Carver and H. J. Hay
Research School of Physical Sciences, Australian National University, Canberra*

[Received July 28, 1953]

The apparent ' resonance ' character of many photo-nuclear reactions is now well known. In the main these processes have been studied with the aid of the bremsstrahlung produced by betatrons and synchrotrons and the reaction identified by activation techniques (a number of references has been given by Carver, Edge and Wilkinson 1953). One of the reactions which has been most thoroughly investigated by this technique is the ^{181}Ta (γ, n) ^{180}Ta reaction. The figure shows the cross section for this reaction as determined by Haslam, Smith and Taylor (1951). Using the gamma-rays from the ^{7}Li (p, γ) reaction, Carver, Edge and Wilkinson (1953) showed that competing reactions did not destroy the ' resonance ' character of the gamma-ray absorption. They found the ratio of the cross sections for ^{181}Ta (γ, 2n) ^{179}Ta at 17·6 MeV to ^{181}Ta (γ, n) ^{180}Ta at 14·6 MeV to be $0{\cdot}29 \pm 0{\cdot}11$.† Taken at their face value these measurements indicate that, at gamma-ray energies of the order of 18 MeV and greater,

---

* Communicated by Professor E. W. Titterton.

† This result agrees with the neutron yield measurements obtained by Halpern, Nathans and Mann (1952) and Whalin and Hanson (1953) using betatron bremsstrahlung and with the indirect estimate made by Eyges (1952).

the gamma-ray absorption occurs almost entirely by means of direct interaction rather than by the immediate formation of a compound nucleus. The (γ, 2n) cross section at 17·6 MeV (Carver, Edge and Wilkinson 1953) is only slightly larger than the (γ, n) cross section at 17·6 MeV (Haslam, Smith and Taylor 1951) whereas calculations based on the statistical theory (Blatt and Weisskopf 1952) indicate that the (γ, 2n) cross section at 17·6 MeV should be some 16 times the (γ, n) cross section at 17·6 MeV.

In order to determine whether or not the high energy tail in the ^{181}Ta (γ, n) ^{180}Ta cross section is indeed as large as is indicated by the bremsstrahlung results we have measured the ratio of the cross sections for this reaction at gamma-ray energies of 14·6 and 17·6 MeV using the

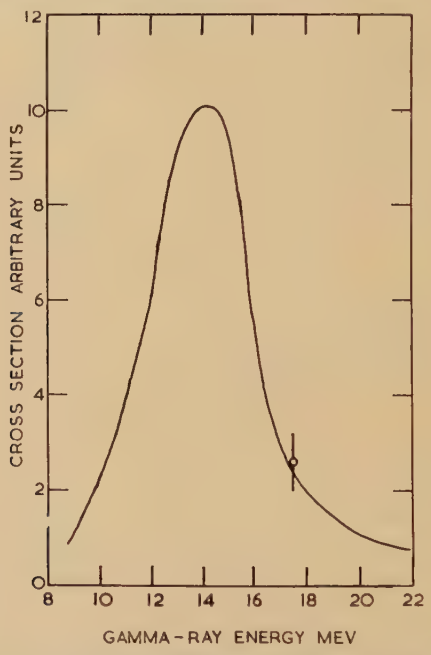

The cross section for ^{181}Ta (γ, n) ^{180}Ta at 17·6 MeV compared with the curve obtained by Haslam, Smith and Taylor (1951).

radiation from the ^{7}Li (p, γ) reaction. The principle of the method was the same as that used by Carver, Edge and Wilkinson (1953) except that a measurement of the induced ^{180}Ta activity (half life 8·15 hr) replaced the total neutron yield measurement.

The proton bombardment of lithium produces gamma-rays of 17·6 MeV (negligible width) and 14·6 MeV (2 MeV width) and the relative intensity of these gamma-rays depends on the proton energy. At a proton energy of 500 keV (thick target) the ratio of the intensity of the 17·6 MeV line to that of the 14·6 MeV line is $1{\cdot}70\pm0{\cdot}20$; at 1·15 MeV (target thickness 250 keV) this ratio is $0{\cdot}45\pm0{\cdot}06$ (Stearns and McDaniel 1951). These ratios apply to radiation emitted at an angle of 75° to the proton beam. We have

irradiated a tantalum Geiger counter under these conditions and determined, at both proton energies, the relative induced ^{180}Ta activity per incident quantum. Throughout the irradiations (which were for periods of about eight hours) the gamma-ray yield was monitored continuously by a NaI (Tl) crystal which was biased so that none of the $\sim$0·5 MEV quanta, due to inelastic scattering at the higher proton energy, was detected. Several irradiations were performed at both proton energies and corrections were made for fluctuations in the gamma-ray yield assuming the half-life of ^{180}Ta to be 8·15 hr. It was found that the ratio of the ^{181}Ta (γ, n) ^{180}Ta cross section at 17·6 MEV to that at 14·6 MEV was $0{\cdot}26 \pm 0{\cdot}06$.* As shown in the figure this result agrees with the bremsstrahlung results and therefore confirms the conclusions drawn by Carver, Edge and Wilkinson (1953) concerning the importance of direct effects at gamma-ray energies above the ' resonance '.

References

BLATT, J. M., and WEISSKOPF, V. F., 1952, *Theoretical Nuclear Physics* (Wiley).
CARVER, J. H., EDGE, R. D., and WILKINSON, D. H., 1953 a, *Phil. Mag.*, **44,** 404; 1953 b, *Phys. Rev.*, **89,** 658.
EYGES, L., 1952, *Phys. Rev.*, **86,** 325.
HALPERN, J., NATHANS, R., and MANN, A. K., 1952, *Phys. Rev.*, **88,** 679.
HASLAM, R. N. H., SMITH, L. A., and TAYLOR, J. G. V., 1951, *Phys. Rev.*, **84,** 840.
STEARNS, M. B., and MCDANIEL, B. D., 1951, *Phys. Rev.*, **82,** 450.
WHALIN, E. A., and HANSON, A. O., 1953, *Phys. Rev.*, **89,** 324.

Introduction of Exchange in the Thomas–Fermi Model for Atoms

By N. H. MARCH

Department of Physics, The University, Sheffield†

[Received August 4, 1953]

IN a recent paper, Scott (1952) has considered the corrections to be applied to the customary formula due to Milne (1927) for the binding energy of the Thomas–Fermi (T.F.) atom, and has obtained results in good agreement with experiment. Scott concluded that two corrections were necessary, the first arising from the so-called ' boundary effect ', due to the failure of the T.F. method in the neighbourhood of the nucleus, and the second from the effect of exchange.

---

* This result applies to a monochromatic gamma-ray of 14·6 MEV and not to the broad line used in the experiment. We have corrected our result for the width of this line (and for the 0·6 MEV increase in gamma-ray energies at the higher proton energy) by assuming that near 14·6 MEV and near 17·6 MEV the shape of the (γ, n) cross section is as given by Haslam, Smith and Taylor (1951) but no assumption as to the relative magnitudes of the 14·6 and 17·6 MEV cross sections has been made.

† Communicated by the Author.

The present work has been carried out with the object of examining the validity of Scott's method of evaluating the binding energy (without the boundary correction, with which we shall not be concerned here) when exchange is included and investigating the possibility of modifying the usual T.F. electron distribution to take some account of exchange. For it is well known that if one attempts to use Dirac's method directly to calculate a modified electron distribution for an atom (Dirac 1930) serious difficulties arise, as there is no solution of the Thomas–Fermi–Dirac (T.F.D.) equation representing an electron cloud which extends to infinity. In fact the only kind of 'atom' in the model is one of finite radius with a discontinuity of charge density at the boundary and this is clearly very unsatisfactory.* Scott avoided the difficulties associated with the T.F.D. model by using the ordinary T.F. electron density to calculate the energy including exchange.

Scott's choice suggested to us the use of the variational function

$$n_\lambda(r)=\lambda^3 n_1(\lambda r), \quad . \quad . \quad . \quad . \quad . \quad . \quad . \quad . \quad (1)$$

for the electron density, $n_1(r)$ being the usual T.F. density. λ^3 is included in (1) simply for normalization purposes. Such a scale factor λ was first introduced by Fock (1932) as a device to enable him to prove the virial theorem in the T.F. theory, and was subsequently put equal to unity. We propose here to use λ as a proper variational parameter. If E_λ is the total energy corresponding to the electron density (1), and T_1, U_1 and A_1 are respectively the kinetic, potential and exchange energies calculated using the unmodified density $n_1(r)$ then it follows that

$$\left.\begin{aligned} E_\lambda &= T_\lambda + U_\lambda + A_\lambda \\ &= \lambda^2 T_1 + \lambda U_1 + \lambda A_1 \end{aligned}\right\} . \quad . \quad . \quad . \quad . \quad . \quad (2)$$

Hence the value of λ, say Λ, for which E_λ is a minimum is given by

$$\Lambda = -\frac{(U_1+A_1)}{2T_1} . \quad . \quad . \quad . \quad . \quad . \quad . \quad . \quad . \quad (3)$$

Thus by choosing λ to have the value Λ given by (3) instead of 1 as in Scott's calculation we find a lower energy and hence an improved charge distribution.

If $E_1(=T_1+U_1)$ is the usual T.F. energy neglecting exchange, we can write, from the work of Milne (1927), Baker (1930) and Scott (1952),

$$\left.\begin{aligned} E_1 &= -\beta Z^{7/3}, & U_1 &= -2\beta Z^{7/3}, \\ T_1 &= \beta Z^{7/3}, & A_1 &= -\gamma Z^{5/3}, \end{aligned}\right\} \quad . \quad . \quad . \quad . \quad . \quad (4)$$

where $\beta=0{\cdot}7687$ and $\gamma=0{\cdot}2208$, both in atomic units.

---

* It should be mentioned here that Plaskett (1953) has recently criticized Dirac's treatment and proposed an alternative equation. This modified equation has associated with it all the difficulties of the T.F.D. treatment.

Hence we obtain from (3) and (4)

$$\left.\begin{aligned} \Lambda &= 1+(\gamma/2\beta)Z^{-2/3} \\ &= 1+0{\cdot}1436Z^{-2/3} \end{aligned}\right\} \quad \ldots\ldots\ldots \quad (5)$$

Equations (1) and (5) completely define a new charge distribution in which some account is taken of exchange.

It is instructive at this stage to write down the separate expressions for the kinetic, potential and exchange energies. They are easily found to be given in terms of β, γ and Z by the following equations:

$$\left.\begin{aligned} T_\Lambda &= \beta Z^{7/3}+\gamma Z^{5/3}+(\gamma^2/4\beta)Z, \\ U_\Lambda &= -2\beta Z^{7/3}-\gamma Z^{5/3}, \\ A_\Lambda &= -\gamma Z^{5/3}-(\gamma^2/2\beta)Z. \end{aligned}\right\} \quad \ldots\ldots\ldots \quad (6)$$

It follows that the energy E_Λ in this approximation is given by

$$E_\Lambda = -\beta Z^{7/3}-\gamma Z^{5/3}-(\gamma^2/4\beta)Z, \quad \ldots\ldots\ldots \quad (7)$$

which agrees with Scott's result apart from the term in Z. Since he neglects terms of order $Z^{4/3}$ it follows that his binding energy formula is left unchanged.

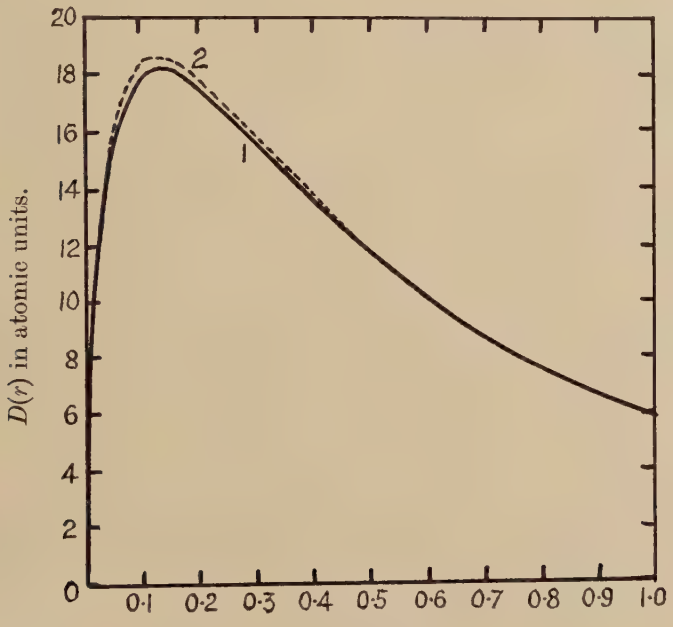

Radial charge distribution for argon.
(1) Without exchange. (2) With exchange.

We see then that whilst the effect of modifying the electron density to take account of exchange is to introduce terms of order $Z^{5/3}$ in the kinetic and potential energies, these terms exactly cancel in the total energy and

Scott's result is effectively regained. It is further interesting to note that from (6)

$$2T_A+U_A+A_A=0, \qquad \ldots\ldots \quad (8)$$

and hence the virial theorem is satisfied in our approximation, whereas it does not, of course, hold in Scott's treatment.

To illustrate the effect of modifying the electron distribution in the manner considered here, we have plotted in the figure the radial charge distribution $D(r)$ (defined as density $\times 4\pi r^2$) for argon, with and without exchange. The contraction of the charge cloud which is known to occur when exchange is introduced is well shown. (For larger values of r than are shown in the figure, curve 2 of course lies below curve 1.)

The method outlined above can also be applied to positive ions, for which a direct application of the T.F.D. equation again leads to difficulties.

References

Baker, E. B., 1930, *Phys. Rev.*, **36**, 630.
Dirac, P. A. M., 1930, *Proc. Camb. Phil. Soc.*, **26**, 376.
Fock, V., 1932, *Phys. Zeits. Sowjet.*, **1**, 747.
Milne, E. A., 1927, *Proc. Camb. Phil. Soc.*, **23**, 794.
Plaskett, J. S., 1953, *Proc. Phys. Soc.* A, **65**, 178.
Scott, J. M. C., 1952, *Phil. Mag.*, **43**, 859.

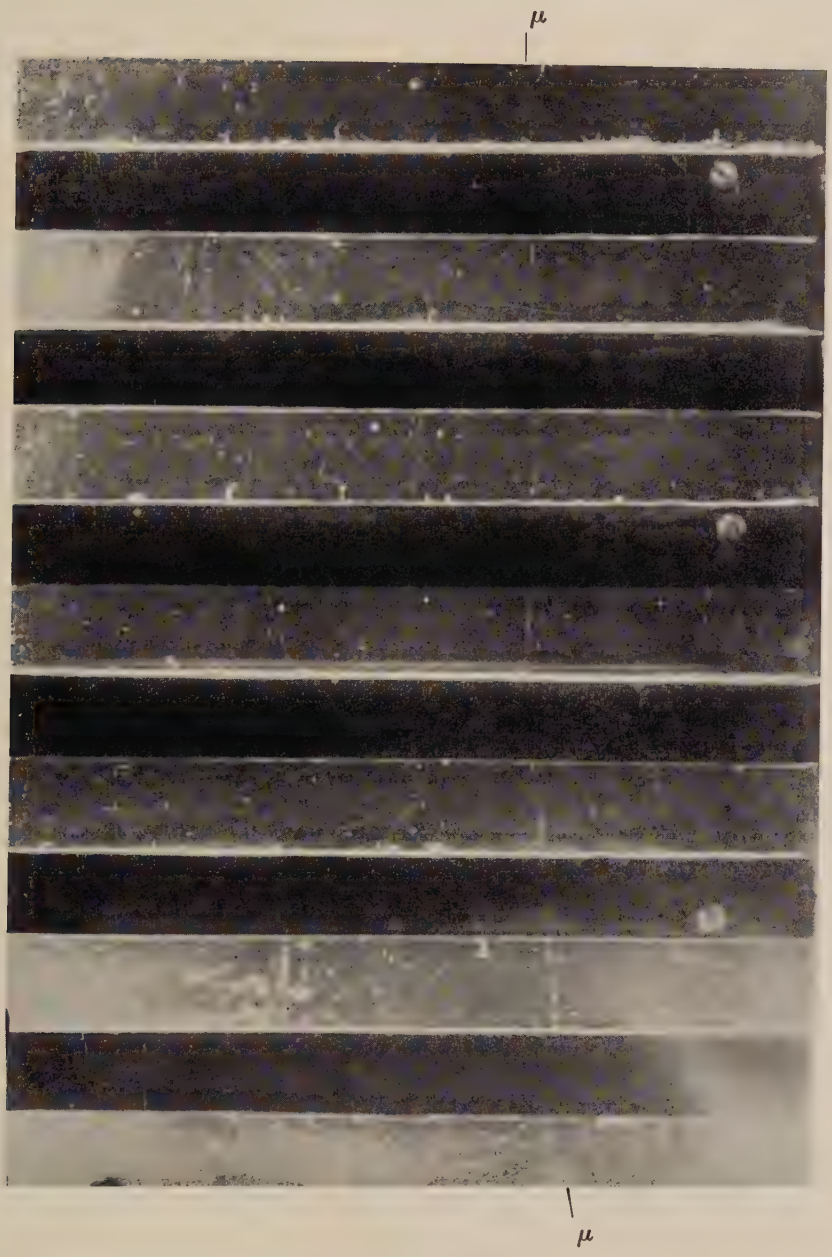

Event No. 5 (table 2). Example of anomalous scattering.

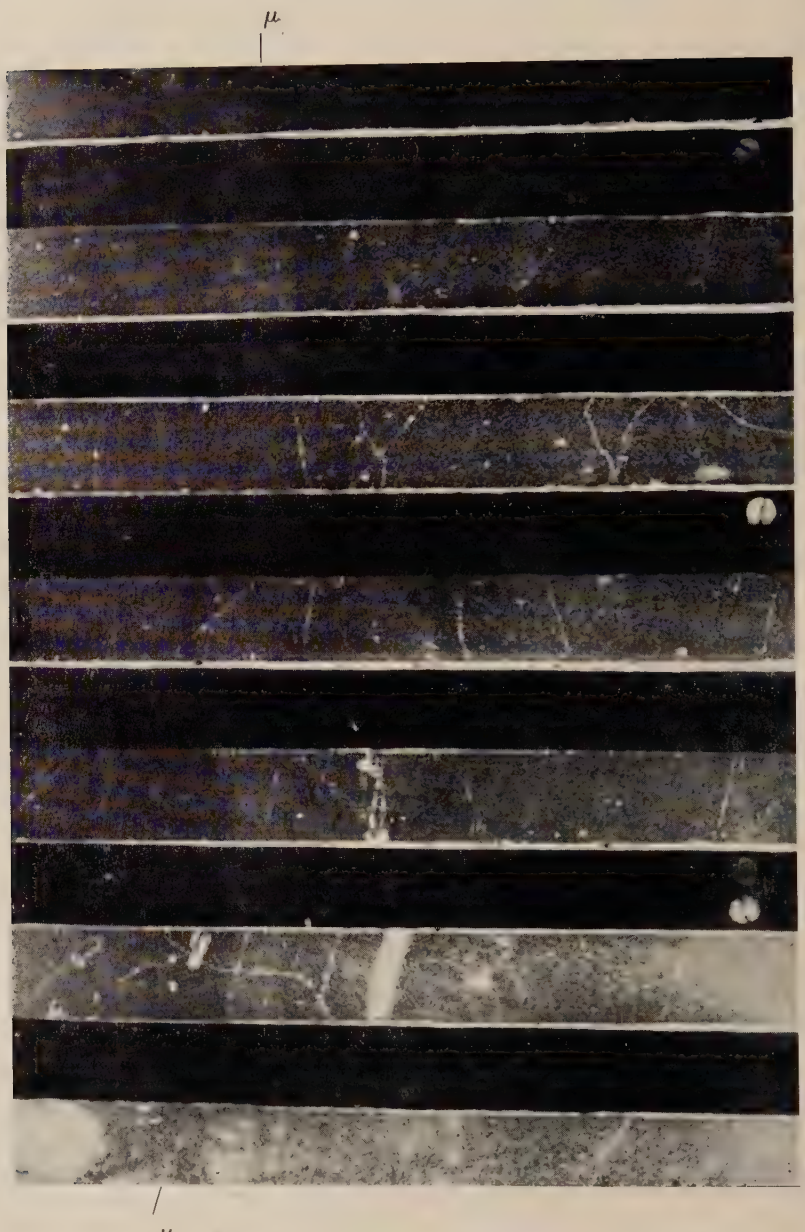

Probable example of anomalous scattering.

Fig. 1

×8000

Growthfronts on 111 face of ZnS.

Fig. 2

×7000

Slip lines on 111 face of ZnS.

Fig. 3

×18000

Enlargement of part of fig. 2.

Fig. 4

×28000

Slip lines on (111) face of ZnS.

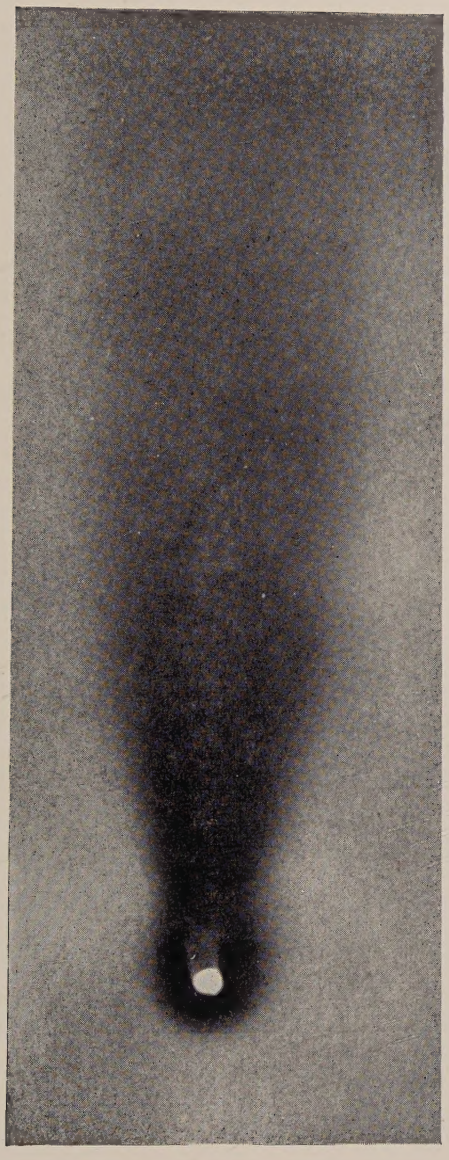

Radioautograph of effect of obstacle on flat plate on deposition of ^{131}I vapour from airstream (wind speed 460 cm/sec).

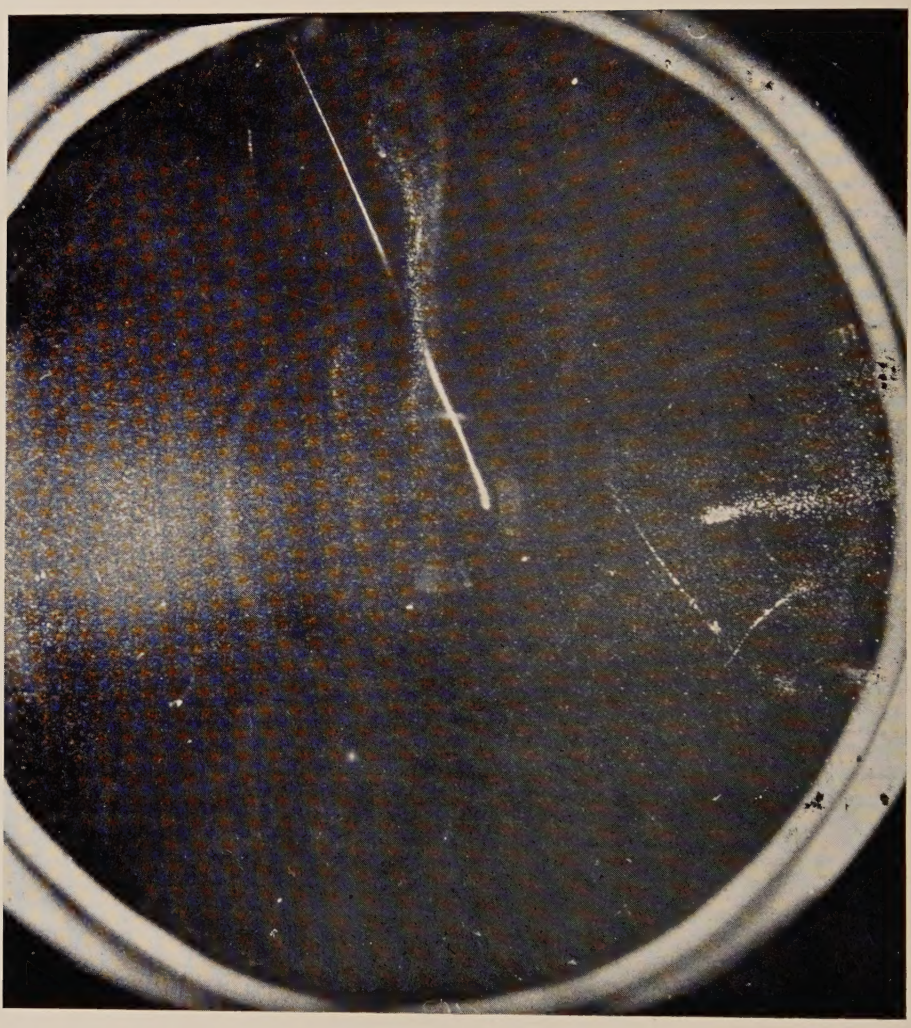

A typical example of a proton track obtained in the diffusion chamber, showing the phenomenon of ' depletion '.

Fig. 1

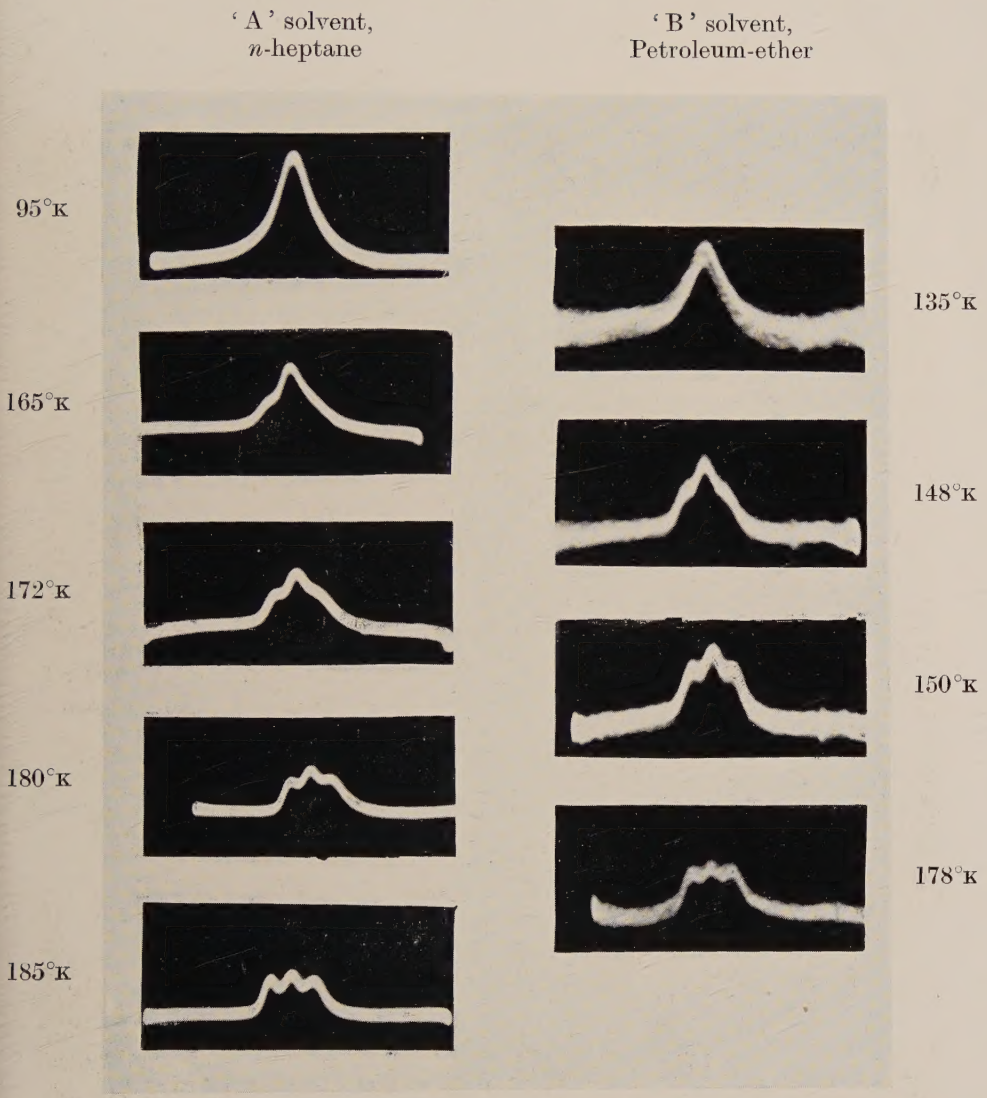

Paramagnetic resonance absorption in solutions of B. and K.'s radical at various temperatures.